Finding the Operating Limits and Optimal Configuration of an Electrically Assisted Turbofan

M.R. van Holsteijn 4143116

Master Thesis

©: NASA

TU Delft Delft University of Technology

Aerospace Engineering

September 5, 2019

Finding the Operating Limits and Optimal Configuration of an Electrically Assisted Turbofan

by

Merijn Rembrandt van Holsteijn

in partial fulfillment of the requirements for the degree of

Master of Science
in Aerospace engineering

at the Delft University of Technology,
to be defended publicly on Thursday September 19th, 2019 at 10:00 AM.

Student number:	4143116	
Thesis committee:	Dr. A. Gangoli Rao,	TU Delft, chair and supervisor
	Dr. F. Yin,	TU Delft, supervisor
	Dr. J. Dong,	TU Delft
	Dr. M.A. Mitici,	TU Delft, external member

An electronic version of this thesis is available at `http://repository.tudelft.nl/`.

TU Delft

Acknowledgements

After having done my Bachelor in Aerospace Engineering at the TU Delft, this master thesis marks the end of my Master Aerospace Engineering, and my study period at the TU Delft. I believe with this thesis I have been able to provide a better understanding of the gas turbine, and in what ways a gas turbine can be redesigned for maximum efficiency in a parallel hybrid electric propulsion Aircraft.

This work would not have been possible without my supervisors Arvind & Feijia. They were able to show me the bigger picture when I was sometimes lost in the details, and provided me with feedback throughout the process. I hope my works also helps them in their future careers, and they are able to improve the aviation industry. Furthermore, I would like to thank Jianning for his help in understanding the workings of an electric motor. A special thanks goes to my fellow students at the FPP-master student rooms for helping me during my thesis with countless discussions on gas turbines, aircraft and all possible other topics. But above all, I would like to thanks my parents Vera & Rob, my sister Freija and my girlfriend Marijke for their years of support, love and kindness.

I hope this thesis provides the reader with new knowledge and insights on gas turbines, electric motors and how they can be combined in an electrically assisted turbofan.

Merijn Rembrandt van Holsteijn
Delft, September 2019

Summary

With an increase in wealth for a growing number of people, the number of flights is increasing. Where in the year 2000 around 20 million flights were conducted, by the year of 2020, it is estimated that the flight number would reach the 40 million, making the aviation industry a sector with a fast growing fuel consumption and related increase of emissions. Since fuel costs are a large part of the operational costs of an airline, reducing fuel consumption is not only beneficial for the environment, but also reduces operational costs.

A promising new technology to reduce emissions and fuel consumption of an aircraft is hybrid electric propulsion (HEP). This technology can be deployed in different ways, depending on the manner in which the gas turbine and electric motor are coupled. In this study the parallel configuration is used, indicating that the electric motor assists the gas turbine in driving the spool(s), using electrical energy from a battery. The power management strategy that is assessed here is based on a fully electric taxi phase; during the high power demanding take-off and climb phases, the gas turbine and motor work together and during cruise phase, the gas turbine will operate on its own. This strategy allows for a redesign of the gas turbine striving for maximum efficiency in cruise, because the take-off and climb thrust requirements do not have to be met by the gas turbine alone. Supplying power to the gas turbine shaft however changes its operating characteristics. The goal of this thesis therefore is to investigate how electrical power can most efficiently and safely be supplied to a gas turbine, and to maximize the cruise efficiency. This will is done by analysing the factors that define the overall efficiency of a gas turbine, the thermodynamic efficiency and the propulsive efficiency. Thermodynamic efficiency is defined by the component efficiencies, turbine inlet temperature (TIT) and overall pressure ratio (OPR). Propulsion efficiency is defined by the bypass ratio and fan pressure ratio.

Due to their limited time in cruise phase, where the battery and electric motor are deadweight, the benefits of the parallel HEP are expected to be most noticeable for regional and short heal flights. Therefore, the Airbus A320neo together with its CFM LEAP-1A engine are used as baseline. Validation of the baseline model is carried out on multiple levels: firstly, on thrust specific fuel consumption in cruise and sea level static conditions, and secondly, on the ability to achieve maximum and minimum thrust settings both in-flight and on ground. To analyse the fuel consumption over a complete flight, a standard mission profile with taxi, take-off, climb, cruise and descent is used over a total range of 1000 km. A320neo flight data is used to validate the mission profile, after which total mission consumption is compared to multiple sources.

Characteristics of an electrically assisted turbofan are assessed by supplying multiple levels of power to the baseline turbofan, and varying the power division between the low pressure and high pressure spool. With the help of the 0-D thermodynamic gas turbine modelling program GSP, it was found that the most efficient combination of power division between the low and high pressure spool depends on the total amount of electrical power supplied. Low power levels are most efficient when supplied to the low pressure spool. By increasing the power supply, a growing fraction is required to be supplied into the high pressure spool for maximum efficiency. The low pressure compressor (LPC) is the component that may cause safety problems when striving for maximum efficiency. If power is supplied to the low pressure spool, the

surge margin of the LPC decreases. On the other hand, when more power is supplied to the high pressure spool, the LPC's surge margin increases. Depending on the component, a certain surge margin is required to allow for safe operation. This safety requirement might therefore limit the options for maximising the overall efficiency of the combined operating mode of gas turbine and electric motor. It was found that type of turbofan impacts this surge margin. A direct drive two spool turbofan like the LEAP-1A has a subsonic LPC, whereas a geared turbofan has a transonic map. Subsonic LPC showed lower surge margins at take-off and climb than the transonic LPC. The geared turbofan therefore shows a greater potential to work at higher efficiencies.

Analysis of the baseline turbofan indicated that both thermodynamic and propulsive turbofan operation leave little space for further cruise efficiency improvements with constant TIT and OPR. In theory, propulsive efficiency can be improved by lowering the fan pressure ratio which would facilitate a higher bypass ratio. However, the required increase in air mass flow would most likely return the effective improvement to zero because of the higher weight and additional nacelle drag. With an electrically assisted turbofan, it is possible to increase both the TIT and OPR in cruise, because both are reduced in their maximum and thus critical values thanks to the electrical assistance in take-off and climb.

By using an average 14% power split between electrical power and low pressure shaft power in both take-off and climb, the TIT is around 100 K lower in both flight phases for the electrically assisted turbofan. At top of climb the OPR is reduced with an electrically assisted turbofan. How much it is reduced, depends on the type of low pressure compressor, around 2.3% and 3.4% for a direct drive two spool and geared turbofan respectively. Using the increased OPR and TIT values in cruise, an analysis was done to find the best possible combination of fan pressure ratio and bypass ratio without significantly increasing the air mass flow. The resulting combination reduced the thrust specific fuel consumption by 1.0%, without increasing the air massflow rate.

Using an optimistic technology level for the electric system in the year of 2030, a hybrid electric Airbus A320neo together with a redesigned CFM LEAP-1A engine, could save 4.7% on fuel consumption over a 1000 km mission. With an even higher technology level in the year 2040, these savings grow to 7.3%. In both cases, the largest share of these savings on comes from the electric taxiing. When a 4 minutes warm-up and 3 minutes cooling of the gas turbines are taken into account, the majority of these savings are lost. Savings for the HEP aircraft are therefore mainly determined by the duration of the taxi phase. The results indicate that the potential savings of a HEP version of the A320neo aircraft are limited in range, mainly due to the mass of the required electrical system which increases the total weight of the aircraft by 5.5% in 2030, or 2.5% in 2040 technology levels. The study shows the increased thrust requirements caused by the additional weight cannot sufficiently be offset by the increase of engine efficiency to allow for longer missions. Additional possible improvements for the hybrid electric aircraft need to come from removing any possible component that the electric system replaces, such as the axillary power unit and the pneumatic starting system of the gas turbines. A redesign of the aircraft for the shorter range of 1000 km for both conventional propulsion and hybrid electric propulsion is therefore suggested. Design of new components specifically for maximum efficiency in cruise could also provide the hybrid aircraft with additional benefits.

Contents

List of Figures

List of Tables

Nomenclature

Acronyms

AC	Alternating Current
APU	Auxiliary Power Unit
ASK	Available Seat Kilometers
BLAC	Brusless Alternating Current
BLI	Boundary Layer Ingestion
BPR	Bypass Ratio
DC	Direct Current
DDTF	Direct Drive Turbofan
EM	Electric Motor
GT	Gas Turbine
Gt	Gigatonnes (10^{12} kg)
GTF	Geared Turbofan
HEP	Hybrid Electric Propulsion
HEPS	Hybrid Electric Propulsion System
HP	High Pressure
HPC	High Pressure Compressor
HPT	High Pressure Turbine
IPM	Interior Permanent Magnet
ISA	International Standard Atmosphere
ITB	Interstage Turbine Burner
LP	Low Pressure
LPC	Low Pressure Compressor
LPT	Low Pressure Turbine
MEA	More Electric Aircraft
min	Minutes
MTOW	Maximum Take-Off Weight
MZFW	Maximum Zero Fuel Weight
NLR	Netherlands Aerospace Centre
OEW	Operative Empty Weight
OPR	Overall Pressure Ratio
PMSM	Permanent Magnet Synchronous Motor
PPMV	Part Per Million Volume
PR	Pressure Ratio
RPK	Revenue Passenger Kilometers
SBT	Science-Based Target
SLS	Sea Level Static
SM	Surge Margin
SPM	Surface Permanent Magnet
SRM	Switched Reluctance Motor
SUGAR	Subsonic Ultra Green Aircraft Research
TIT	Turbine Inlet Temperature
TO	Take-Off

TOC	Top Of Climb
TSFC	Thrust Specific Fuel Consumption
VIGV	Variable Inlet Guide Vane
VSV	Variable Stator Vane

Constants

g_0	Gravitational acceleration at Earth's surface	9.80665 m/s^2
LHV	Lower Heating Value	43.031 MJ/kg

Gas Turbine Stations

0	Ambient
1	Engine Inlet
13	Fan exit bypass
16	Bypass duct
19	Bypass nozzle exit
2	Fan inlet
21	Fan exit core
25	Low pressure compressor exit
3	High pressure compressor exit
4	High pressure turbine inlet
49	Low pressure turbine inlet
54	Low pressure turbine exit
6	Core duct
9	Core nozzle exit

Greek Symbols

η	Efficiency	%
ω	Angular velocity	rad/s
Φ	Power Split	-
π	Pressure ratio	-
Ψ	Low pressure spool power fraction	-
ρ	Density	kg/m^3
σ	Stress	N/m^2
ζ	Magnetic field angle	rad

Roman Symbols

A	Linear current density	A/m
B	Magnetic flux density	Wb/m^2
C	Discharge rating	1/h
C'	Disk shape	-
D	Diameter	m
F	Force	N
G	Tangential stress	N/m^2
k	Electric motor loss coefficient	-
L	Length	m
M	Mach number	-
m	Mass	kg
N	Spool speed	rpm
P	Power	W
r	Moment arm	m

S	Effective flux area	m^2
T	Torque	Nm
V	Velocity	m/s
W	Mass flow	kg/s

Subscripts

C	Corrected
IS	Isentropic
n	net
Poly	Polytropic

1 Introduction

This introductory chapter covers the motivation for the research and explains the research gap that was found. Next, it presents the objective and methodology of the research that has been done. Lastly, it gives the structure of the following report chapters.

1.1. Research motivation

In recent years, more and more news articles, movies, papers and books have been appearing to show the harmful impact humans have on the earth and its other habitants. The increasing population and welfare will cause more people to buy and use more goods, enlarging the negative impact on nature. Part of this harmful impact comes from aviation. In the past decades, the fuel use by aviation has increased rapidly, as is shown in figure 1.1. The figure also shows the revenue passenger kilometers (RPK) which represent the amount of kilometres that have been flown, which shows an exponential as well. It can be seen the RPK increases faster than the fuel consumption, implying planes have gotten more efficient over the past decades, but more on that in the next section.

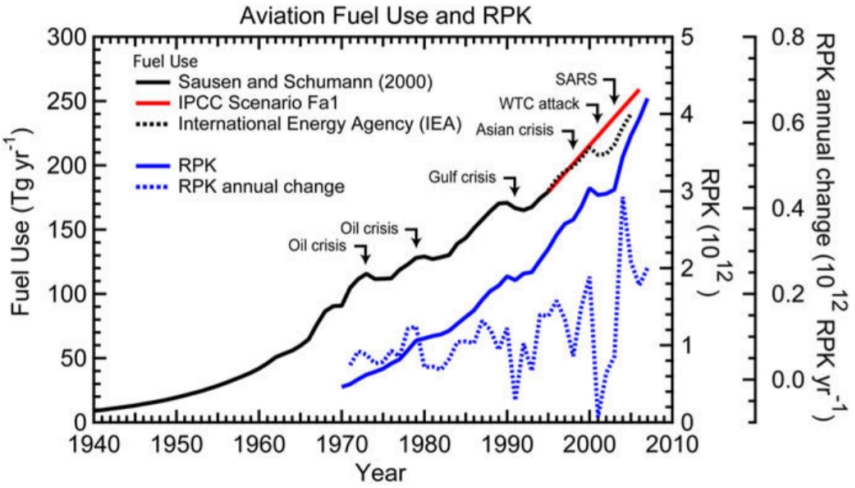

Figure 1.1: Fuel use in aviation and revenue passenger kilometres [1]

As the RPK is expected to keep growing in the future, Airbus and Boeing foresee an annual growth of 4.4% [2] and 4.7% [3] respectively, the total fuel consumption by aviation will continue to grow. This causes a problem not only towards the depletion of fuel reserves, but also to the climate. CO_2 is one of the major green house gasses, and as shown in figure 1.2, the CO_2

emission from aviation keep increasing. In 2005 a total of $0.7 \cdot 10^{12}$ kg of CO_2 was emitted by the complete aviation industry as can be seen in the figure. This accounted for around 2.5% of the global emissions of CO_2 for that year. Additionally, this figure shows that not only the absolute amount of CO_2 emissions of aviation is increasing, but also the relative amount with respect to the anthropogenic CO_2. In the year 2019, this fraction has already grown to 3% [4, 5].

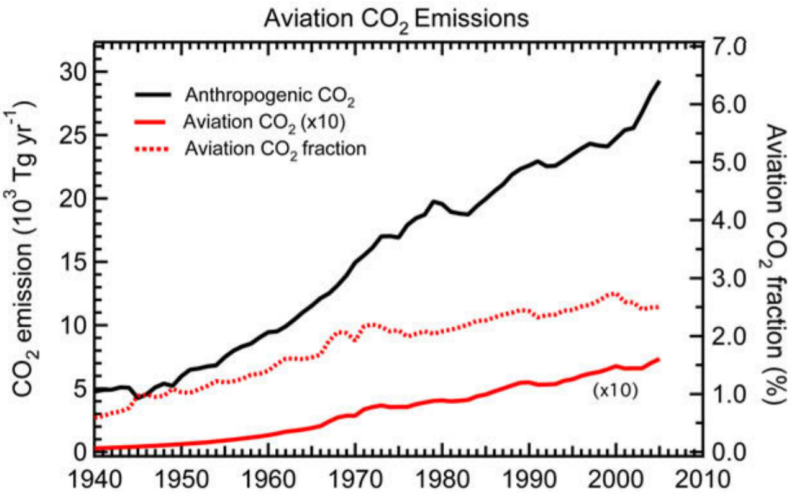

Figure 1.2: CO_2 emissions by the aviation industry [1]

Depending on future developments in aviation legislation, world economic growth and aircraft efficiency improvements, several emission scenarios are sketched in figure 1.3. 'High' emissions estimate increase 5% yearly, while 'mid' and 'low' increase 3.5% and 2% respectively. The figure also shows the goal of the aviation industry itself, the science-based target (SBT) trajectory: half the carbon emissions by 2050 with respect to 2005 levels [5, 6].

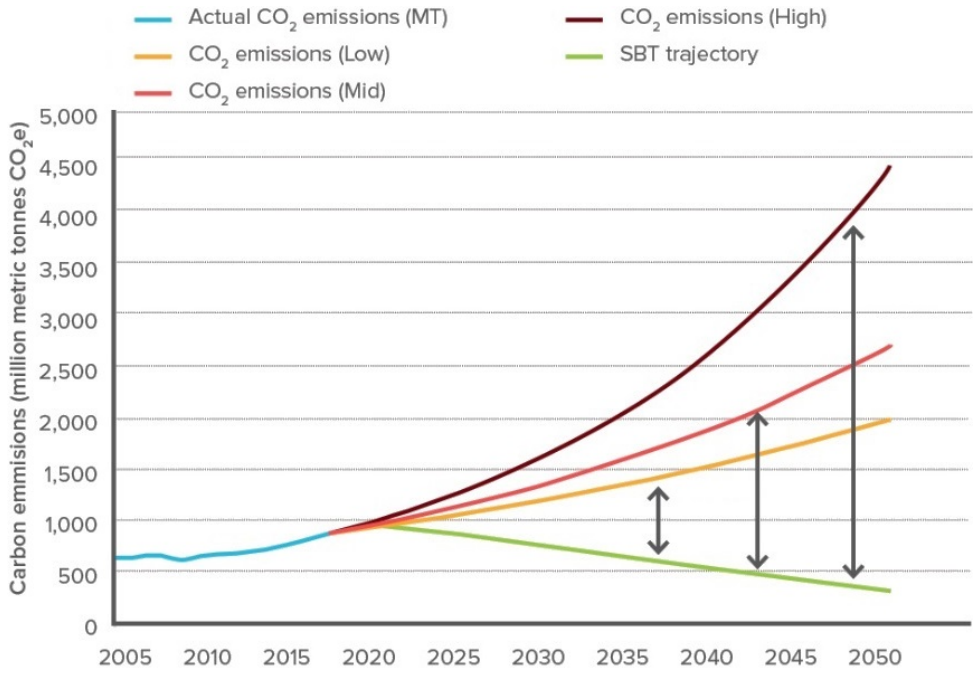

Figure 1.3: Aviation's predicted yearly CO_2 emissions [5]

In the Paris Climate Agreement, almost all countries in the world agreed to keep the temper-

ature increase with respect to pre-industrial time due to climate change below 2.0 ^{o}C. To be able to achieve this, it is estimated that the total amount of CO_2 emissions between 2010 and 2050 should be less than 1020 gigatonnes (Gt). In 2019, 9 years have passed, wherein yearly 35 Gt CO_2 were emitted worldwide [7]. Therefore only around 700 Gt can be emitted in the remaining 31 years to meet the 2.0 ^{o}C goal. Using the 'mid' level CO_2 emission expectancy for, the aviation industry will emit some 50 Gt CO_2 between the year 2019 and 2050 [5]. This would mean the relative impact of the aviation industry increase in the coming years, marking clearly what challenges the world is facing and the responsibility and action that needs to be taken by the aviation industry.

Besides the CO_2 emissions there are other (lesser known) negative consequences due to combustion of fossil fuels. One of them is the emission of NO_x, which causes damage to the ozone layer among others. Aircraft also produce contrails, or clouds, at high altitudes which warm up the earth by acting as a blanket over the earth [1]. At airports and other high air traffic points, local problems of air pollution occur due to soot and NO_x emissions. They cause issues such as acid rain and smog. By combining all the warming effects caused by aviation, it is responsible for 5-9% of the total anthropogenic warming of the earth [1, 5].

The desire to reduce fuel consumption does not only come from an environmental aspect. Aside from government agencies and people's ethics, there is a large financial motivation for it as well. Fuel costs are a major part in the running cost of aircraft, being 22% on average for large commercial aircraft [8]. In the end, a decreased fuel consumption is beneficial for almost everyone.

1.2. Historical improvements in aviation and future outlook

Figure 1.4 illustrates the effects of fuel reduction technologies over the past decades. It shows that from 1960 to 2010 the fuel consumption in terms of fuel per passenger kilometre is reduced by around 80%. Some 45% of this reduction is due to improvements in engine technology. The other 35% points are due to improvements in the airframe and more compact seating arrangements [9].

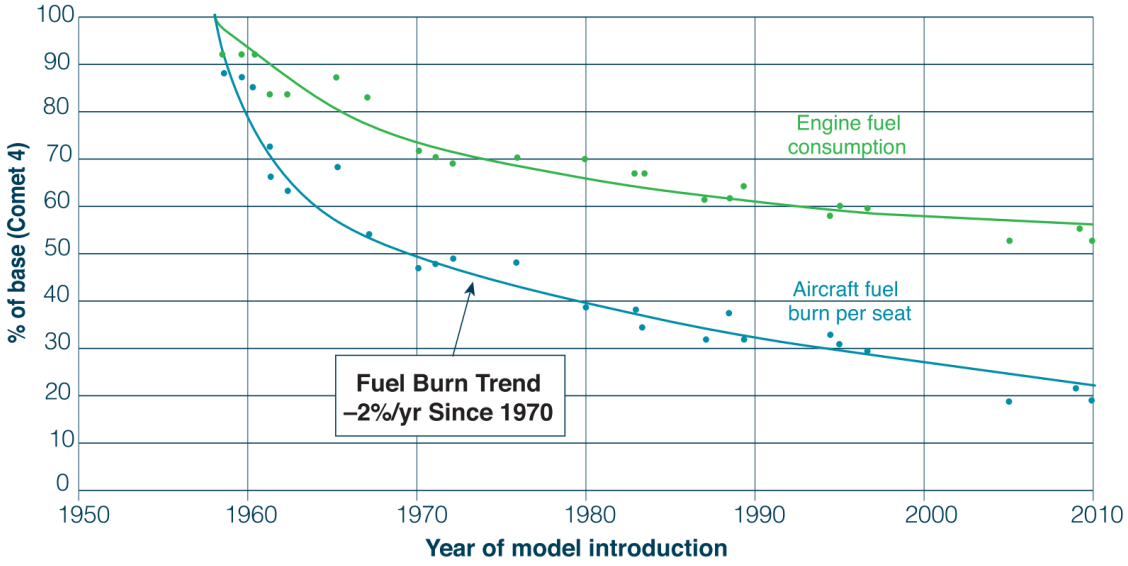

Figure 1.4: Aircraft efficiency improvements over the past decades [9]

In figure 1.4 it is also shown that the average yearly improvement in fuel burn per seat kilometer is around 2% since 1970. Improvements in tighter seating arrangements are hardly possible, and improvements in the current typical airframe of a wing and tube are also limited. On the engine side, historic improvements were made mainly in three aspects. These are: increasing overall pressure ratio (OPR), increasing the bypass ratio (BPR) and increasing the turbine inlet temperature (TIT). However, future improvements on these areas are limited. The thermal efficiency increase that came from the increasing OPR is flattening out, as is shown in figure 1.5. Increasing the TIT causes an exponential increase of the NO_x being created in the combustion chamber, as can be seen in figure 1.6. So by increasing the TIT, thrust specific fuel consumption (TSFC) can be reduced, but it will cause other environmental problems by increased NO_x polution. Besides that, TIT's are limited by the material properties of the components after the combustion chamber and cooling technology of those components. When increasing the BPR, other problems arise. As the diameter of the inlet increases to suck in more air, the fan size and nacelle increase as well. This causes the weight and drag to increase, counteracting the efficiency improvements [10]. Other problems with higher BPR's are the problem between the fan's high tip speed, and the low pressure turbine's (LPT's) relatively low circumferential speed, limiting their efficiency. Up until now, these improvements in the BPR have been made possible by going from turbojet (no bypass) to turbofan, and by increasing the amount of shafts from one, to two or even three on some Rolls-Royce engines. Currently only a few state-of-the-art turbofan engines are fitted with a gear between the low pressure (LP) shaft and the fan, one of them is the PW1000G series [11]. Such a turbofan is called a geared turbofan (GTF), and it allows the fan and LPT to turn at different speeds, improving the component's efficiencies.

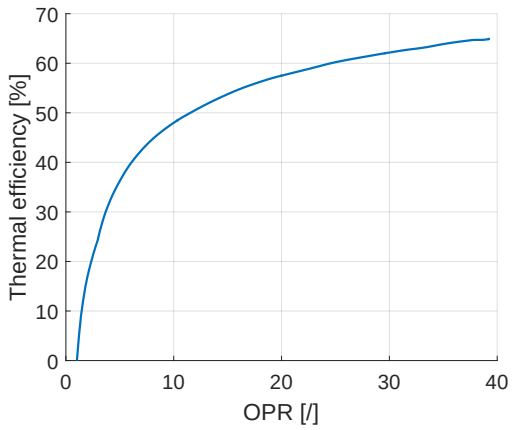

Figure 1.5: Flattening of thermal efficiency compared to OPR, adapted from [10]

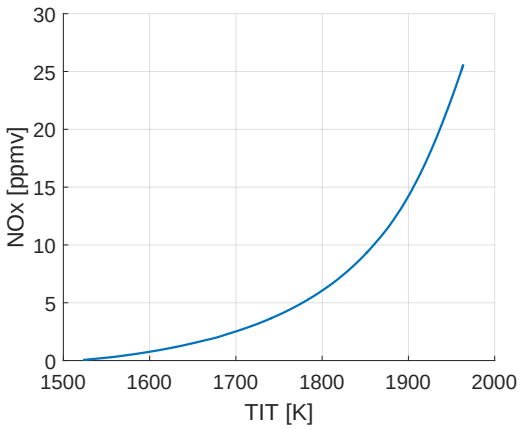

Figure 1.6: NOx creation at different temperatures, adapted from [12]

The aviation industry planned to reach its goal to half their emissions in 2050 with respect to 2005 by improving the fuel efficiency with 1.5% per year [6]. Taking into account the predicted growth of aviation from Airbus and Boeing, and subtracting the efficiency improvements, a yearly increase of 3% in terms of CO_2 emissions can be expected. This is close to the medium prediction from figure 1.3. Governing agencies in the European Union [13] and in the USA [14] have set goals to reduce the negative effects of aviation. The goals for 2050 set by the European Commission are to decrease NO_x emissions by 90%, the fuel consumption by 75% and the noise levels by 65% (compared to a typical new Aircraft in 2000) [13]. Clearly, there is a large gap between the goal of the aviation industry and governmental organisations, and its current direction.

1.3. State of the art in parallel hybrid electric propulsion

One of the promising future technologies to reduce the fuel consumption, hence, emissions of aviation, is hybrid electric propulsion (HEP). Multiple studies show HEP can reduce the fuel burn in regional to short haul flights by 7-10% with the envisaged 2030-2035 technology in comparison to a conventional propulsion system [15, 16]. Multiple types of HEP exist, a basic distinction can be made based on the way electric motor and gas turbine are coupled, parallel or in series. The different types are discussed in more detail in the next chapter, but the parallel type is expected the be introduced first [17]. A parallel configuration would require less modifications on the overall aircraft is therefore easier to implement. For this reason, the parallel type is considered in this study.

Multiple configurations for attaching an electric motor to the low pressure (LP) spool on a geared turbofan have been investigated in terms of efficiency and ease of installation [18]. The most promissing configurations are the ones where the electric motor is attached to the relatively fast spinning shaft of the low pressure compressor (LPC) and low pressure turbine (LPT). In terms of positioning, the cold end of the gas turbine, in front of the combustion chamber, is selected. A problem with the operation of compressors in an electrically assited turbofan (EATF) is a shift in operating point. This could put the compressor in less efficient operation, or into surge, as was also explained by another research [19]. In that study a solution was investigated to mechanically couple the two spools via a gearbox, to be able to deal with the added electrical power.

1.4. Problem description

Most of the previous studies into HEP have mainly been focusing on the overall feasibility of such a propulsion system, and on finding solutions for dealing with the effects of added power from an electrical motor on the shift in compressor and turbine operating characteristics. The approach in solving this problem so far has been to mechanically connect the two shaft via a gearbox [19]. Industrial gas turbines used to generate electricity also have high power off-takes, but these work only at one speed, to keep the electricity grid's frequency constant. The aero engine turbines on the other hand have to deal with a lot more speed and thrust variations. As shown in that study [19], the gas turbine might not only work less efficient in its operating points due to the power on- and off-take, but the compressor might also be put into surge or chocking conditions. This problem of shifting operating conditions, overall efficiency and safety will serve as starting point of this study. Primary goal of this study therefore is to investigate the specifics of these shifts in operating conditions due to the EATF and to design a parallel EATF configuration that operates safe and efficient during all operating conditions.

1.4.1. Research objective

The goal of this research is stated as follows:

The objective of this research is to find the operating limits of the combined hybrid-electric turbofan engine by modelling these two components and to find an optimized engine design in terms of specific fuel consumption for a fixed power split ratio.

To come to this final objective, the following research questions are defined:

- What are the operating limits of an electric motor?
- What are the operating limits of a gas turbine (turbofan)?
- How can the performance of various components be individually modelled?

- How should the electric motor and gas turbine be coupled?
- In what ways can the electric motor assist or replace other components?
- How to achieve the optimal cycle efficiency of a HEPS?
- What are the limits of the design space of electrically assisted turbofans?

1.4.2. Research methodology

To find answers to the research questions, the following methodology is used. The modular Gas Turbine Simulation Program, GSP® is used to build a gasturbine model [20]. GSP® is a component based modelling environment, which makes it flexible to model various gas turbine configurations. Furthermore, GSP® can be extended with MATLAB® via the Application Programming Interface (API), which provides the possibility for EAPS modelling [21]. The program is based on a 0-D thermodynamic model, making it very fast and suitable for conceptual study (for more information, see references [20, 22]).

From a baseline model of an existing turbofan, the characteristics of an electrically assisted turbofan are analysed with some basic information from a study on parallel hybrid electric propulsion [16]. The gas turbine will then be redesigned to achieve maximum efficiency during cruise. This is done because it is questioned whether a conventional turbofan is compromised in cruise efficiency due to the take-off thrust requirement. Although the maximum required take-off thrust will not change for the EATF because the same MTOW is considered, the gas turbine is assisted by electric power to achieve this thrust. With this new EATF, the total fuel consumption and electrical energy required are calculated and compared to a conventional engine.

1.5. Structure of the report

The following chapter, chapter 2 provides the background information, required to better understand the research in the later chapters. Chapter 3 covers the modelling of the baseline gas turbine together with the modelling of the flight mission, where after chapter 4 explains the modelling specific for the hybrid electric engine. The results are presented and discussed in chapter 5, from which the final conclusions and recommendations for future work are given in chapter 6 gives the final conclusions of this report together with recommendations for future work.

2

Background Information

To help the reader with a good understanding of the executed research, this chapter provides the necessary background information. It is divided between the working principles a a gas turbine in section 2.1, the working principles of an electric motor in section 2.2 followed by more information on hybrid electric propulsion in section 2.3.

2.1. Working principles of a gas turbine

Because of the relative low energy density of batteries compared to fossil fuels, the main propulsive devise in a HEPS will remain a gas turbine. This chapter will present the most important knowledge to understand its working principle and limitations. Gas turbines have been used for aircraft propulsion since they where introduced in the commercial aviation market in 1949 by the Comet. They have been enormously improved since that time in every aspect. SFC has been improved by 45%, noise has been reduced by 20 dB all while improving the thrust to weight ratio by a factor of 3.5 [23].

2.1.1. Fundamentals

In modern day commercial aviation a high BPR turbofan engine is the most common. Figure 2.1 shows a cross-sectional view of an high BPR engine [24]. It provides the most widely used nomenclature for numbering different stations in the engine.

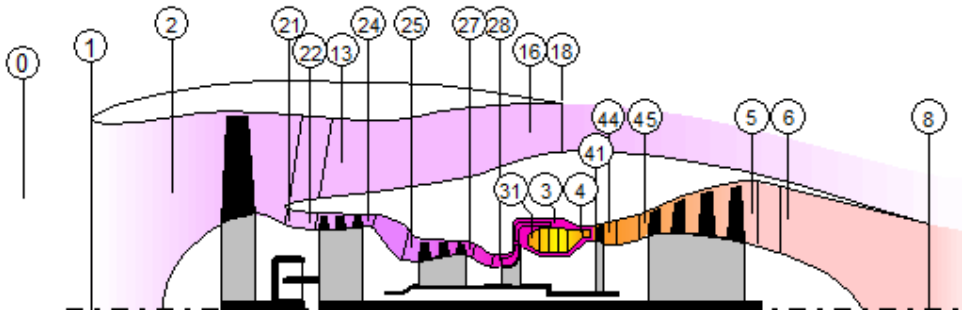

Figure 2.1: Lay-out and numbering of a twin spool turbofan engine [24]

A relative brief description of what happens in a turbofan engine:
The air in the far field free stream has number '0', when the air enters the inlet of the engine it passes through station '1'. At station '1' the total air mass flow of the engine can be defined. This differs from the combined (bypass and core) mass flow at the exhaust by the fuel mass flow. At

the end of the inlet just before the fan, station '2' is defined. The fan then gives a pressure ratio rise in the order of 1.5, after which it is defined as stage '21' for the core flow and '13' for the bypass flow. The largest part (90% and more in current engines) of the mass flow of this engine type flows through the bypass. The rest of the mass flow goes through the core of the engine. To explain the core flow better, a temperature-entropy (T-S) diagram of an ideal Brayton cycle is provided in figure 2.2.

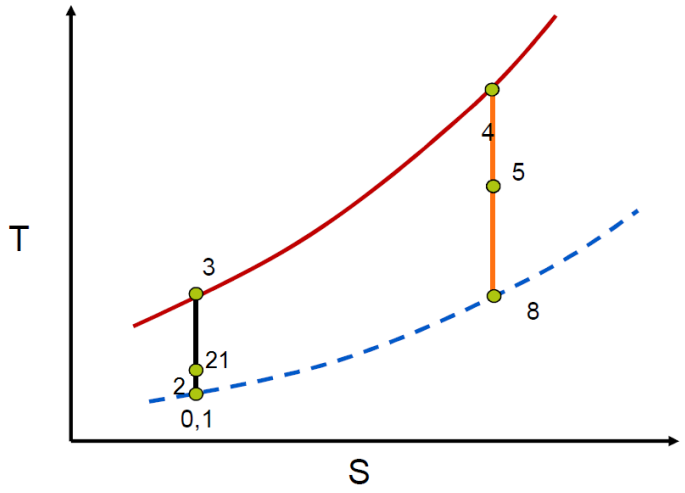

Figure 2.2: T-S diagram of an ideal Brayton cycle [23]

The figure shows that from point '0' and '1' to point '21' air is compressed, but the largest compression takes place from point '21' to point '3', which is down by the low pressure compressor (LPC) as well as the high pressure compressor (HPC). Point '3' is the exit of the HPC as well as entrance of the combustion chamber. From this point the fuel is added and combusted under constant pressure (ideal case), after which the end of the combustion chamber is reached at point '4'. Next the line between point '4' and '5' represents the power that is extracted by the turbine to drive the compressor(s). The line from point '5' to point '8' represent the power that provides the thrust, being it via the bypass, or the core exhaust. To have the highest propulsive efficiency, it is best to have a small amount of velocity increase for a large amount of mass flow. As most of the mass flow is going through the bypass, most thrust is created here. Beside the thrust due to this velocity increase, thrust can also be exerted by a pressure difference between the exit of the nozzle and the inlet. This will only happen in case the nozzle is chocked. The major differences between the ideal cycle shown in figure 2.2 and the real Brayton cycle are an increase in entropy during compression (from point '1' to '3'), a pressure loss during the combustion process (from '3' to '4') and an increase in entropy during expansion in the turbine ('4' to '8').

2.1.2. Operating limits and efficiency map

A real gas turbine is a complex machine, it has a lot of operating restrictions in different flight phases. One of the most convenient ways to show these restriction is by showing it together with the efficiency profile in a 'performance map'. Figure 2.3 shows such a map, with pressure ratio on the y-axis versus corrected mass flow rate on the x-axis. Corrected values are often used in describing the operation of the gas turbine and its components because the velocity triangles and Mach number are the same for when the corrected properties are the same. Therefore the behaviour of the components will be the same.

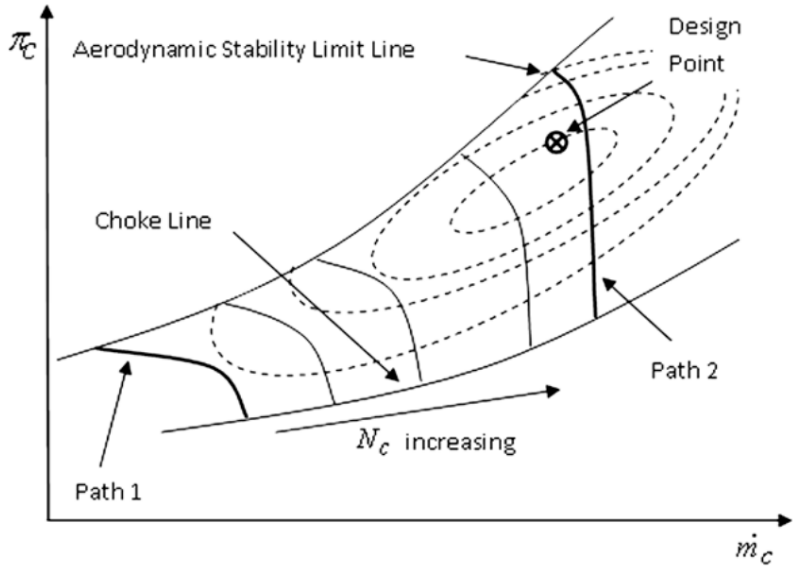

Figure 2.3: Axial compressor efficiency map with operating limits [25]

The figure does not show the complete engine, but only the compressor's efficiency and restrictions. Nonetheless, because the compressor is in most cases the restricting component, it is used as a starting point for the engine's limitations. The graph shows lines of constant rational speed (N_c), and the direction of increasing rotational speed. It furthermore shows lines of constant compressor efficiency with dotted ovals, and at the highest efficiency point also the design point is marked. For every constant rotational speed there is an upper, and a lower limit of pressure ratio. At the lower limit, the air speed reaches the speed of sound at some cross-section in between blades. This makes it impossible to increase the mass flow by decreasing the pressure ratio. On the upper limit, the mass flow is too low for this pressure ratio and rotational speed. It causes a large inflow angle on the rotor blades, which they cannot handle. The blades are now stalling as shown in figure 2.4. It shows that large inflow angles causes the blade to stall. There are several causes for the high inflow angle on the rotor blade. It can be caused by the relative low mass flow, which reduced the axial velocity of the air, or the rotational speed might be too high (especially at the first stages), also causing an inflow angle which is too high for the flow to remain attached on the rotor blade.

Possible ways to prevent stall in the compressor are also shown in figure 2.4. The normal design point of the compressor is presented in black. In case of start up of the engine or in idle, the mass flow rate is low. This is presented by the red velocity triangle. The peripheral velocity of the blade is lower compared to the design point, but the axial air velocity is reduced even more in comparison, causing the high inflow angle. For the operating scheme of a gas turbine, a safety measure in terms of 'surge margin' is used. This should make it impossible for the engine to approach compressor stall. Such a safety margin is required because surge can heavily damage or destroy the engine. Three possible ways to recover/prevent where shows in figure 2.4, which are now explained. In the early days of the gas turbine engine only one shaft was used, causing the first compressor stages to turn faster then ideal because the higher speed was required for the aft compressor stages. Implementing an additional spool would let the front stages turn slower. This way the peripheral speed of the rotor blade is lower and the inflow angle is acceptable, as shown by the green velocity triangle in figure 2.4. In newer engines, an other way to fix the stall problem is shown by the blue velocity triangle. In this case, variable

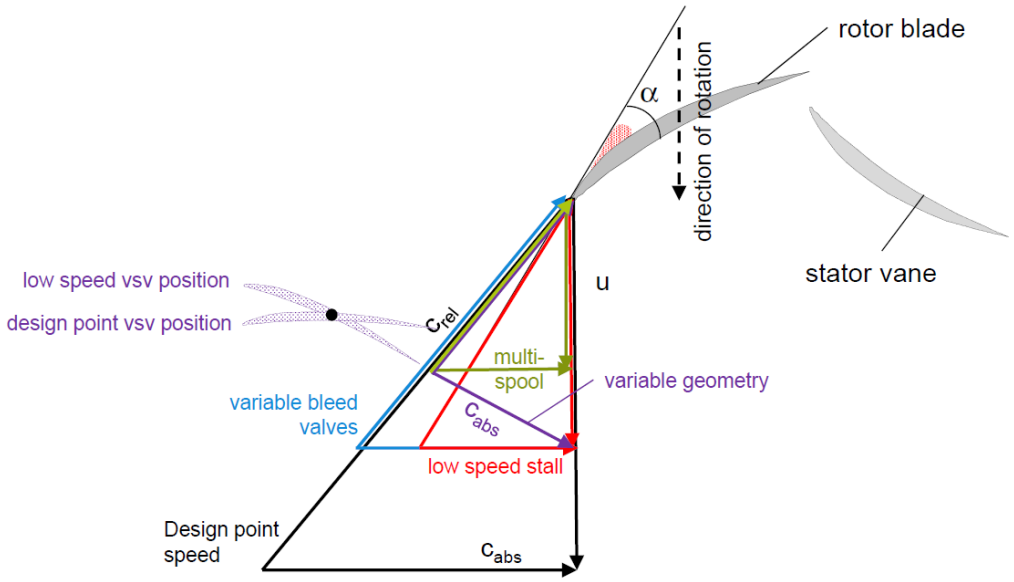

Figure 2.4: Compressor stall and measures to prevent it [26]

bleed valves are used. These bleed valves open up behind the stage in case of stall. Now the compressed air can easily flow out, creating an increase in mass flow through the compressor. This is seen as the increased axial velocity in the velocity triangle. A third way of preventing stall is with variable stator vanes (VSV's), might also be called variable inlet guide vanes (VIGV's) in the case these blades are in front of the first rotor row of the compressor. These VSV's and VIGV's are essentially a set of airfoils in front of a rotor. The angle under which these vanes are positioned can be changed, allowing to change the angle of the flow and with that also the inflow angle on the rotor blades. Positions of these VSV's are shown in purple in the figure, for both design point and low speed operation. The effect on the velocity triangle is also shown in purple.

Besides aerodynamic limitations the gas turbine has other limits. The temperature at the end of the combustion chamber/turbine inlet (stage '4' in figures 2.1 and 2.2) is limited due to material properties of the turbine blades. Depending on the engine, the temperature at the compressor exit (point '3') might also be limited. This temperature limit will be lower due to the fact that these compressor blades cannot be cooled, unlike the turbine blades [27]. An internal pressure limit is also present, especially important for modern day engines, as they can have pressure ratio's of up to 50. The center part of the engine, around the combustion chamber, must be capable of dealing with these stresses. Next, there is a speed limit at which shafts can spin. This limit comes from stresses inside the fan, compressor and turbine blades, but also the bearings of the spool and cooling of them approach their limits.

2.1.3. Design points

Aviation gas turbine engines are used under a wide variety of operating conditions. This requires that a proposed/designed engine is assessed under all of these different conditions. Figure 2.5 shows some of the most stringent operating conditions. It is important to bare all these conditions in mind, and realize that the engine cannot only be optimized to have minimal TSFC at cruise conditions. In case of an electrically assisted turbofan, the gas turbine constraints are slightly relieved in the take-off and climb parts. The electric motor is assisting the gas turbine in these phases, allowing the gas turbine to work closer to its cruise design point.

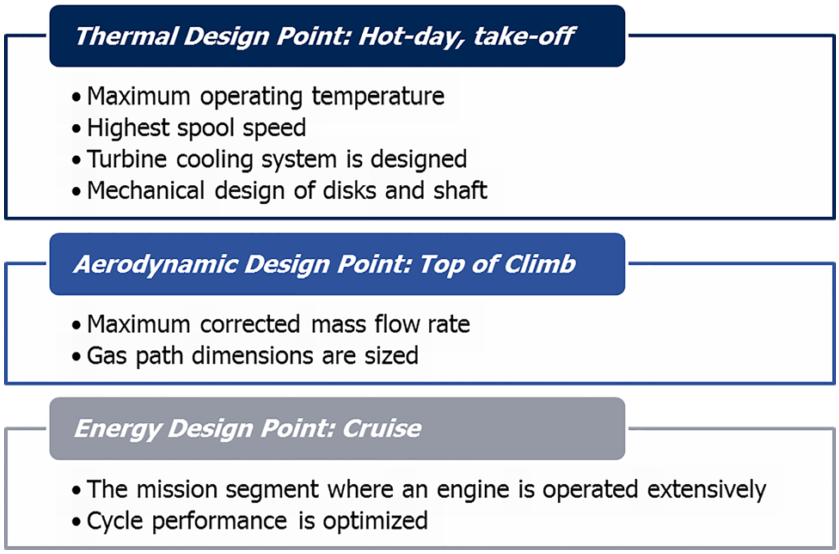

Figure 2.5: Engine design conditions [28]

2.1.4. State of the art in aircraft propulsion

As said in the previous section, the ways how improvements in aero engines have been accomplished in the past are fading out. To meet the goals set by the European Commission and NASA more drastic measures need to be taken. Several possible future concepts will now be discussed.

Open rotor

To partly mitigate the problems of higher BPR engines, the open rotor concept is made. In figure 2.6, a counter-rotating open rotor concept is shown. The open rotor design makes it possible to have a higher BPR without increasing the nacelle drag and weight as much. This is due to the fact that the nacelle is no longer around the main fan, but only around the engine core. Nonetheless, a study from NASA showed that an open rotor is still expected to be 50% heavier than a comparable (in terms of thrust) turbofan engine [29]. As weight is a key factor in aerospace, this seems like a major problem. Although, when taking into account the predicted 36% decreased fuel consumption (with respect to 1990 engines), the required fuel for a mission might be so much lower, the take-off weight of the aircraft might be reduced [29]. Weight problems are therefore depending on the aircraft's mission, long distance flights save more fuel in absolute terms, possibly offsetting the weight increase of the gas turbine. Other roblems that are present, no matter the mission, are in terms of noise, as was found by a another study [30]. With modern day turbofan engines, a large part of the noise comes from the fan. Normally this fan is surrounded by a nacelle that absorbs a large part of the noise, so the noise created by the fan is less noticeable. The whole idea of the open rotor is however, that there is no nacelle around the large fan, and the noise levels will therefore be higher. Additional drawbacks are mentioned in a report from 2015 [31]. In traditional turbofan engines, the nacelles also serve as blade containment barrier in case one of the blades would break off. A possible, but also heavy option to mitigate this, is to strengthen the fuselage and wing for such impact. The absence of a nacelle around the fan also means that at high speeds, the efficiency drastically reduces, meaning that the aircraft would only achieve its higher efficiency at lower flight speeds compared to standard turbofans. A lower flight speed means a longer flight duration. More problems arise with respect to the placement of the open rotor motor, as they will most likely get too big to

place under the wing (which is currently the most used location). This means that also the aircraft will need to be redesigned, enlarging the costs for company's to design and build an open rotor aircraft. An under wing placement is beneficial for airlines as well, because the maintenance is relatively fast and cheap. A different placement (above the wing or aft-mounted) would increase the operating costs for them.

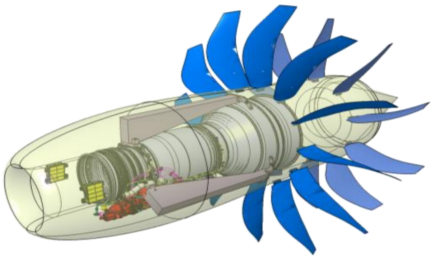

Figure 2.6: Open rotor concept [32]

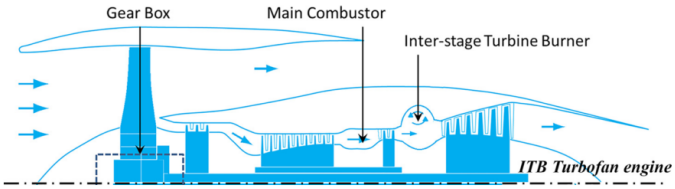

Figure 2.7: Layout of a turbofan with ITB [28]

Interstage turbine burner

A different concept for possible future use is the interstage turbine burner (ITB) turbofan engine. This concept uses, as the name suggest, a second combustion chamber in between the high pressure turbine (HPT) and LPT, as shown in figure 2.7. By doing so, a lower TIT is possible for a given thrust setting. This helps to reduce the NO_x emissions as well as it improves the life of the components. The downside of an ITB is that the part of the fuel is burned at a lower pressure. Efficiency of a cycle decreases when fuel is burned at lower pressures and therefore the TSFC will be higher when in the same engine all fuel would have been burned in the main combustion chamber. However, when taking into account expected future technology, such as a higher OPR and a larger bypass ratio, a reduction in both SFC and NO_x can be realized [28]. Having two combustion chambers makes it possible to have different fuels in each of them. One has the option to, for instance, use liquid hydrogen in the main combustion chamber, and kerosene in the ITB. Hydrogen has the advantage of a higher energy per unit of mass compared to kerosene, as well as no formation of CO_2 when it is burned. A downside to hydrogen is the large volume required per unit of energy. Even in liquid form, it requires about three times the volume of kerosene. A combination of hydrogen and kerosene was therefore used in a study into multi-fuel interstage turbine burner. It was found that with an 88% energy fraction of hydrogen, CO_2 could be reduced by 87% [33]. This result is for comparing an engine with set BPR, OPR and components efficiency and therefore purely comparing kerosene only in the main combustion chamber against a combination of two fuels with the ITB.

Distributed propulsion

Distributed propulsion is also a way to improve future aircraft. Often distributed propulsion is combined with boundary layer ingestion (BLI). A similarity between the distributed propulsion and BLI is that they both decrease mixing losses, and thereby improves performance. With distributed propulsion, this decrease comes from the fact the thrust is created by accelerating a large amount of air, by only a small amount, so there are no large velocity differences. With BLI the slow moving air in the boundary layer is accelerated so there are less losses in the wake. BLI alone is said to have a fuel saving of around 10% [34, 35]. A larger amount of air around the aircraft can be accelerated by using more fans/propellers than what is normally done on aircraft (which rarely have more than 4 fans/propellers). This is possible with conventional turbofan/turbojet/turboprop engines, but these engines are expensive. Additionally, larger engines are more efficient than smaller ones. Putting a lot of small engines together therefore has

downsides. It is possible to have for instance two large turbofan engines, which mechanically transfer power to additional fans, but such systems are complex and heavy. Electric motors come in handy here. Power transfer is easy and these compact motors can be positioned almost anywhere. A propulsion system as such is called a hybrid electric propulsion system or HEPS for short, and is explained further in the next subsection.

Hybrid electric propulsion

With hybrid electric propulsion, the propulsion is (similar to a hybrid car) a combination of conventional propulsion and electric propulsion. Dozens of studies have already been performed into the topic. A study called SUGAR (Subsonic Ultra Green Aircraft Research) [36] was done to find the most promising concepts for the future to reduce fuel consumption and emissions on medium range missions. In phase 1 of that research, several different airframe concepts were studied. Amongst others, a conventional, a hybrid wing body and several different propulsion systems. A very promising outcome of this research is the SUGAR Volt aircraft, shown in figure 2.8. The airframe used is very similar to the conventional layout, but the wings are placed above the fuselage and support struts are added. For propulsion, a hybrid electric system is used. Expected fuel savings go beyond 70% compared to 2005 best in class aircraft. Similar studies were also performed on aircraft for long ranges. By combining several studies, the N3-X concept was created and is shown in figure 2.9) [37]. By using a hybrid wing body and distributed hybrid electric propulsion with BLI, a fuel burn reduction of 72% compared to the B777-200LR (year 2005) is expected. For power generation, two turbogenerators are used, one on each wingtip. The electricity created by these generators is transferred to 15 electric motors attached to the top aft part of the fuselage, as shown in the figure. Major challenges that need to be overcome to make HEPS possible all have to do with energy and power density of the electric motor and the battery. Kerosene has a energy density that is about 50 times higher than today's (2018's) batteries. Although the energy density of batteries has been improving over the past decades, and is expected to also do so in the future, the added weight is a real problem for the aircraft. Other challenges are cooling problems in the electrical components, as they need to have the highest power density possible and also be compact. In section 2.3, HEP is explained in more detail.

Figure 2.8: SUGAR Volt concept [38]

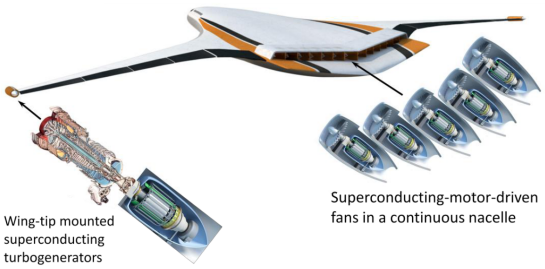

Figure 2.9: N3-X concept [37]

2.2. Working principles of an electric motor

This section is aimed to give a better understanding of the electric motor, which is required to understand the practical limitations and considerations for the following master thesis.

2.2.1. Types of electric motors

One can basically divide all electrical motors into two groups: direct current (DC) and alternating current (AC) motors. This classification follows from the type of electric power supply to the motor. A further division of the types of motors is shown in figure 2.10. The different motors vary in the power density (kW/kg), efficiency, starting torque, requirement of an electrical drive and several other factors.

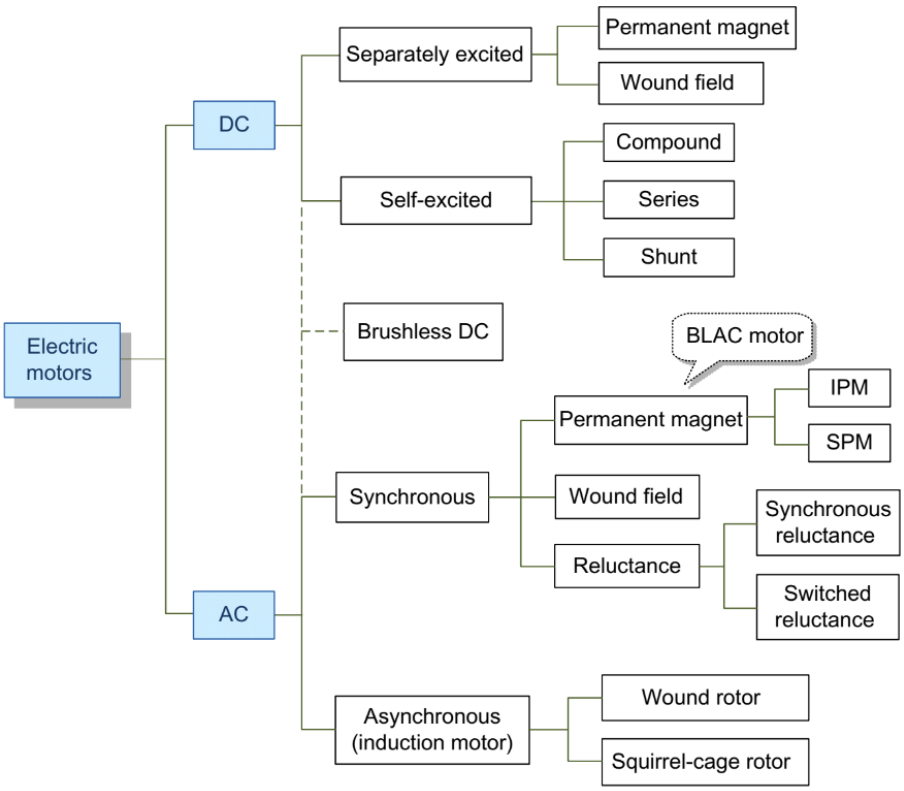

Figure 2.10: Electric motor classification [39]

2.2.2. Fundamentals

The general workings of all electric motor types are pretty similar, figure 2.11 shows several types. An electric motor can be divided into two parts, there is a stator (which does not move) on the outside part of the motor, and a rotor (that rotates) on the inside. This rotating motion is created by two magnetic fields of which one is in the rotor and the other in the stator. Type A of the figure shows that a DC-motor (generally) has one standing magnetic field created by permanent magnets, and a rotating magnetic field in the rotor imposed by a current running through different windings. In type B an AC synchronous motor is shown, the stator and rotor configuration is the same as type A, but flipped. Now there are permanent magnets on the rotor, and the stator has a magnetic field created by current flowing through windings. As a results of the AC current through the rotor windings, both magnetic fields are rotating. Because the rotational speed of the rotor and rotating frequency of the magnetic field in the stator are equal, it is called synchronous. Lastly motor C shows an asynchronous AC induction motor, which also has two rotating magnetic fields, but are in this case both created by current flowing through the windings on the stator and rotor. It is called asynchronous as the rotational speed of the rotor is lower than the speed at which the magnetic field of the stator rotates.

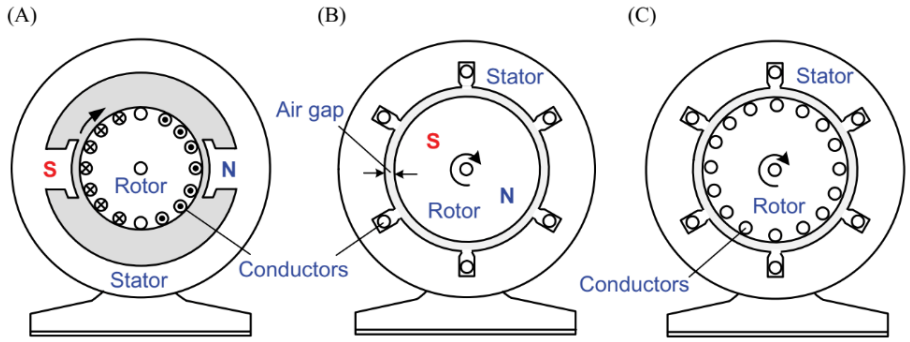

Figure 2.11: Workings of different types of electric motors [39]

As stated before, these are only three of the motor types shown in figure 2.10. A permanent magnet electric motor can already be divided into three types, as shown in figure 2.10. There are: interior permanent magnet (IPM) motor, surface permanent magnet (SPM) motor, or brushless AC (BLAC). The first two (IPM and SPM) are only different in the way the permanent magnet is positioned inside the rotor. In motor type B from figure 2.11, the magnets are placed inside the rotor, so it can be either an IPM or SPM. The physical workings of these two types are therefore exactly the same. Type A from figure 2.10, a BLAC, is somewhat different. Here the permanent magnets are placed in the stator instead of the rotor [40]. Beside the differences, all electric motors have in common that the force to rotate the rotor relative to the stator is created by the two magnetic fields. The strength of these magnetic fields determine the force (and with it torque) with which the motor can rotate.

Besides the method with which the two magnetic fields are formed, there are differences in electric motor topologies. The topology used in all three sketches of figure 2.11, is radial flux. An axial flux motor has the magnetic forces between the stator and rotor working in the same direction as its axis of rotation, as is shown in figure 2.12.

2.2.3. Operating limits and efficiency map

Similar to the gas turbine, an electric motor has operating limits. The most important ones are:

- maximum temperature
- maximum torque
- maximum speed
- maximum power

In a permanent magnet AC motor the temperature is mainly limited, because of the permanent magnets' properties. These magnets lose their magnetic properties at higher temperatures. The temperature limitation becomes even more stringent during high power operation in thin air, at higher altitudes due to a lack of cooling [42]. The torque, speed and power limits are also shown in figure 2.13 where also the generic efficiency of the motor is shown. At lower speed ranges, the motor is limited by its maximum torque. This can be seen by the torque remaining at a value of 1 for increasing speed. When the speed is increased, the maximum torque will go down because of the power limitation (the power scales with torque times speed). If the speed keeps increasing, there is a sudden drop in the torque that can be applied, as the maximum speed of the motor is reached (pointed out as max torque at max speed). Maximum efficiency contour is located at relatively high speed with low torque in this figure, but that will depend on the type of electric motor and its specific design.

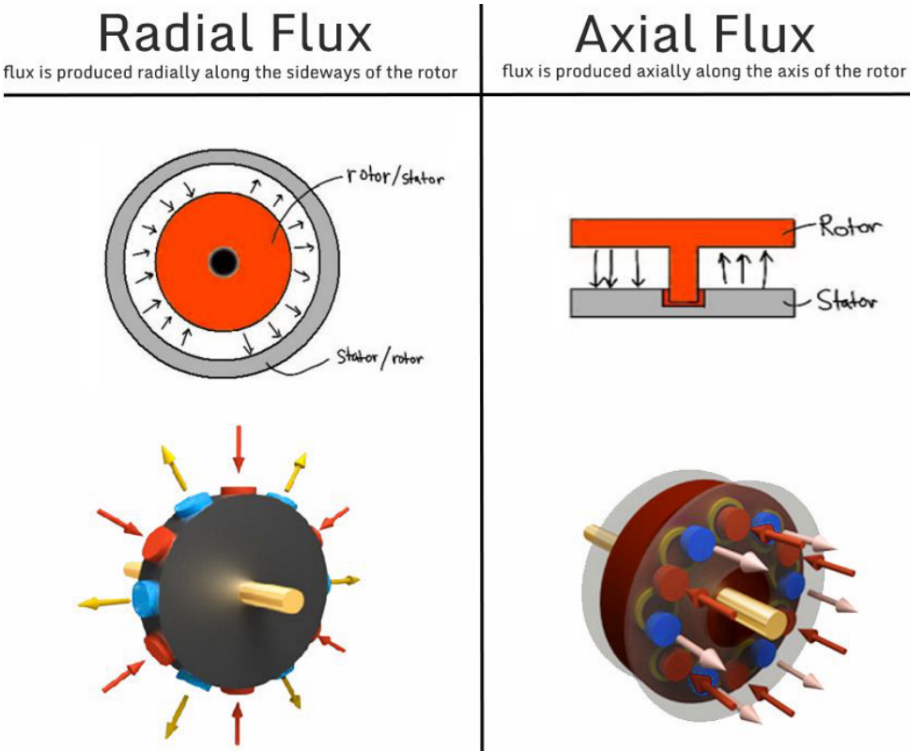

Figure 2.12: Radial vs Axial Flux Electric Motor [41]

2.2.4. State of the art electric motors

A lot of research is going on and has already been done on high performance electric motors. Some of the most relevant studies are discussed below.

Current electric motors in aircraft propulsion

A key factor for any aircraft is weight. Electric motors used to have far lower power densities than gas turbines had, but that difference is disappearing and can even flip in favour of electric motors. One very important factor in the ability to have a high power density and therefore lightweight machine is to make it efficient. When only a small amount of heat is generated, the electric motor is easier to cool and can be made smaller. Siemens' SP260D is one of the most efficienct and power dens electric motors in 2019. It achieves a maximum efficiency of 95% with a power density of 5.2 kW/kg for a 260 kW permanent magnet motor [44]. This motor powers the Extra 330LE electric aircraft from Siemens, called the Extra 330LE. It shows that with the state-of-the-art technology, electric aircraft are possible, but range is limited with only 20 minutes of flight time.

Electric motors research

Because of the before mentioned importance of efficiency and weight, superconductivity would allow for a big improvement in performance. It is estimated it would be possible to have 25-40 kW/kg electric motors, together with an efficiency of 98-99% [45]. Such a large increase comes from superconductivity of metals at very low temperatures. Almost no losses are present in this state, meaning only a small amount of heat is generated. Although additional systems are required to cool the metal to these temperatures by means of cryocoolers, it could still provide major improvements in the far future. Unfortunately the technology for this has not yet matured, and is to be expected in around 10-20 years [45].

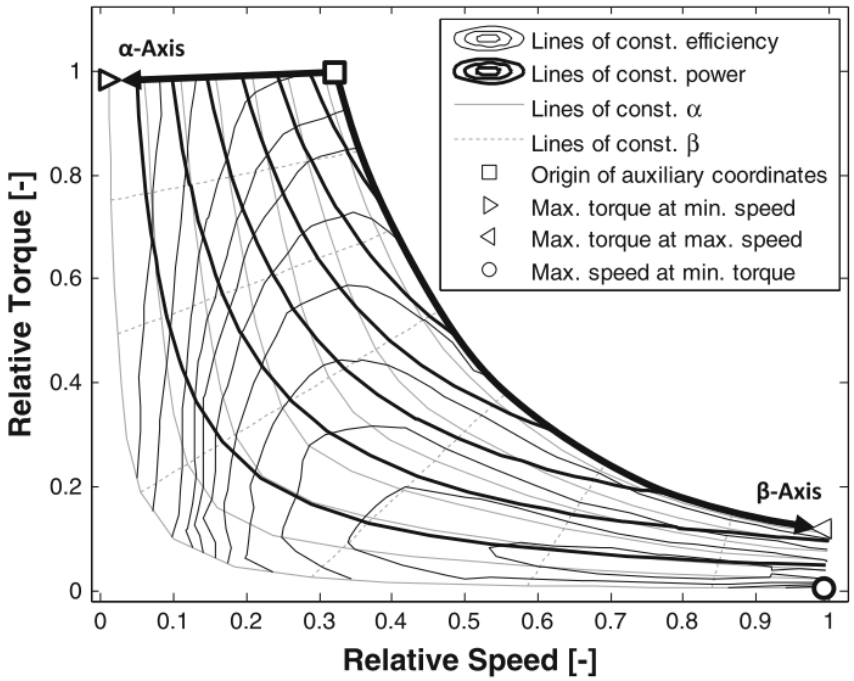

Figure 2.13: Generic performance map of an electric motor including operating limits [43]

Electric motors in hybrid electric aircraft propulsion research

Several studies that have been performed into HEPS, have also designed the electric motor and position to some extend. The SUGAR study came up with the concept of their so called 'hfan' [36]. It was the gas turbine engine that was used in their SUGAR Volt aircraft concept. Figure 2.14 shows the layout of this engine. At the right side of the figure, a switched reluctance motor is positioned. Normally a tail cone is positioned here, as can be seen the layout of a gas turbine in figure 2.1, which has empty space inside. The rest of the gas turbine layout can therefore largely remain the same.

In a different study, specifically focused on designing an electric motor for this application in the tail cone of a turbofan, several designs were made of the switched reluctance motor [46]. The study took into account a maximum outer diameter, so that the electric motor fits inside the same dimensions as where the cone would normally be, and a minimum internal diameter was used so that the low pressure shaft is attached to the electric motor. Phase 2 of the SUGAR study went deeper into the overall design of the engine scaling of the SUGAR Volt [47]. It was found that optimum fan size and pressure ratio remain the same for conventional gas turbine and a HEPS. This means that one can design an aircraft's engine without HEP and later on make an updated version without requiring changes in fan diameter, which translates to nacelle and possibly engine ground clearance and landing gear, saving a lot of time and money for re-design.

Back to the placing of the electric motor in the SUGAR study, the placement of the electric motor was in the aft part of the gas turbine. A downside to this placement is the high temperature. Placing it more in front, especially in front of the combustion chamber, allows a much lower operating temperature. This grants access to the use of permanent magnet synchronous motors. These motors are expected to outperform switched reluctance motors and others in terms of efficiency and power density [48, 49]. It makes therefore most sense to try and incorporate

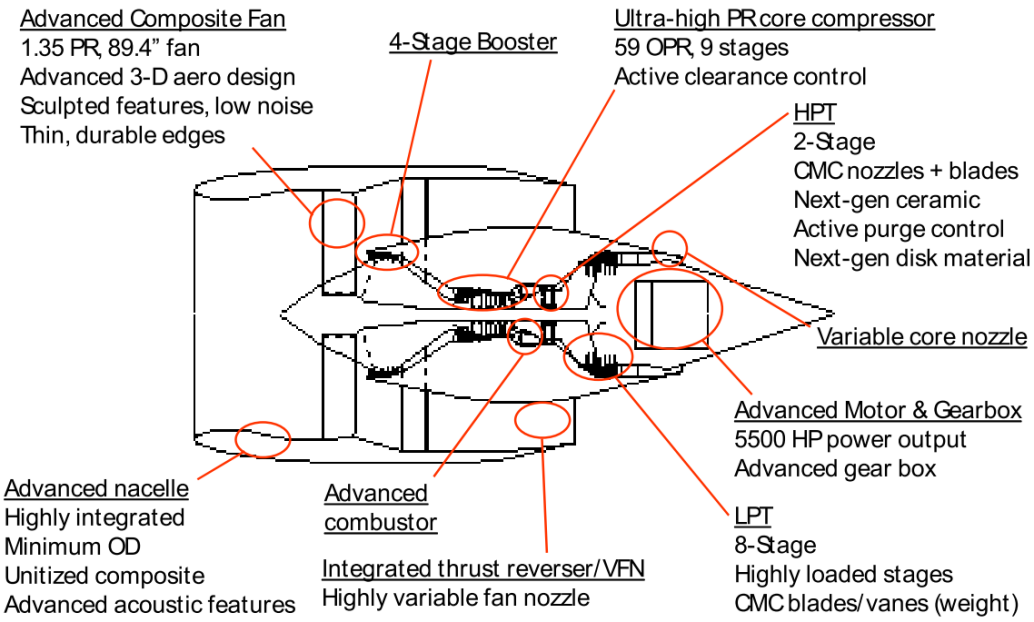

Figure 2.14: Layout of the SUGAR hfan gas turbine [36]

these motors, if temperature allows.

2.3. Hybrid electric propulsion

Studies into HEP have been growing exponentially lately, especially after the automotive industry showed that hybrid electric systems can reduce fuel consumption in cars, and NASA showed their aircraft and propulsion concepts for drastic fuel consumption reductions. This section explains the basics behind HEP, what the advantages are, as well as the downsides.

2.3.1. Types of hybrid electric propulsion

The general idea of HEP is that besides turbofan/turboprop engines also an electric motor and a battery are present in the propulsion system of the aircraft. Multiple configurations are possible to connect these components, figures 2.15 and 2.16 show the two basic configurations possible. In the parallel HEPS, from figure 2.15, the basic idea is that a turbofan or turboprop engine is assisted by an electric motor to drive the shaft. Such a configuration is called parallel as the electric motor and combustion engine can provide shaft power side-by-side. Figure 2.16 shows the series configuration. Here the combustion engine and electric motor are put after one another (in series). Power is first created in a combustion engine, and then converted into electrical power by a generator. A power converter then directs where the power needs to go to, to or from the battery and to or from the electric motor, or it may also be a combination of both. In any way, only the electric motor is connected to the fan/propeller.

Series HEP is expected to be heavier, as it consists of more components. Compared to the parallel configuration, the electric motors need to be able to supply 100% of the shaft power for propulsion. The combustion engine needs to supply a large part of the power in the take-off and climb phase, while a generator still needs to convert it to electrical power. An advantage of this, is that the decoupling of the combustion engine from the propeller/fan allows it to operate at its peak efficiency [51]. A small comparison is made in table 2.1. In the table, conventional propulsion is taken as baseline, to which parallel and series HEP are compared. The term conventionality stands for how much redesign is required of the aircraft for that propulsion type.

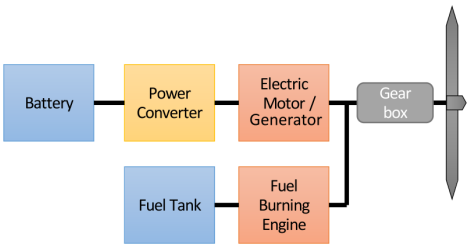

Figure 2.15: Parallel HEPS [50]

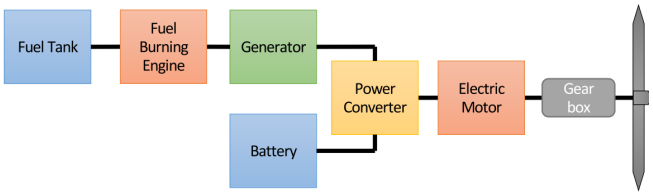

Figure 2.16: Series HEPS [50]

From this table it becomes clear that an upfront decision for choosing one configuration over the other is difficult to make. Depending on the exact integration of these two configurations and the mission of the aircraft, either one can be preferable over the other.

Table 2.1: Comparison of parallel and series HEPS against conventional propulsion

Propulsion:	Conventional	Parallel HEPS	Series HEPS
Weight:	0	-	- -
Efficiency:	0	+	+ +
Conventionality:	0	-	- -

Combinations of parallel and series are also possible. By doing so one can make use of (part of) the benefits of each system. An example is to combine tip mounted propellers to the SUGAR Volt, which uses a parallel HEPS. On the wingtip, an electric motor can than be mounted which uses power from the gas turbine. However, because of additional complexity of these systems, they are not treated in more depth in this study.

2.3.2. Benefits of HEP and its dependence on technology

Beside fuel and emissions savings, HEP has a lot more benefits to offer. It enables the aircraft to taxi electrically, greatly reducing the local air quality around airports. Taxiing electrically also is almost silent as the gas turbine is not running, something also set as a goal by the EU [13]. Furthermore, the aircraft produces less noise during take-off, as a smaller amount of power is provided by the gas turbine. Some airports are limited by the created noise of aircraft, so more take-offs and landings can take place if the noise per aircraft is reduced [16, 52]. HEP makes it also possible to partly use energy from other (renewable) sources than fossil fuel, reducing its dependency on fossil fuels as well as its price fluctuations.

Expected fuel savings and emission reductions heavily depend on the gravimetric energy density of the batteries. Figure 2.17 shows how the battery mass changes for a certain power split ratio, with different energy densities of the battery. The lower limit used in this figure, 750 Wh/kg, is already quite high. The study from which this graph came, used an ATR-72 as reference airplane. It is a regional turboprop aircraft with a range of around 1500 km. In the reference case, the aircraft needs 2000 kg of fuel for this mission, but as seen in the figure, a battery mass of 2000 kg is required when a constant power split of 20% is used over the entire mission. Required fuel for this mission will go down in this case with around 250 kg, but this clearly does not offset the 2000 kg of additional battery mass [53]. Luckily, battery technology is improving rapidly. Figure 2.18 shows how the energy density of batteries have been increasing over the past decades. From 2010 onward, the technology showed another step forward, as there are currently battery cells available with capacities of 240-250 Wh/kg [54, 55]. Although such energy density is good enough for hybrid and fully electric cars, regional and short range

commercial aircraft will require more energy per kg battery. In comparison, Jet A1 fuel has an energy density (lower heating value) of 43 MJ/kg or 12 kWh/kg. The battery cell energy density is however not the actual usable energy density, because cooling, heating and battery management systems come on top of it. In the Tesla Model 3, this reduces the cell energy density of 250 Wh/kg to a system energy density of around 160 Wh/kg [55]. Very promising research is going on with other types of batteries than today's standard Lithium-Ion batteries, showing very promissing energy densities. In one research was capable of building an aluminium-air battery in a lab with a energy density of 2552 Wh/kg [56]. These technologies are however still far away, as energy density expectations for the year 2030-2035 often range from 500-1000 Wh/kg. The efficiency of a battery depends in reality on the state of charge and the rate of charge or discharge. However, often it is averaged out for simplicity, in which case batteries can be expected to have efficiencies of 98.2% and 97.6% for charge and discharge respectively [43].

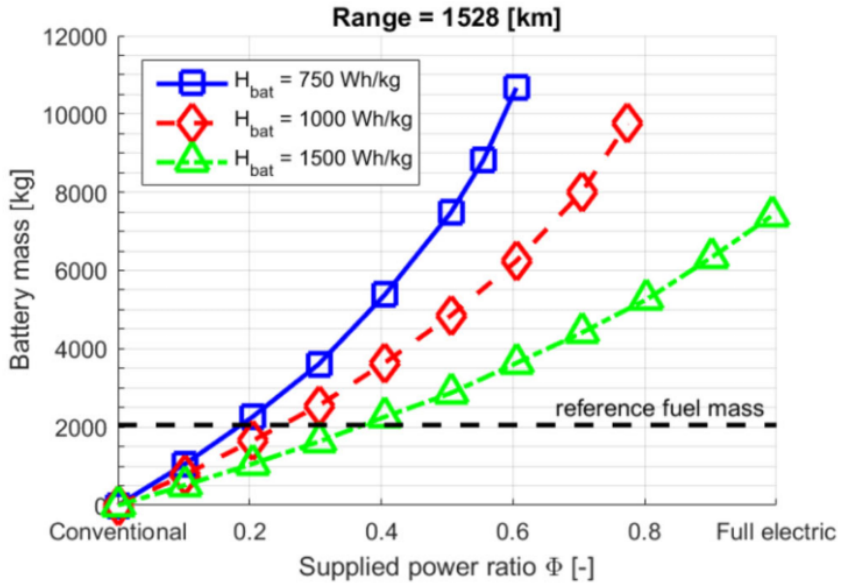

Figure 2.17: Importance of energy density for HEPS [53]

Together with the electric motor, gas turbine and battery, the inverter forms the basic components of a HEPS. Therefore its efficiency and weight are important for the overall feasibility and performance of a HEPS. An inverter is responsible to convert the DC-power from the batteries to AC-power for the electric motor. With today's technology, inverters can be made to transform around 14 kW/kg with an efficiency of 98.9% [58]. Future expectations are even higher, where values of 23 kW/kg and efficiencies of 99.5% are expected [59, 60].

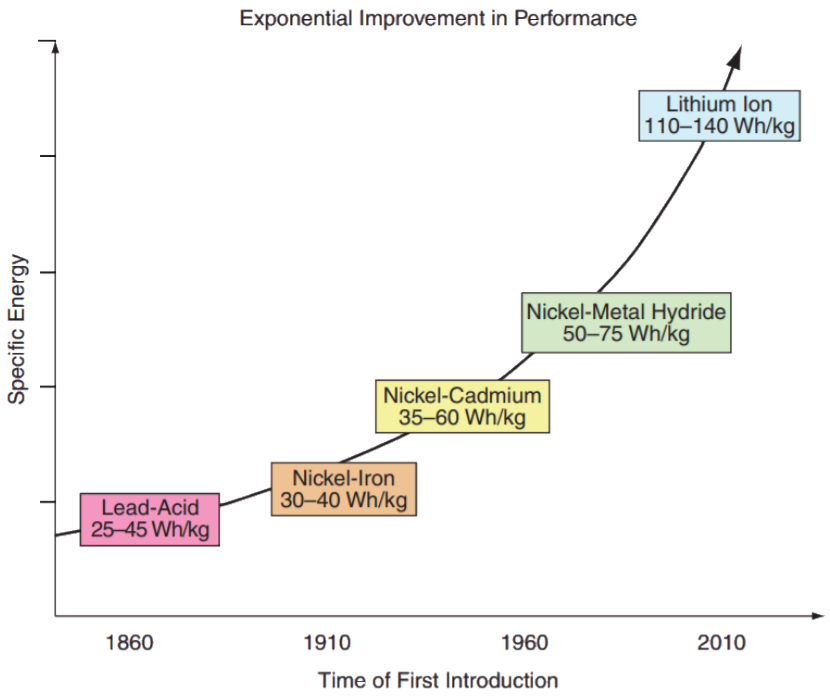

Figure 2.18: Specific energy density of batteries over the years [57]

3

Baseline Engine and Aircraft

To be able to calculate possible fuel savings, first a reference or baseline model needs to be created. This chapter covers the selection of a reference aircraft and the build-up of the baseline gas turbine.

3.1. Reference aircraft selection

As reference aircraft the Airbus A320neo is selected. From figure 3.1, it can be seen that the largest amount of available seat kilometers (ASK) are with narrowbody jet aircraft in the range of 1000-2000 km. If one is therefore able reduce the fuel burn on these mission with such an aircraft, a large amount of fuel can be saved and emissions reduced. The Airbus A320 and Boeing 737 are the largest competitors in this market, from which the Airbus is selected. This type of aircraft has also been examined before, and shows possibilities in terms of fuel reduction with HEP [16, 36].

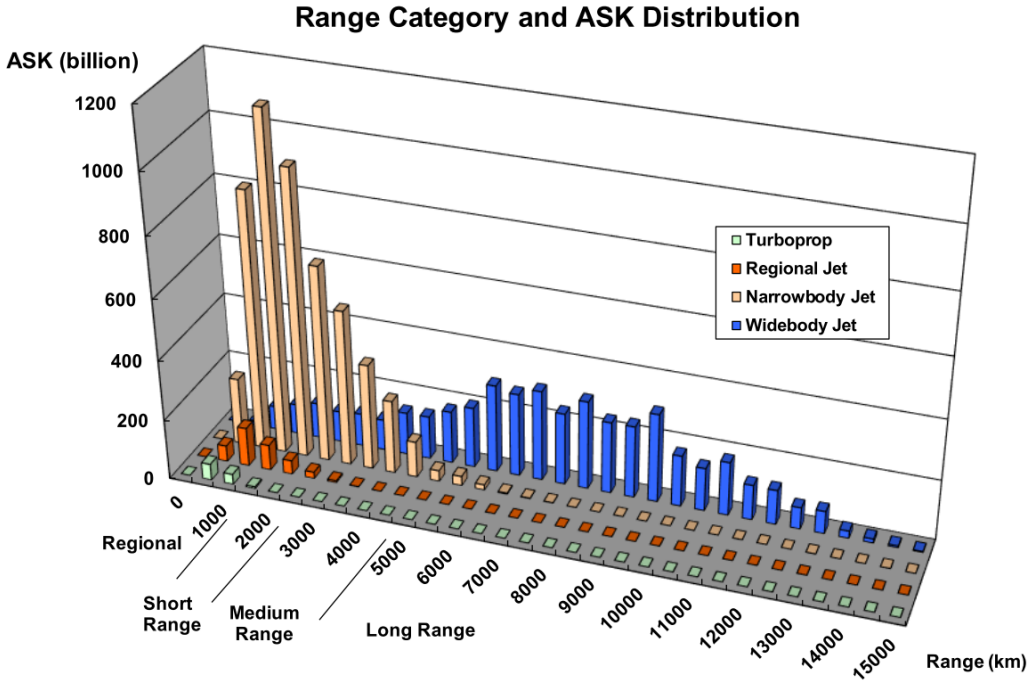

Figure 3.1: ASK grouped to mission length and aircraft category in 2017 [61]

3.2. Airbus A320neo main specifications and requirements

Some of the main parameters of the A320neo are gathered in table 3.1 below.

Table 3.1: Main Airbus A320neo Specifications

Parameter	Value	Unit	Source
Weights			
MTOW	73500	[kg]	[62]
OEW	44400	[kg]	[62]
Max Payload	18400	[kg]	[62]
Max zero-fuel weight	62800	[kg]	[62]
Maximum landing weight	66300	[kg]	[62]
Cruise			
Cruise Mach number	0.78	[-]	[63]
Cruise Altitude	11280	[m]	[63]
Cruise L/D ratio	16.8	[-]	[64]

An aircraft has all kinds of subsystems, which require electric and/or pneumatic power. This power is provided by the gas turbines on the aircraft and thus affects its fuel consumption. On a flight from Hamburg to Toulouse, the electrical and pneumatic power requirements of an Airbus A320 where shared by reference [65]. The data provided does not include taxi power requirements, but it is assumed to be similar to the approach flight segment, since both are around sea level and at relative low thrust requirements. A different engine was used on this A320 flight, the V2500 from International Aero Engines, than this study uses as baseline. However, since the power requirements mainly depend upon the aircraft, and the A320 and A320neo have a high similarity, the same power requirements are used in this study for the A320neo. Table 3.2 shows the bleed-off and power requirements per flight segments that is used.

Table 3.2: Bleed and shaft power requirements per engine [65]

Mission segment	Electric power requirement [kW]	Fan bleed air requirement [kg/s]	HPC bleed air requirement [kg/s]
Taxi	68.6	0.453	0.453
Take-off	73.8	0.463	0.579
Climb	83.5	0.308	0.710
Cruise	79.0	0.186	0.481
Descent	68.6	0.332	0.429
Approach	68.6	0.453	0.453

3.3. Gas turbine

The gas turbine is the main focus of this study, this section will explain both the modelling procedure for it, and the requirements from it in the baseline model. An A320neo has two engine series as options, the PW1100G and the LEAP-1A, each with multiple variants. The LEAP-1A26 series is selected as reference engine for this research, because more date was available.

3.3.1. Gas turbine modelling program

As said before in section 1.4.2, GSP is used as program to model the gas turbine. Figure 3.2 shows the layout of a LEAP engine model that has been built in GSP. It shows the bleed control schedule with number 1, which contains a schedule for the LPC bleed-off at low N1 speeds to

prevent surge. Then all the standard gas turbine components, which are numbered from 2 up to 13. First, there is an inlet (number 2), followed by a fan (number 3) with the bypass and core exits. The fan core exit is followed by the LPC (number 4) and the HPC (number 5). Number 6 is the control for component number 7, the combustion chamber (CC). This is followed by two turbines, the HPT (number 8) and LPT (number 9). Then, aft of both the fan bypass and LPT, a duct (number 10 and 12) and an exhaust (numbers 11 and 13) are present.

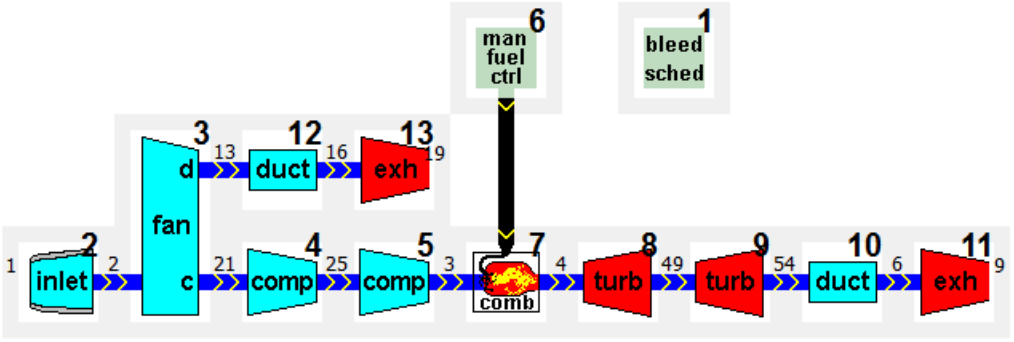

Figure 3.2: Two spool turbofan model in GSP

The performance simulation follows a sequential procedure starting from a reference point (cruise condition in the current paper) and followed by off-design performance calculation at other operating conditions. The calculation at the reference point follows a standard thermodynamic procedure [27]. More information on the workings of GSP can be found in references [20, 22].

3.3.2. Thrust requirements

An aircraft is required to be able to take-off within a certain maximum distance and to climb with a specific speed, also with MTOW. To achieve this, the gas turbine has thrust requirements at these points. At take-off, the maximum rated thrust of the selected engine is 120.6 kN at sea level static (SLS) conditions [66]. Initial cruise thrust is calculated by assuming that the amount the of fuel burnt during take-off and climb is insignificant to the MTOW, so the MTOW is divided by the cruise L/D ratio. This gives 21.5 kN of thrust per engine. To calculate the top of climb (TOC) thrust requirement, the initial cruise thrust is multiplied by a factor, as presented in another research [67]. For the same MTOW, similar aircraft require similar take-off thrust for similar performance. A320neo's predecessor, the A320, was powered by the CFM56-5B4 for aircraft with similar MTOW weight and it produced the same take-off thrust as the LEAP-1A26. This CFM56 provided a TOC thrust of 25.0 kN together with an initial cruise thrust of 22.3 kN [68]. A320neo climb requirements are assumed to be the same as the A320, meaning a TOC thrust requirement of 24.1 kN per engine. Average cruise will be set as the reference point of the gas turbine model. It is calculated by averaging the MTOW and zero fuel weight from table 3.1, dividing the weight by the cruise L/D ratio, which comes to 19.9 kN per engine. Table 3.3 summarises the thrust requirements per stage with appriorate mach number and altitude [63].

Table 3.3: Thrust requirements per flight segment, per engine

Flight segment:	Thrust: [kN]	Mach: [-]	Altitude: [m]
Take-off	120.6	0.0	0
TOC	24.1	0.78	11280
Cruise	19.9	0.78	11280

3.3.3. Baseline turbofan engine model

In table 3.4 the specifications of the baseline engine in the reference point (cruise) are given. It has been setup with the help of references [27, 66, 68–70] and trial & error. The table comprises of the BPR of the turbofan, as well the pressure ratio (π) of several components, and their efficiency (η)

Table 3.4: Turbofan model reference point specifications

Component:	Notation:	Value:	Component:	Notation:	Value:
Engine	BPR	11.1	HPT	$\eta_{poly\ HPT}$	92%
Inlet	π_{inlet}	0.99	LPT	$\eta_{poly\ LPT}$	92%
Fan	π_{fan}	1.54	CC	π_{cc}	0.95
Fan	$\eta_{poly\ fan}$	92%	CC	$\eta_{combustion}$	99.5%
LPC	π_{inlet}	1.70	Core duct	$\pi_{core\ duct}$	0.98
LPC	$\eta_{poly\ LPC}$	91%	Bypass duct	$\pi_{bypass\ duct}$	0.98
HPC	π_{inlet}	14.5	HP spool	$\eta_{mechanical}$	99.5%
HPC	η_{HPC}	92%	LP spool	$\eta_{mechanical}$	99.5%

3.3.4. Performance maps

Component performance maps are of great influence for the total gas turbine characteristics. In figures 3.3 and 3.4, two performance maps of a fan duct are displayed. The first is GSP's standard map, while the second is performance map created from measurement data of reference [71]. GSP's fan map shows the highest efficiencies at very high corrected speeds, close to the surge line, while the EEE fan map shows its highest efficiency regions at a relative broad speed range, in between chocking conditions and the surge line. Although performance maps can differ a lot, none of the available axial compressor/fan maps from Smooth C [72], nor any NASA rotor study maps looked like the GSP fan map. It is also worthwhile to note that the standard GSP LPC and HPC performance maps show very similar characteristics as the GSP fan map, with the highest efficiency at high corrected speeds, located close to the surge line.

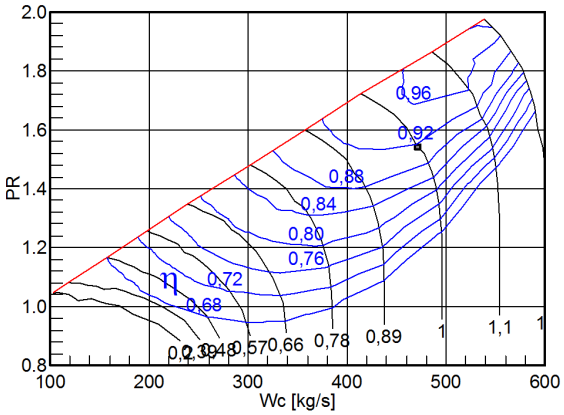

Figure 3.3: GSP Fan duct map [20]

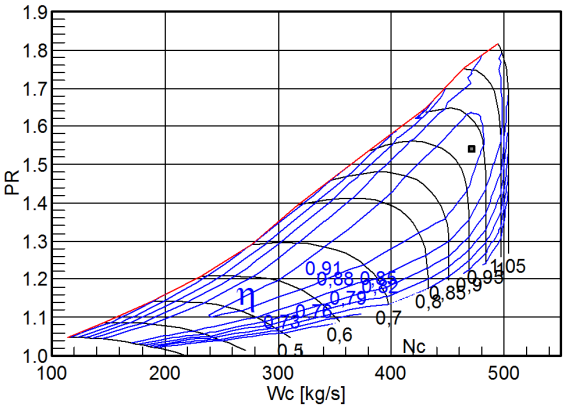

Figure 3.4: EEE Fan duct map [71]

Two turbofan models are created with the exact same settings at the reference point. One model makes use of all the standard GSP performance maps, while the other makes use of open literature performance maps. For the open literature, the EEE fan map is used together with a subsonic LPC map of the CFM56-3 [73] and a HPC map from a NASA test [74]. In both models, the turbine maps are the same, as the standard GSP performance maps of the HPT and LPT

showed the same characteristics as maps of open literature. These two models are then compared for their TSFC over a thrust range from 10 kN to TOC thrust (24.1 kN) at cruise altitude and speed. Figures 3.5 and 3.6 show the results for the GSP and literature maps respectively. Because the maximum efficiency location of the standard GSP maps is at high corrected speeds, the gas turbine operates most efficiently in these conditions, as can be seen in figure 3.5. In figure 3.6, the lowest TSFC is not obtained at maximum thrust settings, but just below because the components efficiencies are decreasing at higher corrected speeds. Therefore, depending on the types of performance maps used different conclusions can be drawn. With the standard GSP performance maps, the conclusion would be that a turbofan operating at higher thrust settings in cruise would provide an efficiency benefit. This would mean that the cruise TSFC of a downscaled engine would be higher, since working at maximum thrust setting in cruise would be beneficial over a larger engine operating at more moderate thrust setting. With the open literature performance maps however, the opposite is true. The open literature maps are expected to be more realistic, as there are a lot of similar maps, while the GSP maps are different from any of them. It can also be expected that turbofans operate most efficiently at cruise thrust settings, because they are designed to be most fuel efficient in that operating point. Therefore, the open literature maps will be used in the rest of the report.

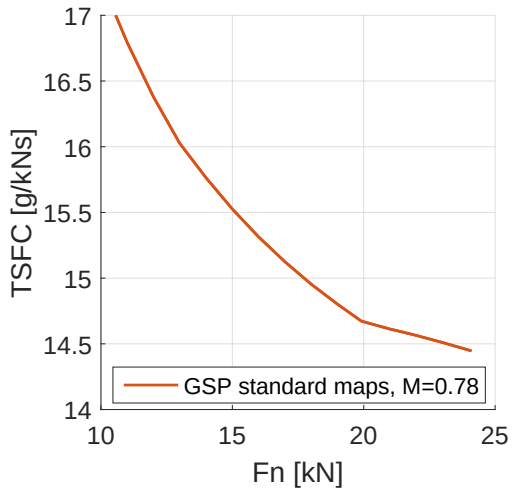

Figure 3.5: Cruise TSFC trend GSP performance maps

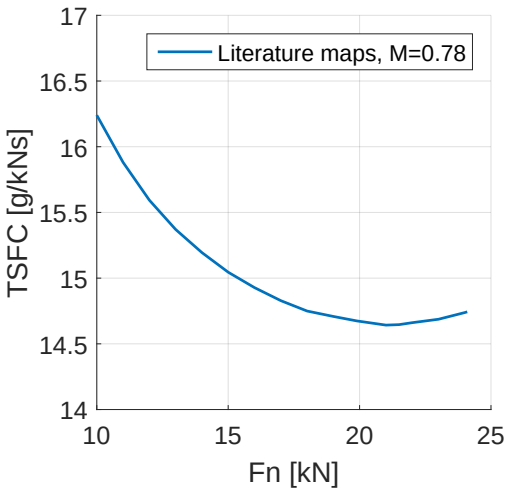

Figure 3.6: Cruise TSFC trend open literature performance maps

3.4. Mission profile

Since HEP is expected to provide most benefits in relatively short flights [53, 75], the mission used in this research is only 1000 km. Comparing that to the maximum range of 3000 km at maximum payload [62], the aircraft is most likely not operating at is range for maximum efficiency, but that is out of the scope of this study. The same mission profile is used as created in reference [75], which is the master thesis behind reference [16]. It created an aircraft model with basic flight dynamics. Figure 3.7 shows the altitude as well as the Mach number over the complete mission. With the altitude and speed from reference [75], together with the international standard atmosphere (ISA) the Mach number is obtained. Explanation of the ISA is provided in appendix A. The mission consist of 5 minutes taxi-out, together with a take-off (TO) on the runway of 0.7 minutes, a climb phase of 25 minutes and 35 minutes cruise. Afterwards, the aircraft descents for 20 minutes, followed by a 5 minutes taxi-in. Cruise takes place

at the before mentioned speed and altitude of Mach 0.78 and 11.28 km respectively. Validation of the mission profile is done with an actual A320neo flight of Lufthansa, and is described in appendix B. From the validation it can be concluded the mission shows a good approximation for the majority of the mission. However, both taxi-in and taxi-out are relatively short, and lift-off and touch-down occur at Mach 0.4 instead of 0.2. Since the take-off phase is very short, it will not have a significant effect on the mission fuel consumption. Just before cruise, and just after cruise, the Mach number shows a quick increase and decrease respectively. The sharp increased occurs when the aircraft has reached it cruise altitude, but has not yet obtained its cruise Mach number. At that time, more energy is put into acceleration rather than climb. Just after cruise, the thrust is already reduced before the aircraft starts to descent. For that reason it loses speed relatively quickly, while it slightly increases its speed when descent starts. Later on this report, in chapter 5 which discusses the results, the length of the taxi phases will be investigated to determine its affect on the results.

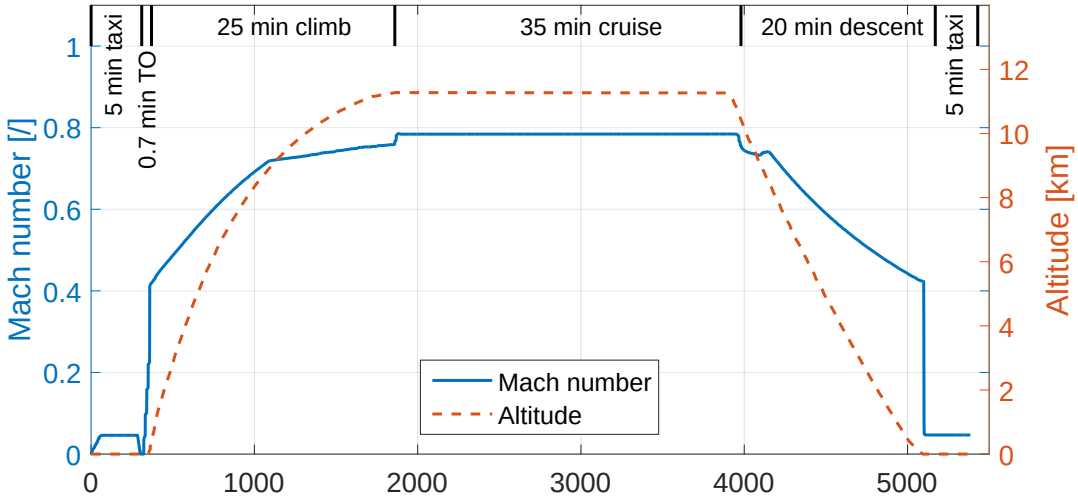

Figure 3.7: Mission profile, data adapted from [75]

3.5. Validation

Validation of the baseline aircraft is done for the gas turbine, in terms of efficiency, as well as the off-design simulation ability. Next, the mission fuel consumption is compared to other sources.

3.5.1. Gas turbine TSFC

TSFC is checked in several different ways. First, in table 3.5 the fuel consumption is compared to ICAO data [66]. At higher thrust settings the model shows good agreement. Lower thrust settings show larger differences, 18.7% at 7% thrust, but during the mission analysis these are only used during taxiing. This large deviation can be caused by several aspects: the use of generic performance components instead of the actual performance maps, and the simplification of a constant mass flow percentage for cooling at all thrust settings. However, these low thrust settings are not stressing the operating limits of the turbofan, and are therefore not expected to influence the overall results. An important note to the ICAO test data is that during the tests, no bleed and no power off-takes were applied and 100% ram recovery was ussumed in the inlet [70]. It is not stated how exactly the reference data is corrected for the 100% ram recovery,

but in the simulation result below, a constant inlet efficiency of 99% was used to obtain these results. In reality these values can therefore never be obtained since the inlet will always have ram recovery losses. During the other simulations in this report an inlet performance map is used. This map has 99% ram recovery as was specified in table 3.4, while at maximum thrust setting in SLS conditions, the ram recovery is 5% [20].

Table 3.5: Turbofan model validation at sea level with ICAO data [66]

Thrust level:	Thrust:	ICAO fuel flow:	LEAP-1A26 model:	Difference:
100 %	120.6 [kN]	0.861 [kg/s]	0.879 [kg/s]	2.1%
85 %	102.5 [kN]	0.710 [kg/s]	0.719 [kg/s]	1.3%
30 %	36.2 [kN]	0.244 [kg/s]	0.248 [kg/s]	1.6%
7 %	8.4 [kN]	0.091 [kg/s]	0.074 [kg/s]	-18.7%

A cruise efficiency validation is done by combining data from multiple references. The predescesor of the LEAP-1A26, the CFM56-5B4, has a TSFC of 16.98 g/kNs [68]. This is assumed to include power and bleed requirements for the aircraft. CFM, the manufacturer of the LEAP-engine, claims a TSFC reduction of 15% [69]. LEAP-1A26's cruise TSFC is therefore expected to be 14.43 g/kNs. A TSFC of 14.67 g/kNs is found, meaning an 1.7% higher value than expected. Another cruise TSFC was found from reference [76], where it stated 15.4 g/kNs for the CFM56-5B. Since this is considerably lower than the other cruise TSFC found, it is therefore expected to be without bleed-off and electrical power off-take. The modelled engine has a cruise TSFC of 13.79 g/kNs, or 10.5% below the CFM56-5B. Because of the unknown exact conditions of the CFM-56 cruise TSFC's, it is difficult to point out where the deviations from expectations and results come from. The modelled gas turbine does show good overall agreement with expectations under the limited data available.

3.5.2. Gas turbine off-design simulation ability

The gas turbine should be able to reach not only the maximum thrust levels, it also needs to operate safely at lower thrust settings. In this section, multiple operating lines are shown. Figures 3.8, 3.9 and 3.10 show these operating lines for the Fan, LPC and HPC respectively. The dark green line represent the thrust sweep from 24.1 kN until 5 kN at cruise conditions. In red the thrust is varied from 120.6 kN down to 8.4 kN in SLS conditions. Both the cruise and take-off operating lines in all three components show the exact same trends in terms of slope and relative positioning of the two operating lines on the map as in literature [77]. Besides the operating lines, the reference point is indicated in all of the maps, with a small square as well as the arrow pointing it out. This reference point is used to scale the map, and is the point in which the cruise point operates from table 3.3. At SLS maximum thrust, the minimum surge margin (SM) requirements are specified per component in table 3.6 [27].

Table 3.6: Minimum surge margin requirement in SLS maximum thrust [27]

Component:	Fan	LPC	HPC
SM requirement	10%	15%	20%

Equation 3.1 gives the definition for the SM, where it relates the PR of operating line to the PR of the surge line, at constant correct massflow [27]. The fan is the component with the largest difference in operating lines between cruise and take-off, because of the high BPR of the turbofan. For the fan, the cruise SM is therefore significantly larger than the SM at SLS take-off.

$$SM = 100 \cdot \frac{PR_{surge\ line} - PR_{operating\ line}}{PR_{operating\ line}} \tag{3.1}$$

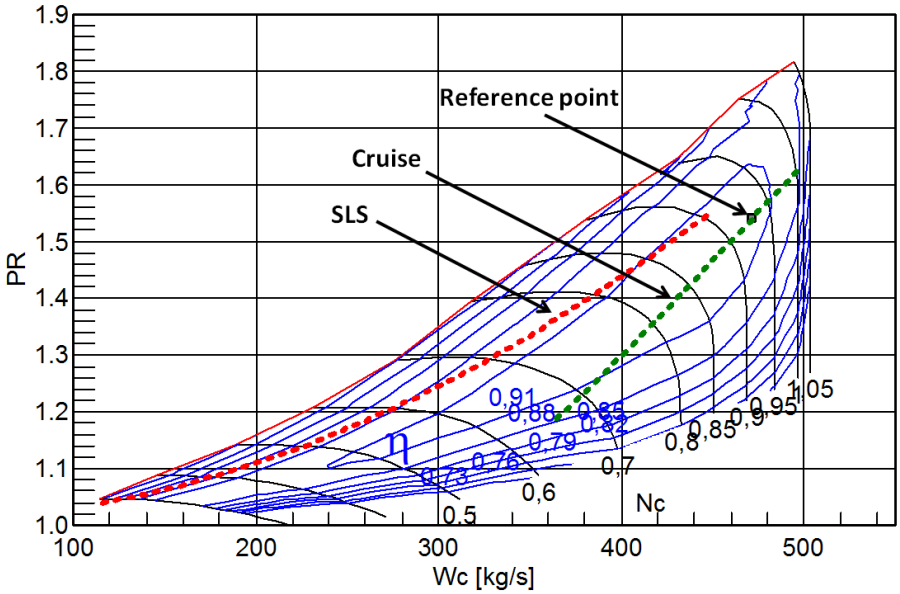

Figure 3.8: Fan operating lines at different conditions

Operating lines of the LPC in figure 3.9 show a reversed characteristic from fan, since in the LPC the cruise operating line is closer to the surge line. For that reason, the reference (cruise) point was selected for the LPC to satisfy the SM requirement.

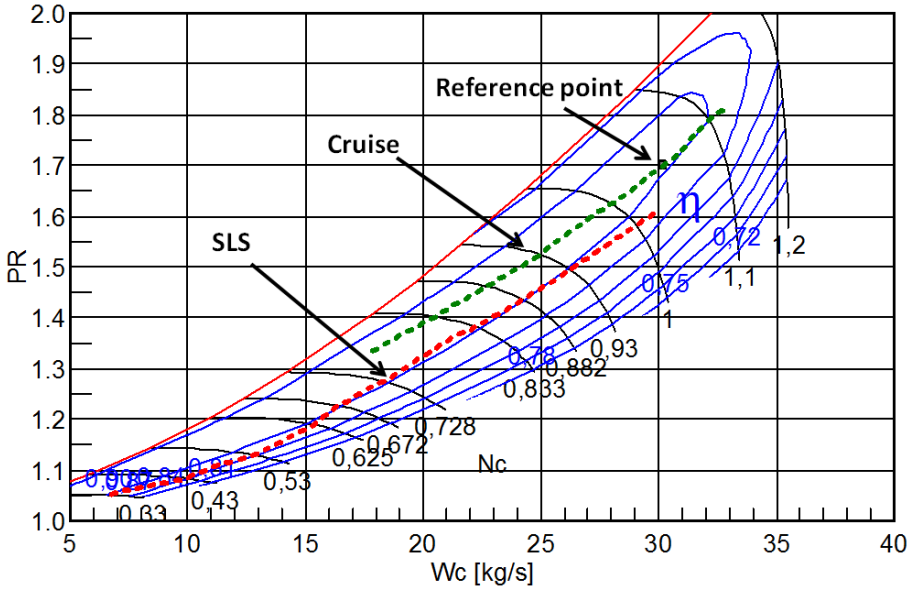

Figure 3.9: LPC operating lines at different conditions

The HPC has almost no difference in position of the operating lines between SLS and cruise, as show in figure 3.10. At very low thrust values, the HPC is surging in the current analysis. The gas turbine simulation model is not able to take into account variable stator vanes however. These would in a real gas turbine change the flow over the compressor blades to prevent the compressor from surging. Therefore this operating line outside the operating map is not a result of a fault in the modelling and will not significantly impact the results.

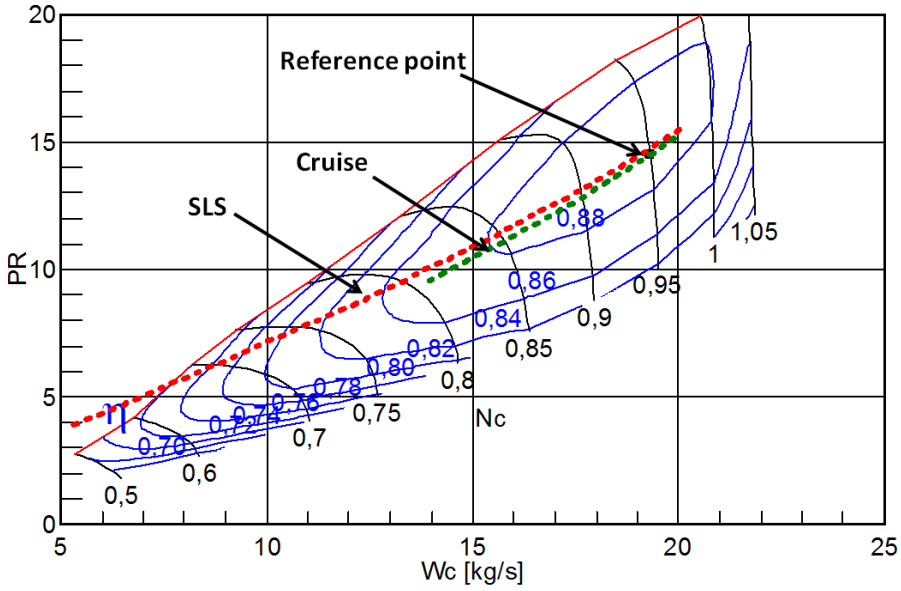

Figure 3.10: HPC operating lines at different conditions

3.5.3. Mission fuel consumption

Lastly, the mission fuel consumption is validated. In figure 3.11, the consumed fuel during the entire mission is shown. The reference mission is the same as that was used for the mission profile [75]. Since the thrust over the complete mission was for the A320neo, and considered the same mission length with maximum payload, the same thrust is used for this reference mission. Total fuel required for the mission of the reference case was 3231 kg, compared to 2836 kg of the current simulation, showing a 12.2% decrease. Although the aircraft's mission and thrust requirement were the same for both missions, the gas turbine model is different. The reference modelled a gas turbine with rated SLS thrust of 143.1 kN (CFM LEAP-1A35) and is not used to power the A320neo but the A321neo instead. Because of this, it operates at lower thrust settings than it actually would. Another point to be taken into account, is that the reference used standard GSP maps (discussed in section 3.3.4). With these maps, the TSFC vs thrust trend is different and together with the fact that the reference engine would operate at lower thrust setting, the total fuel consumption is therefore overestimated in the reference.

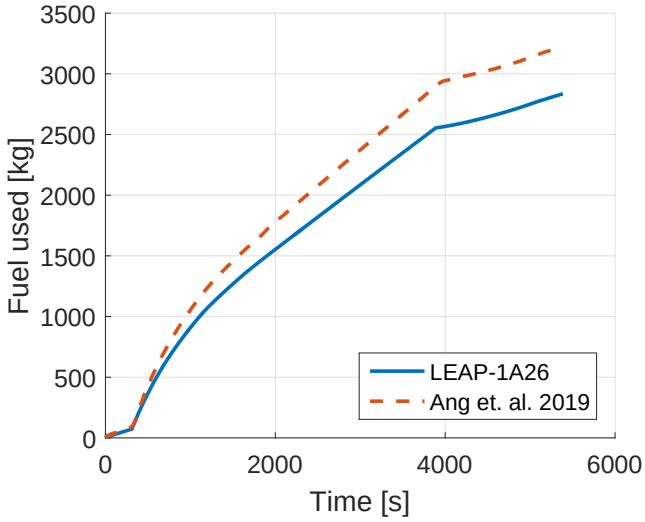

Figure 3.11: Mission fuel consumption validation, with data from [75]

From open literature, the A320neo fuel consumption on a 1222 km mission is said to require 4228 liters or 3400 kg of kerosene. Correcting this to a mission of 1000 km by assuming the cruise segment is 222 km shorter and using the simulated cruise fuel flow of 0.55 kg/s, the fuel consumption is 2869 kg. This neglects the snowball effect of carrying less fuel during the beginning of the mission, but acceptable for this relatively short distance. Only a very small deviation of 1.1% is found in that case between the simulated 2836 kg and reference [78]. Since the exact details of payload and length in taxi that is considered, this result lies well within the fault margin. Another reference to the mission fuel consumption is found by combining an A320ceo mission with the 20% fuel savings of the A320neo compared to its predecessor by airlines [79, 80]. On a 960 km flight from Frankfuhrt to Rome, the A320ceo uses 4077 kg of fuel according to reference [81]. For an A320neo, the expected fuel consumption would be 3262 kg, or 15% higher than simulated, showing more resemblance to reference [16]. Depending on the reference used, and the unknown factors like duration of taxi, payloads etcetera, the simulation shows a good agreement. Combining this with calculating possible savings of the HEP aircraft in percentages of this created baseline, the conclusions will remain the same.

4

Electrically Assited Turbofan and HEP Aircraft

The modelling procedure of the EATF, together with the HEP aircraft is explained in this chapter. It explains the modelling of the individual components and wraps up with a validation on multiple points of the created model.

4.1. HEP A320neo specification and requirements

For the hybrid electric propulsion A320neo, the same base aircraft model is used as for the non HEP case. This means the same specification and requirements defined in section 3.2 apply to this aircraft. Although the aircraft will become heavier due to the added electrical system, the standard A320neo has a larger maximum range than the mission that is considered in this study. Therefore, the decrease in required fuel for this mission gives option to add the electrical system. From the MTOW and maximum zero fuel mass from table 3.1 together with the fuel use of the baseline aircraft on this mission (roughly 3000 kg), 7700 kg can be added before the MTOW is exceeded.

4.2. Mission profile

The mission flight profile of the HEP aircraft is exactly the same as that of the baseline aircraft, described in section 3.4. A different aspect in the mission profile is the power management strategy of the HEP aircraft, because of the hybrid electric propulsion system. In figure 4.1 the strategy used in this research is shown. It shows purely electric taxi-in and out, electrically assisted take-off and climb, and cruise on solely the gas turbine. During the descent, an option is to recharge the batteries, but because this will consume more fuel, and the first goal of this study is to reduce fuel consumption, no charging is applied. From an operational point of view, the in-flight charging could however help because less charging (time) would be required on-ground, and the aircraft could fly more trips a day.

The reasoning behind this power management strategy is that at cruise, it is best to use the gas turbine, because the specific energy density of batteries is far lower than that of kerosene. Too much heavy batteries would therefore be required if they would be needed during cruise. If the electric part of the HEPS is used to assist the turbofan in the take-off and climb, the turbofan is no longer required to meet the take-off and TOC thrust requirements on its own. It can then be sized more specifically for cruise and possibly improve its TSFC. During taxi, the gas turbines operate at very low power settings, at which they perform poorly in terms of efficiency.

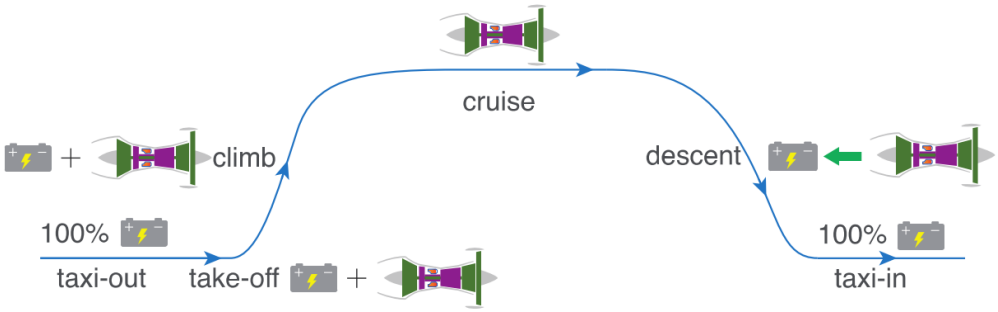

Figure 4.1: Power management strategy of the HEP aircraft [16]

Electric motors do not have this problem and would therefore provide the thrust during taxiing.

For the take-off and climb, a ratio between electric power and power of the gas turbine is required. Equation 4.1 gives the power split ratio (Φ) definition, introduced by [16]. It is the ratio of electrical power supplied by the electric motor(s) (P_{EM}), to the total LP-shaft power of the gas turbine (P_{total}). For simplicity reasons, the power split is averaged over the take-off or climb phase. The electrical power supply is constant during a mission phase, but because the gas turbine power changes over both mission phases, the actual power split during a mission phases changes slightly from beginning to end.

$$\Phi = \frac{P_{EM\ LP-shaft} + P_{EM\ HP-shaft}}{P_{total\ LP-shaft}} \tag{4.1}$$

With figure 4.2 from reference [16], the power split ratio's for take-off and climb are selected. The figure shows for a range of take-off and climb power split's the fuel consumption and total energy consumption over the complete mission. That research proposed a power split of ≈ 14% during climb for a combination of fuel savings and total energy savings. 14% power split for climb shows the largest decrease in fuel consumption, while keep total energy consumption low. The most promising take-off power splits with 14% climb power split are encircled in red in the figure. During take-off a different power split is selected as was suggested in that study, because the study suggested a engine scaled down in massflow, which would require 25% power split in take-off to not exceed its TIT. From section 3.3.4 however, it already was made clear scaling the engine down in mass flow would not yield any benefits. Therefore a more moderate 14% is selected for take-off as well for the EATF.

To be able to fly the same mission profile with a heavier aircraft, more thrust is required. Together with the assumption that the L/D ratio at every point in flight will remain the same as in the A320neo mission, the thrust can be calculated at every point in time. Figure 4.3 shows the flow chart for how this is done. Starting with the weights and engine model of the A320neo and CFM LEAP-1A26, together with it thrust requirements during the complete mission, a mission analysis is done of the A320neo. From this, the total fuel consumption is calculated, and the weight of the A320neo at every moment during the complete mission by calculating backwards from the maximum zero fuel weight (MZFW). Next, a fuel guess is done, which is equal to the fuel consumption of the A320neo in the first iteration. Then the weights of the A320HEP are calculated from the power splits and technology levels of the components. A mission analysis is then carried out with the thrust increased for the added mass of the HEP aircraft. At every point in the mission the consumed fuel is calculated, so the current weight of the aircraft is known for the thrust requirement. After the mission analysis is carried out, it is iterated for ac-

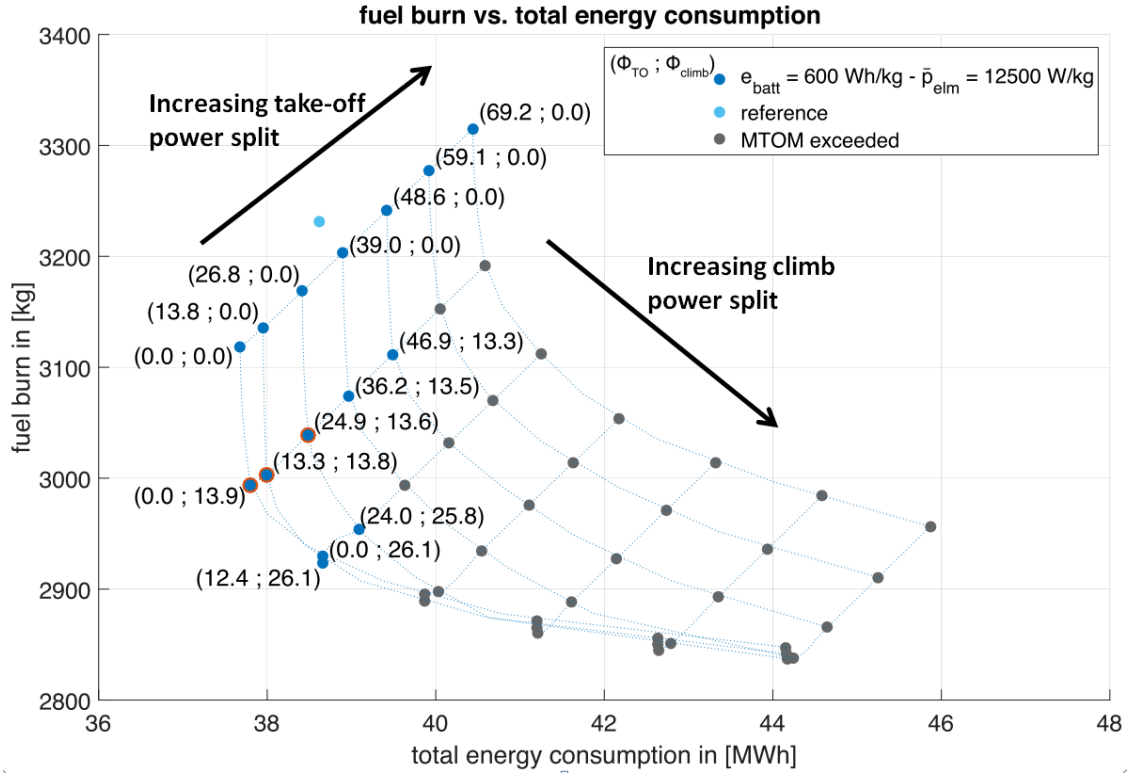

Figure 4.2: Effects of power split on fuel consumption and energy consumption [75]

tual fuel consumption and what was assumed before the mission analysis. After it is converged, the fuel consumption of the A320HEP is known.

4.3. Gas turbine

Modelling of the EATF is done via GSP as well. It allows to have power off-take in the turbines (HPT and LPT), where a negative power off-take implies power is added to the turbine. This way the turbine needs to extract less power from the flow to be able to provide power to the fan and/or compressor. The maximum thrust requirements of the EATF are the same as those of the baseline turbofan, because the MTOW of the aircraft will not be exceeded. To model the EATF, another variable needs to be defined besides the previously mentioned power split. This new variable is the LP-power fraction (Psi), equation 4.2 states that it is defined as the electrical power supplied to the LP-shaft compared to the electrical power added to both the HP- and LP-shaft. A LP-power fraction of 1 therefore means all the electrical power will be supplied to the LP-shaft, and nothing to the HP-shaft. Vice-versa, a LP-power fraction of 0 will be no power is supplied to the LP-shaft, and all the power is supplied to the HP-shaft.

$$\Psi = \frac{P_{EM\ LP-shaft}}{P_{EM\ LP-shaft} + P_{EM\ HP-shaft}} \tag{4.2}$$

4.4. Electric motor

With the electric motor supplying a substantial amount of power to the gas turbine shafts, it is important to take into account the losses of the electric motor and how its performance scales

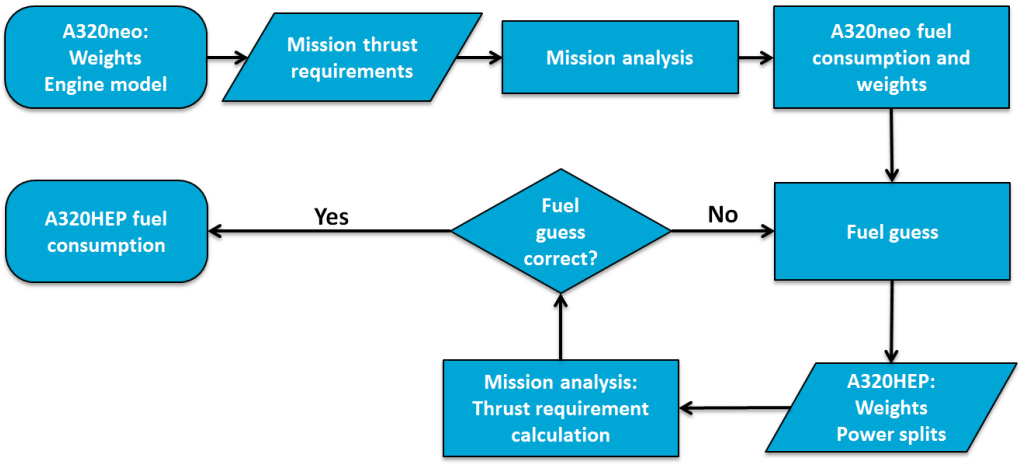

Figure 4.3: Flow chart of the HEP aircraft mission

with total power output and rotational speed range.

4.4.1. Losses of an electric motor

Losses of an electric motor can be divided in copper losses, iron losses, friction losses, windage losses and constant losses. Copper losses are those created from friction in the windings due to the current being proportional to the torque, $T \propto I$ and the losses are proportional current squared, $P_{loss} \propto I^2$, the current losses scale with torque squared, as is shown in equation 4.3. The moving magnetic field of the rotor creates losses inside the stator. These are called iron losses, and can be further divided into hysteresis losses and eddy current losses. Hysteresis losses are caused by the magnetizing and demagnetizing of the iron in the stator. Eddy current losses are losses due to the current created by a changing magnetic field. Iron losses therefore depend on the speed of the electric motor, as shown in equation 4.4.

$$P_{copper} = k_c \cdot T^2 \tag{4.3}$$

$$P_{iron} = k_i \cdot \omega \tag{4.4}$$

Windage and friction losses are both due to the movement of the rotor, but the first are created by air resistance of the moving rotor, and the second is friction from seals and bearings. These are assumed to have a constant torque, and are therefore only scaling with rotational speed, giving equation 4.5. An air drag force scales with velocity squared, making windage power losses cubed, as shown in equation 4.6.

$$P_{friction} = k_f \cdot \omega \tag{4.5}$$

$$P_{windage} = k_w \cdot \omega^3 \tag{4.6}$$

Lastly, there are losses independent of rotational speed or torque. Combining all the above described losses, equation 4.8 is obtained [82].

$$P_{constant} = C \tag{4.7}$$

$$P_{losses} = k_c \cdot T^2 + (k_i + k_f) \cdot \omega + k_w \cdot \omega^3 + C \tag{4.8}$$

Since no in depth design of the electric motor is available, it is hard to select the good k-factors for the considered electric motor. With the help of reference [83], these loss factors can be rewritten into more meaningful characteristics of maximum efficiency, rotational speed and torque of maximum efficiency and a factor for the constant losses. Together with a known maximum torque and speed, a complete efficiency map of the electric motor can be created. A basic efficiency model is shown in figure 4.4. The maximum efficiency is placed at normalised speed, torque and power of '1', with all their maxima shown by thick lines at values of '2'.

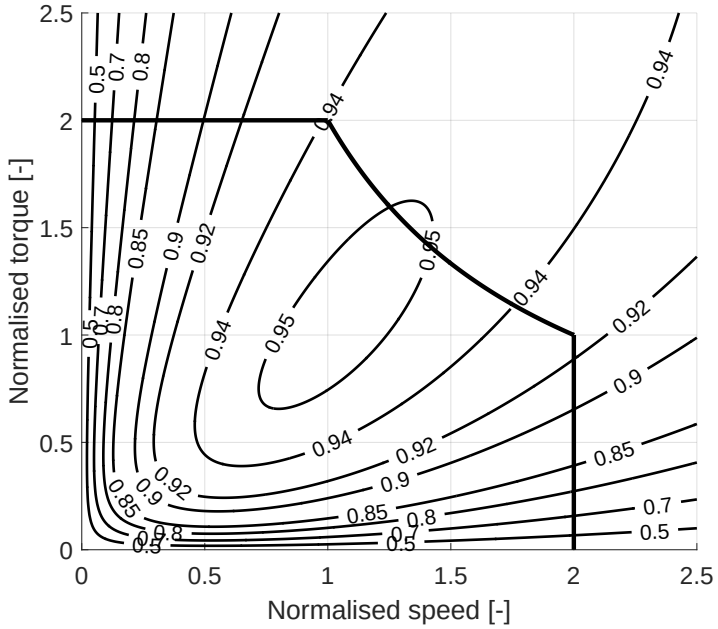

Figure 4.4: Basic electric motor efficiency map

From this figure, it can be noted that the efficiency of the electric motor would still be very efficient above its maximum power. After the validation of this model it becomes clear this is indeed not in line with reality (see section 4.6.2. Losses for field weakening and magnetic saturation are missing [84]. Field weakening depends on both the torque and the speed of the electrical machine. However, if over the complete efficiency map of the electric motor an additional loss is applied, the complete map is changed. Therefore the field weakening factor is altered depending on the manufacturer's efficiency map, and is only applied at high speed and power values, above the maximum efficiency. Similarly, magnetic saturation is accounted for by an additional loss factor at high torque values, where this loss is the largest [84]. These losses are taken into account by adjusting them via trial and error to mimic the performance of an actual electric motor. The shape of the electric motor efficiency map scale largely with the size of the electric motor [85]. In reality larger electric motors can achieve higher efficiencies, but these effects are not considered in this study [41].

It is important to take into account that during cruise, the electrical machine still spins since it is attached to the LP- or HP-shaft, even though it does not supplying power to the shaft any more. Depending on the type of electrical machine, SRM / PMSM, the constant losses, friction losses, windage losses and iron losses are still present, creating an additional power requirement from both the HPT and LPT (if two motors are used).

4.4.2. Scaling laws of an electric motor

For an aircraft, weight is crucial, and therefore power density (or power to weight ratio) of an electric motor. The power of an electric motor scales with torque and rotational speed ($P = \omega \cdot T$). Per unit area between the stator and rotor surface, a certain amount of tangential force can be exerted. This value largely depends on the type and configuration of the electric motor. Equation 4.9 shows this tangential stress depend on the current density 'A', the average magnetic flux density 'B', and a correction factor the possible offset between the two magnetic fields. With synchronous machines this offset (ζ) is zero, and therefore the tangential stress does not decrease [84]. The torque of an electric machine can be calculated with the surface area ('S') in the direction of the magnetic field, and the distance between this surface area and the axis of rotation (arm 'r'). See equation 4.10 [84].

$$G_{tangential} = \frac{A \cdot \hat{B} \cdot cos(\zeta)}{\sqrt{2}} \tag{4.9}$$

$$T = \int_S G \cdot r \cdot dS \tag{4.10}$$

Depending on the type of electric motor, axial or radial flux, the torque equation will look as equations 4.11 and 4.12 respectively. The outer and inner diameters are of the rotor, which is not important for the radial flux motor, but is important for the axial flux motor. Its inner diameter is mainly limited by the drive shaft through the electric motor. The length of the rotor 'L' comes into play with radial machines, but not with axial flux machines. From these equations one can see the torque of an radial motor increases quadratically with diameter, while the axial flux motor increases cubically with diameter. This falls in line with other studies [86].

$$T_{radial} = \frac{D_{outer}^2 \cdot \pi \cdot L}{2} \cdot G \tag{4.11}$$

$$T_{axial} = \frac{2\pi \cdot G}{3} \frac{D_{outer}^3 - D_{inner}^3}{8} \tag{4.12}$$

The other side of the electric motor power density relation is the rotational speed of an electric motor. An increase in diameter limits the rotational speed because of mechanical stresses inside the rotor. Equation 4.13 shows that the mechanical stress inside the rotor is a factor of C', which describes the layout of the rotor, assumed constant since the design is only scales. The material density ρ, also not changing with scaling, and both the radius and rotational speeds squared. For an increasing diameter, the maximum speed therefore reduces inversely, which applies to both axial and radial machines.

$$\sigma_{mechanical} = C' \cdot \rho \cdot r_{rotor}^2 \cdot \omega^2 \tag{4.13}$$

Combing this with the relation between torque and diameter, equations 4.14 and 4.15 show the relations of power with diameter of the machine. The radial machine increases power linearly with diameter, whereas the axial machine increases power quadratically with diameter. When also taking into account the weight of an electric motor, which roughly scales with volume, the power density an axial flux machine stays the same with diameter, whereas the power density of a radial flux electric motor decreases linearly with diameter.

$$P_{radial} \propto diameter \tag{4.14}$$

$$P_{axial} \propto diameter^2 \tag{4.15}$$

4.4.3. Scaling point

Sizing of the electric motor can be done in multiple ways. From figure 4.4 one can see the most efficient point of operation of the electric motor is not a its maximum power. Therefore one needs to make a trade-off between the weight of the electric motor, the required size of the battery and the weight of the cooling system. In this study the electric motor is sized at continues power for the climb phase, because it operates at a constant power setting for the complete climb length of 25 minutes. Meaning that the weight of the electric motor is minimal, later on, in section 5.3 this decision will be further explained. In take-off the required power is around twice as high as in climb, but this only needs to be supplied for 42 second (0.7 minutes). Therefore the electric motor can be used at its peak power. For more information on the operation of the electric motors during flight, please see section 5.3 in the results chapter.

4.5. Battery & inverter

Both the inverter and battery are modelled in a basic manner, their exact performance is beyond the scope of this study. The inverter and battery are therefore only simulated with a constant efficiency, and a power density and energy density for the inverter and battery respectively. In chapter 5 the assumed values are shown depending on the technology level.

The total battery energy and mass are calculated based on the set power split ratio during take-off and climb. Because the length of each flight segment is known, the required energy from the battery can be calculated. Together with the losses in the electric motor, the inverter, the battery discharge efficiency and the maximum depth of discharge, total battery size and weight are obtained. Another important specification of a battery is its rate of discharge, which is described in a 'C' rating. Often the maximum C rating is around 2 for short duration [54]. This means the battery can fully discharge in 1/2 hour. Since the climb segment of the aircraft is about 25 minutes, the batteries would require 3C continuous. Take-off requires roughly twice the power from the battery, so 6C would be needed for around 42 seconds, which is above today's ratings. Energy density is therefore not the only concern for batteries, also their discharge rate. This will definitely need to be investigated in future research, but is outside the goal of this study.

4.6. Validation

Validation of the electrically assisted aircraft is done component wise and on a mission level in terms of fuel consumption.

4.6.1. Gas turbine shaft power

In a high bypass gas turbine most of the thrust is produced by the fan in the bypass. The LP-shaft power is therefore highly correlated to the amount of thrust. To check weather the gas turbine simulation is capable of simulating an EATF correctly, electrical power is supplied to the LEAP-1A26 model, and set to maximum SLS thrust (120.6 kN). Figure 4.5 shows the LP-shaft power (combined power of fan and LPC), under increasing electrical power supplies. Three different LP-power fractions are used, to show the effect of this parameter as well. One can see the LP-shaft power does actually change under power supply. The LP-power fraction is affecting the speed at which LP-shaft power varies under power supply. The difference in LP-shaft power comes from a reduction in thrust produced by the core, as shown in figure 4.6. Since total thrust is the same at every point in the figures, the fan needs to produce more thrust, increasing the LP-shaft power. The trends of figures 4.5 and 4.6 are therefore exactly opposite. A deeper explanation of the characteristics of the EATF together with the explanation of this

can be found in chapter 5. Since these changes in LP-shaft power can be explained, simulation of the EATF is possible in the simulation model.

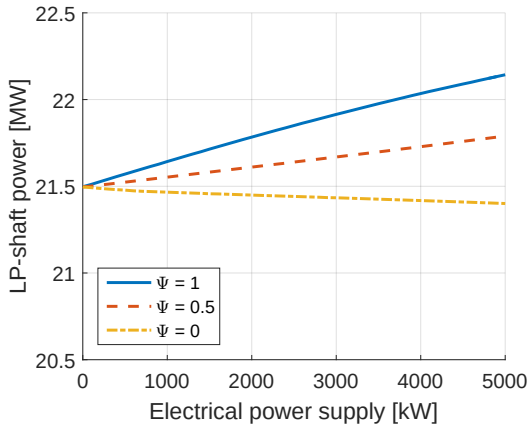

Figure 4.5: LP-shaft power under different electric power supplies

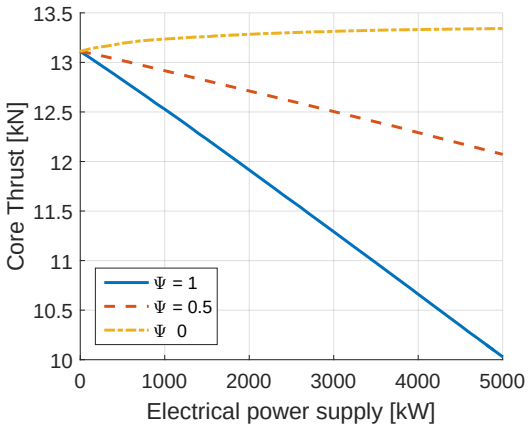

Figure 4.6: Thrust produced by the engine SPcore

4.6.2. Electric motor

For the validation of the electric motor model, figure 4.7 shows the basic model described before, without field weakening and magnetic saturation. When comparing this to figure 4.9, which is the efficiency map of a 400 kW axial flux permanent magnet motor from EMRAX, it is clear the standard model overestimates the efficiency especially at high torque and high speed operation [85]. By adjusting the loss factor for the iron (k_i) and copper (k_c) losses when the speed and torque surpassed the maximum efficiency point, figure 4.8 is obtained after some trial and error. Figure 4.8 figure clearly shows a lot better agreement with the efficiency map of the manufacturer (figure 4.9, but at high rotational speed with low torque, the efficiencies are a bit off and will be discussed in the next paragraph. It was found that the required adjustments of the k_i and k_c largely depend in the motor. EMRAX's motor shown here, mainly required adjustments for the magnetic saturation of the materials. Which means the magnetic field and thus torque do not increase linearly any more with an increase in current, which happens at high torques. An electric motor from Magnax [41, 87] showed that field weakening was the main cause for differences between the basic model and the manufacturer's map. Field weakening occurs when rotational speeds are very high, and the machine is limited by its maximum power.

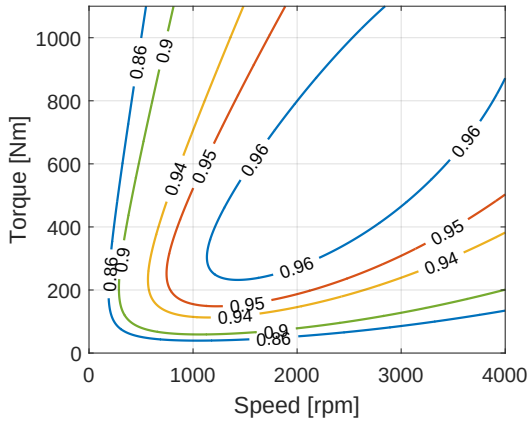

Figure 4.7: EMRAX 348 simple simulation efficiency map

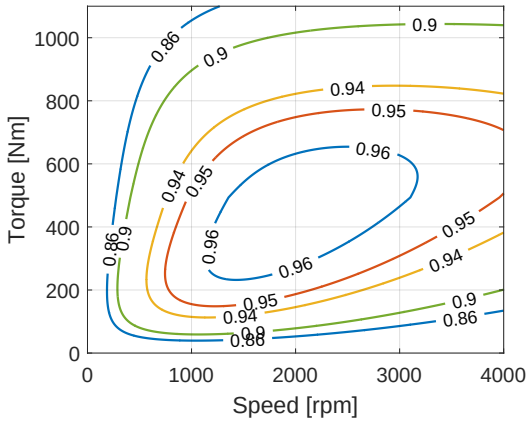

Figure 4.8: EMRAX 348 improved simulation efficiency map

At high speeds with low torque, there is a difference between the simulation and validation data as just mentioned. This becomes even more apearant when looking at the free run losses. These losses occur when no external load is applied to the electric motor. Figure 4.10 shows the simulated free run losses as well the manufacturer's data [85]. One can see the simulated loses are higher than expected, performance is therefore underestimated at high speeds. Free run losses need to be overcome during the flight phases where the electric motor rotates, but does not deliver power. These phases are cruise and descent in this study.

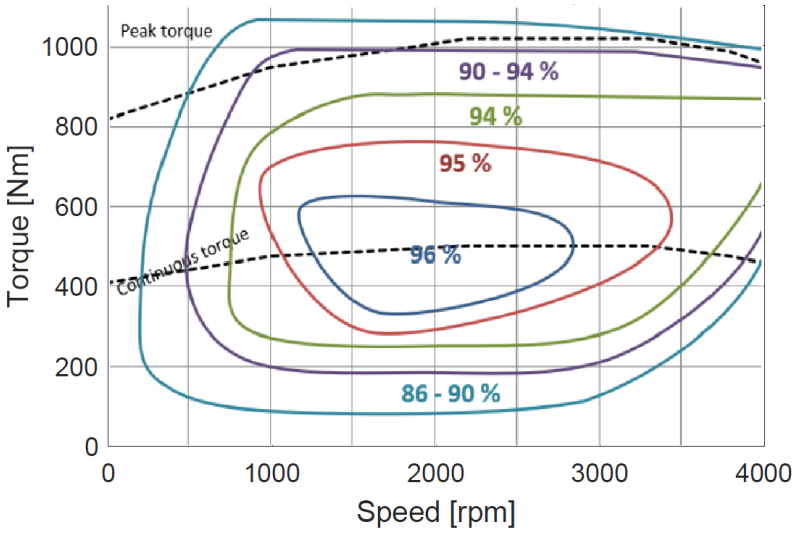

Figure 4.9: EMRAX 348 manufacturer's efficiency map [85]

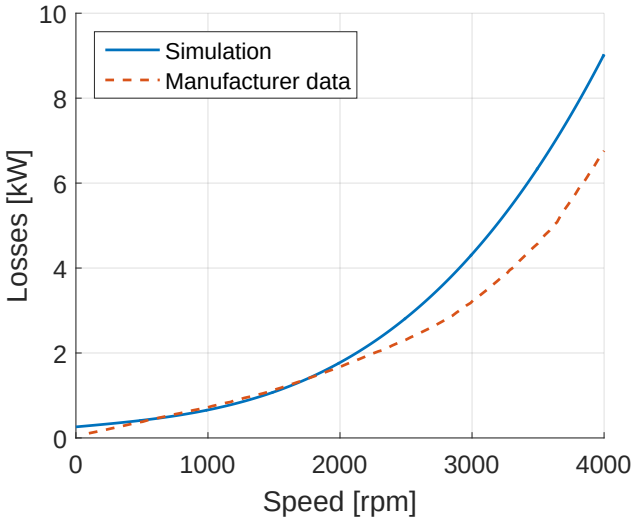

Figure 4.10: EMRAX 348's free run losses, with data from [85]

4.6.3. Mission fuel consumption

Validation of the fuel consumption is done through a complete mission of HEP aircraft with data from reference [75]. The assumed performance of the electrical motor, battery and inverter is set the same to the reference case (largely similar to the later described technology level of 2030). A power split ratio of 13.3% and 13.8% at take-off and climb respectively is used to directly compare to the reference data. In all cases shown in this validation, the turbofan engines are the baseline engines. So, for the validation the turbofan engines are not redesigned for cruise. Figure 4.11 shows the results of both the conventional aircraft and the HEP aircraft in terms of fuel consumption over the same mission, while figure 4.12 shows the fuel flow rate of the simulated flight missions in this study.

For a clear recap of the total fuel consumption validation, table 4.1 gives a summary of the total fuel consumed for a given mission in different simulations. Although both studies show a clear reduction in fuel consumption, 4.4% vs 7.2% reduction for the current study and reference

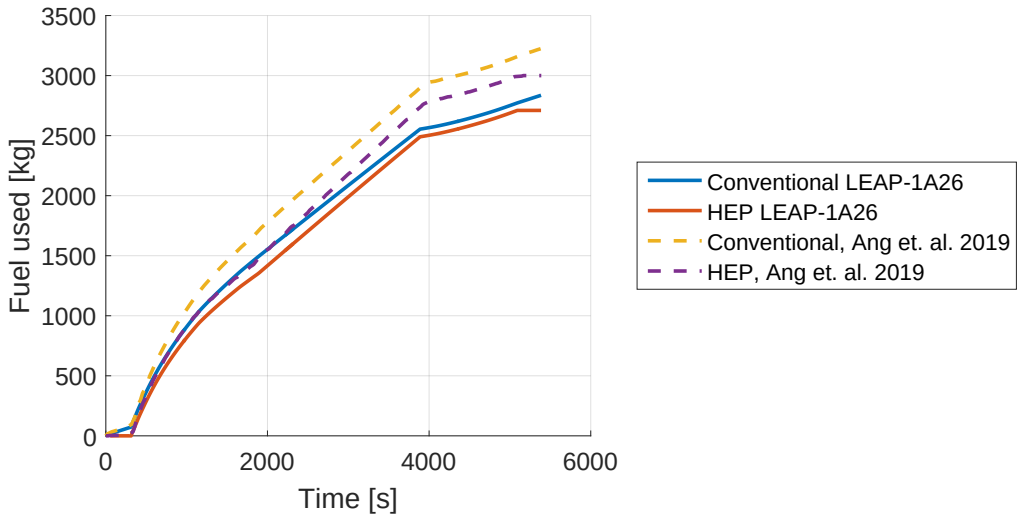

Figure 4.11: HEP aircraft fuel consumption validation, with data from [75]

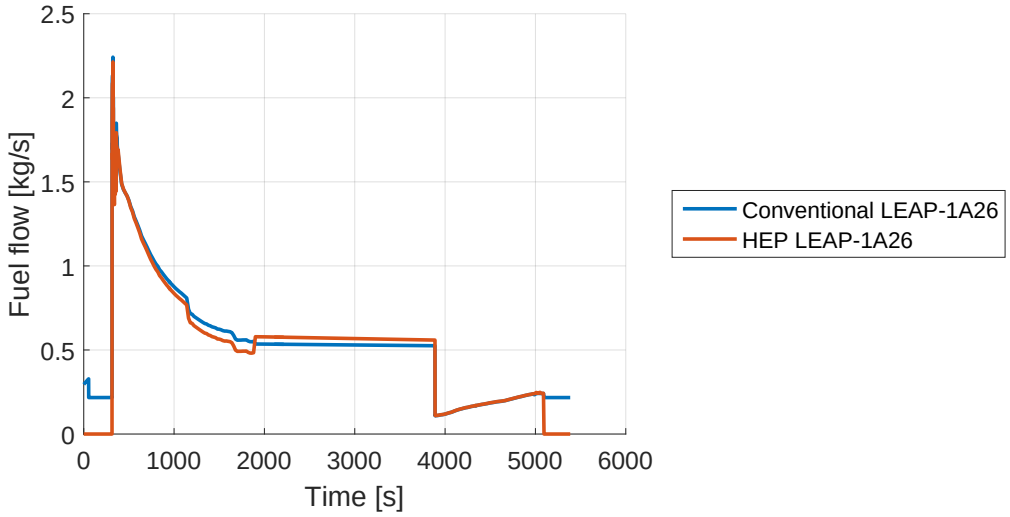

Figure 4.12: HEP aircraft fuel flow comparison

study respectively, the difference is significant. Unfortunately it is unclear where the difference comes from. The characteristics of the fuel consumption over the missions, very similar as can be seen in figure 4.11. In both cases the HEP aircraft have consumed less fuel at TOC, after which the savings decrease during cruise as well for both. But because the current simulation does not show the same savings at TOC, at end of cruise almost all savings are gone. With help of figure 4.12 the difference in fuel flow rate between the HEP and conventional aircraft can be seen more easily. In the taxi-out phase, the HEP aircraft shows the most significant savings, and keeps saving fuel until TOC (at around 1900 seconds mission duration). But at cruise the electric motors are turned off, showing a clear increase in fuel flow rate due to the extra thrust required by the heavier aircraft. In the descent phase, no significant difference can be seen because the aircraft mostly glides down. Since the L/D ratio is assumed the same for both aircraft, the higher mass of the HEP aircraft does not affect its fuel consumption in this phase. During taxi-in, the HEP aircraft can again taxi fully electric, making a significant saving. Overall, the trends shown by the simulation as well as the reference are the same, but the exact magnitude

of the savings differ. With that the HEP simulation is considered validated, keeping in mind that the exact savings might differ.

Table 4.1: HEP aircraft fuel consumption validation, with data from reference [16]

Type:	Total fuel consumption:	Difference w.r.t. conventional:
Conventional, LEAP-1A26	2836 [kg]	
HEP, LEAP-1A26	2710 [kg]	-4.4 [%]
Conventional, Ang et. al. 2019	3231 [kg]	
HEP, Ang et. al. 2019	2999 [kg]	-7.2 [%]

5

Results & Discussion

In this chapter, first the characteristics of the EATF are presented. From this information, a redesign of the turbofan is made with the electrical assistance in mind. The operating point of the electric motors during a mission are investigated. And lastly, different technology levels are compared in terms of total fuel consumption of the complete mission.

5.1. Characteristics of an electrically assisted turbofan

To find the characteristics of an EATF, the baseline LEAP-1A26 model used. It is examined at SLS, as well as TOC conditions, since those are most stringent operating conditions for the turbofan. The selected 14% power split (see section 4.2) is used in the analysis, together with 50% less power (Φ=7%) and 50% more power (Φ=21%), to show the EATF characteristics .

5.1.1. Sea level static

EATF characteristics at sea level static take-off thrust are analysed with the three different power split levels, 21%, 14% and 7%. These correspond to 3.9 MW, 2.6 MW and 1.3 MW respectively. Each of these power splits has a color, as shown in figure 5.1. Every power split ratio is varied from a LP-power fraction of 1 to 0. These results are obtained by setting GSP to off-design calculated, with a thrust requirement of 120.6 kN in this case. It then finds the operating point by varying the fuel flow rate.

The first figure, 5.1, shows fuel flow required to achieve maximum SLS take-off thrust. A reference line is added to show the fuel flow required by the un-assisted LEAP-1A26. To show the trend in minimum TSFC, an additional line, called the minimum fuel line, goes through the LP-power fractions with minimum TSFC. One can see that an increase in power split (available electrical power) decreases the optimum LP-power fraction. Or in other words, if one wants minimal TSFC with a high power split, two electric motors are required. One on the LP-spool and one on the HP-spool.

In figures 5.3 and 5.4 the operating points of the LPC and HPC are shown on the performance map respectively. The arrow indicates the direct of increasing LP-power fraction. No figure is given of the fan, because it's operating point hardly varied, which makes sense since the total thrust requirement remains the same and the fan produces most of the thrust. From figure 5.3 one can see that LPC cannot operate safely with the highest power split (yellow line, Φ=21%) and a LP-power fraction of 1. The surge margin is way too small here, as is also shown in figure 5.2. Also the middle power split (red line, Φ=14%) would not meet the 15% surge margin requirement of the LPC. The lowest power split under a LP-power fraction is just below 15% surge

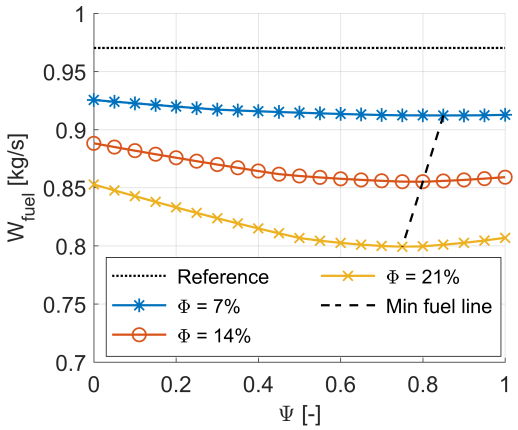

Figure 5.1: Fuel flow rate under different power splits and power fractions at sea level static take-off conditions

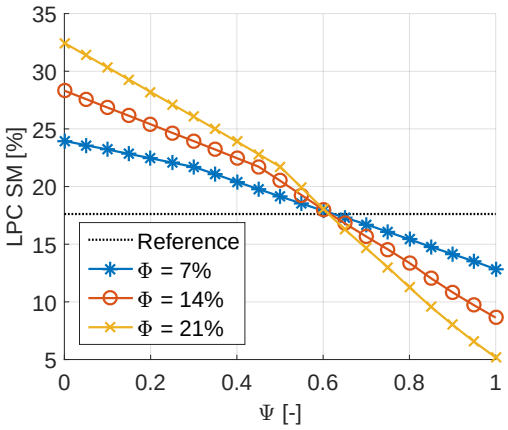

Figure 5.2: LPC surge margin under different power splits and power fractions at sea level static take-off conditions

margin, but this might be because of the use of a generic performance map. Another point to notice from the LPC operating points, is that the corrected speed hardly changes. Which is due to that LPC and fan are on the same shaft.

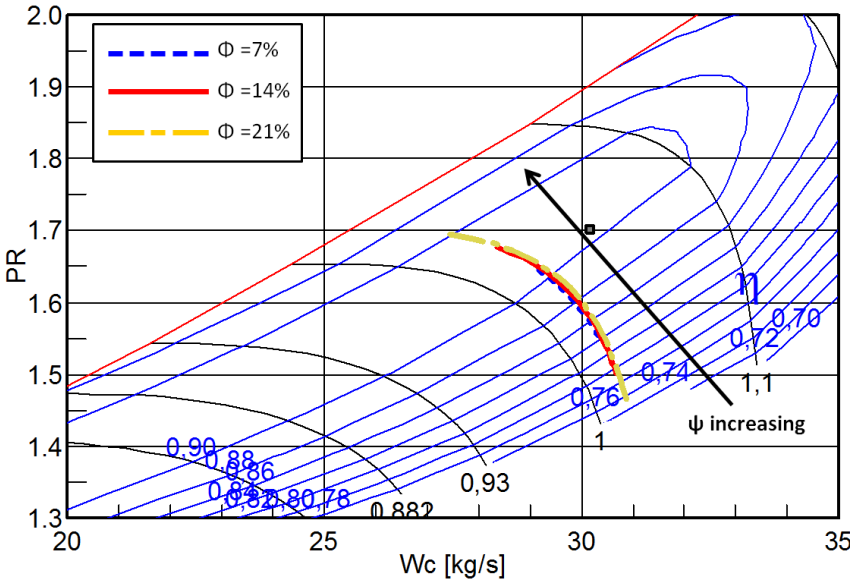

Figure 5.3: Characteristics of the LPC at SLS TO under electrical power supply

The trends of the HPC with electrical assistance is quit different, as is shown in figure 5.4. An increasing LP-power fraction means a decrease in corrected speed, and a lower pressure ratio of the HPC. This follows from the lower TIT due to a reduction is fuel flow (see also figure 5.5. Less energy in the flow and still a power requirement from the LPT in terms of thermal energy, the HPT receives less power. When it receives less power the speed goes down, and so does the HPC's pressure ratio. It is worthwhile to note in figure 5.5 that the TIT is not lowest at the exact same points where the fuel flow is minimal. At lower LP-power fractions, the OPR is higher, and thus the combustor entry temperature (or TT3) will be higher.

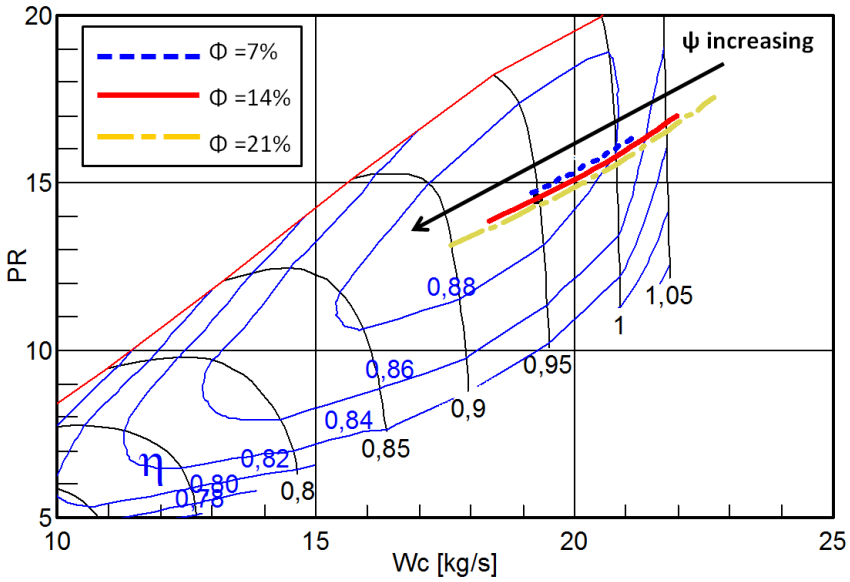

Figure 5.4: Characteristics of the HPC at SLS TO under electrical power supply

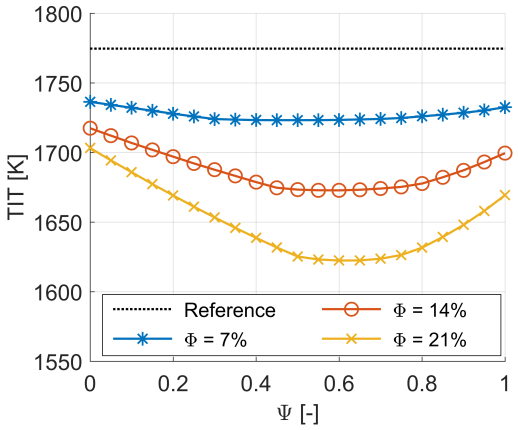

Figure 5.5: TIT under different power splits and power fractions at sea level static take-off conditions

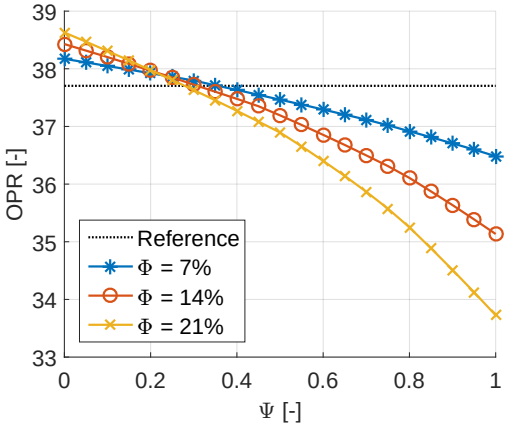

Figure 5.6: OPR under different power splits and power fractions at sea level static take-off conditions

When looking at the efficiency of the fuel combustion, which is largely a factor of OPR, the EATF's efficiency is lower compared to a conventional turbofan. Figure 5.6 shows that the OPR is highest for low LP-power fractions, which is because of the large amount of power that is added to the HPT.

5.1.2. Top of climb

The EATF characteristics at TOC are very similar to those at max SLS take-off thrust. Power split levels at TOC are different, here the avialable levels are lower, because reference [16] showed that a high climb power split is not beneficial. Due to the relative long climb segment, a larger power split requires a lot of additional battery weight. Same power splits as at take-off are used, 21%, 14% and 7%, which correspond to 2.1 MW, 1.4 MW and 0.7 MW respectively. The effective power is lower in TOC compared to SLS, because the overall power of the turbine decreases due to lower air density. First, the efficiency of the gas turbine is examined by looking at the

required fuel flow to meet the TOC thrust of 24.1 kN. In figure 5.7 it is shown that a high power split has its most fuel efficient point under lower power fraction than low power split levels. With the lowest power split level analysed in TOC, the most fuel efficient LP-power fraction is 1.

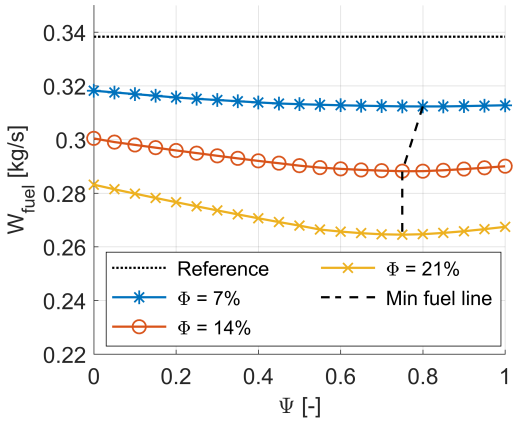

Figure 5.7: Fuel flow rate under different power splits and power fractions at TOC conditions

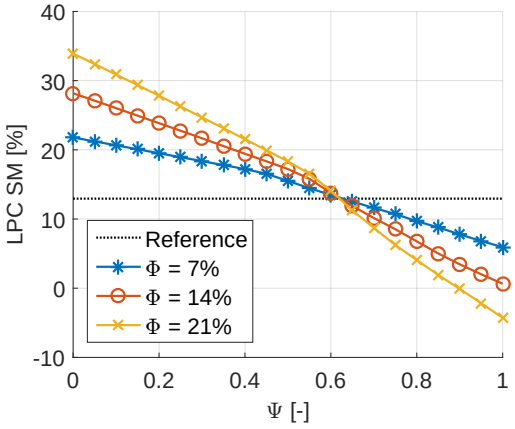

Figure 5.8: LPC surge margin under different power splits and power fractions at TOC conditions

Figure 5.9 now shows that the high LP-power fractions are even closer to the surge line, which is confirmed by figure 5.8. None of the analysed power split ratio's is capable of a safe operation under a LP-power fraction of 1, meaning in climb two electric motors are required, one on each spool. It should also be noted that none of the most fuel efficient LP-power fraction are capable with a sufficient surge margin.

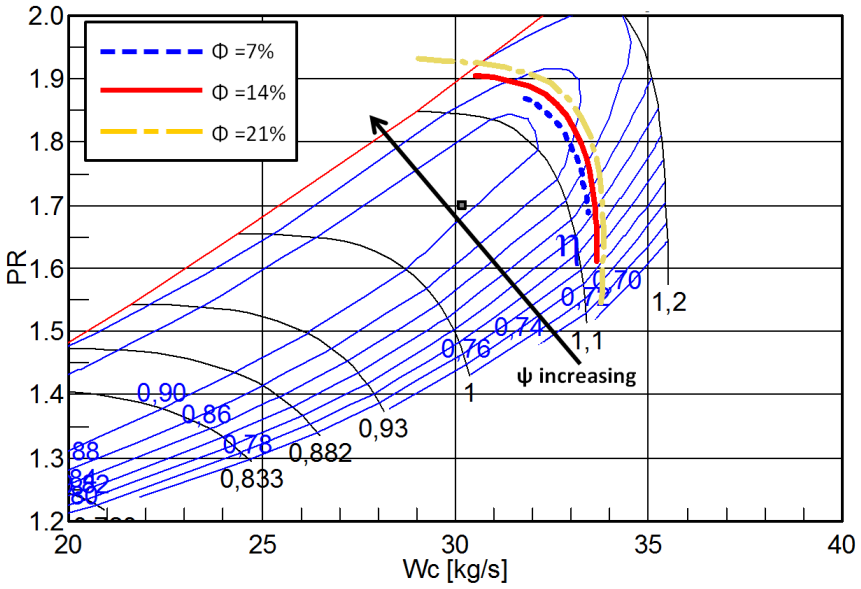

Figure 5.9: Characteristics of the LPC at TOC under electrical power supply

Two very similar higher between TOC and SLS are the trends shown in by the TIT and the OPR in figures 5.10 and 5.11 respectively. The TIT is the lowest between LP-power fraction of 0.6

and 0.8, where especially in the higher power splits of 14 and 21% show a significant decrease. The OPR in figure 5.6 on the other hand shows the highest values at low LP-power fractions, and decreases with increasing Ψ. From the analysis of the EATF it becomes clear that in TOC and take-off very similar trends occur. In TOC the LPC surge margin is however clearly more stringent.

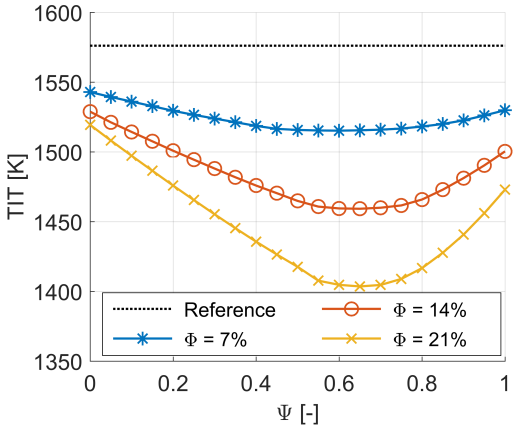

Figure 5.10: TIT under different power splits and power fractions at TOC conditions

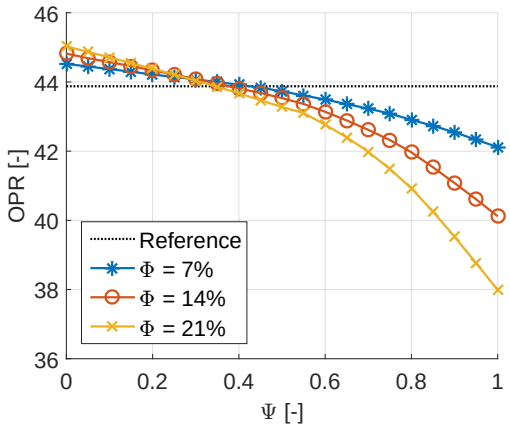

Figure 5.11: OPR under different power splits and power fractions at TOC conditions

The effects of the electrical power can also be expressed in terms of thermal efficiency, which is done in figure 5.12. It uses the definition of thermal efficiency from equation 5.1, which relates the power added to the gas through the gas turbine to the total supplied power of the gas turbine. Where the P_{EM}, the power of the electric motors, is added to the standard definition because in case of the EATF, energy is not only supplied via fuel but by the electric motors as well. Figure 5.12 shows that the thermal efficiency is largely dependant on both the power split and the LP-power fraction. At low LP-power splits, the efficiency hardly changes with different power splits. Around a LP-power fraction of 0.7 the thermal efficiency is however largely impacted, meaning less thermal energy (heat) is left at the exhaust of the gas turbine. The decrease in thermal efficiency at even higher LP-power fractions is due to several aspects. Firstly, the OPR is decreasing rapidly, as was shown in figure 5.11. Secondly, the LPC's efficiency is decreasing, see figure 5.9. Lastly, the HPT's efficiency is decreasing, as shown in figure 5.13. The efficiency of the HPT shows a sharp decrease in efficiency at higher LP-power fractions than 0.7, in all of the power splits. This decrease is caused by the HPT moving out of its most efficient operating region, which is on its hand caused by the decreasing shaft speed, and a decreasing pressure ratio of the HPT [77].

$$\eta_{thermal} = \frac{\Sigma\left(0.5 \cdot \dot{m}\left(v^2_{jet\ effective} - v^2_0\right)\right)}{\dot{m}_{fuel} \cdot LHV_{fuel} + P_{EM}} \tag{5.1}$$

Besides the thermal efficiency, the overall efficiency is defined by the propulsive efficiency. With the definition from equation 5.2, which relates the effective power of the gas turbine (net thrust multiplied by speed) to the power that is was added to the gas flowing through the gas turbine. Or in other words, how effectively kinetic energy is converted into propulsive energy. Figure 5.14 shows this propulsive efficiency, with a very clear trend, of higher efficiencies at higher LP-power fractions. The increasing LP-power fraction puts more power into the LP-

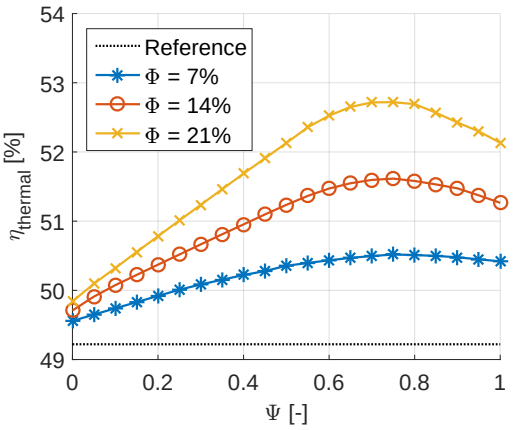

Figure 5.12: Thermal efficiency at TOC under different power splits and LP-power fractions

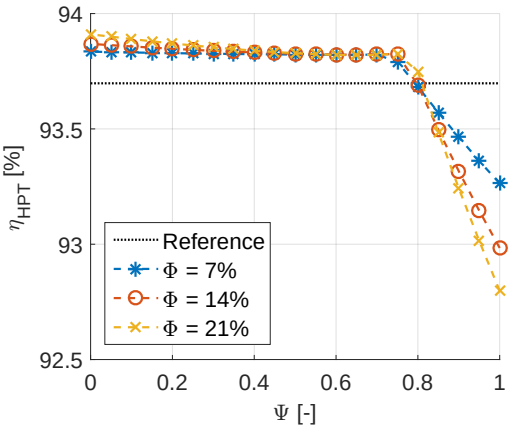

Figure 5.13: HPT efficiency at TOC under different power splits and LP-power fractions

spool, which produce most of the thrust via the fan. Because the fan accelerates the air only by a relatively small amount compared to the gas turbine core, it produces thrust more effectively from kinetic energy. Higher LP-power fractions therefore result in higher propulsive efficiencies.

$$\eta_{propulsive} = \frac{\Sigma\left(\dot{m}\left(v_{jet\ effective} - v_0\right)\right) \cdot v_0}{\Sigma\left(0.5 \cdot \dot{m}\left(v^2_{jet\ effective} - v^2_0\right)\right)} \tag{5.2}$$

By combining equation 5.1 and 5.2, equation 5.3 is obtained. It gives the total efficiency of the gas turbine, by linking the thrust power to the total supplied power to the gas turbine. Since the total efficiency is the multiplication of the propulsive and thermal efficiency, the total efficiency trend lays in between the two of them. This is shown in figure 5.15, showing the total efficiency of the gas turbine. Although the trends are very similar to the thermal efficiency plot of figure 5.12, the total efficiency does not show an equally steep drop at higher LP-power fraction than 0.7. As a result of the higher propulsive efficiency at high LP-power fraction.

$$\eta_{total} = \frac{\Sigma\left(\dot{m}\left(v_{jet\ effective} - v_0\right)\right) v_0}{\dot{m}_{fuel} \cdot LHV_{fuel} + P_{EM}} \tag{5.3}$$

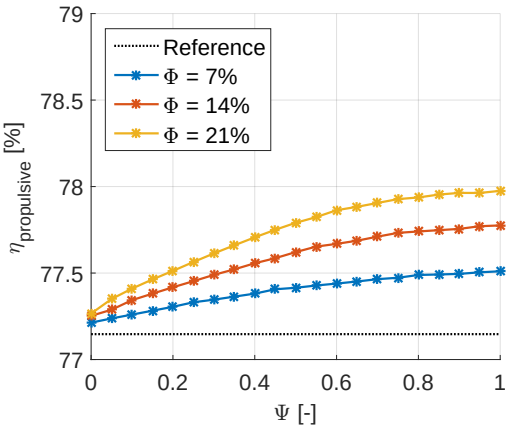

Figure 5.14: Propulsive efficiency at TOC under different power splits and LP-power fractions

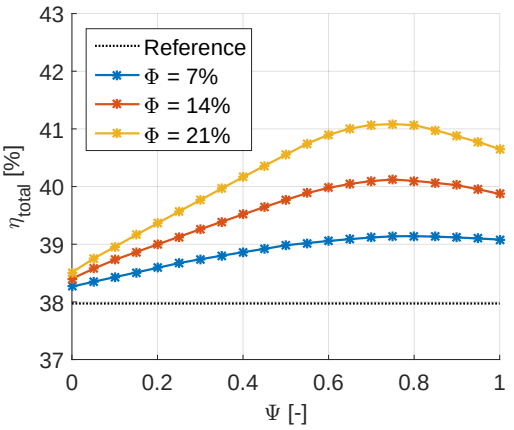

Figure 5.15: Total efficiency at TOC under different power splits and different LP-power fractions

5.1.3. Geared turbofan

A GTF has a different performance map of the LPC when compared to a direct drive turbofan (DDTF) such as the LEAP-1A. In a GTF, the LPC turns faster than the fan, and thus operates at higher circumferential speeds [77]. Although a GTF differs in more ways from a DDTF because the fan rotates slower and the LPT turns faster, it is able to obtain higher efficiencies [77]. It will also affect the shape of primarily the fan performance map. However since it was found the fan map does not affect the results of this study, the GTF is modelled by changing only the LPC performance map to the transonic map from reference [88]. All other setting where kept the same as the baseline model of the LEAP-1A.

In figure 5.16 the operating points at TOC under the supply of electrical power are shown of the transonic LPC in the GTF. The highest efficiency contour is located further away from the surge line compared to the subsonic LPC map of the DDTF. Therefore a larger surge margin is present, meaning the EATF is not restricted as much by the surge margin of the LPC.

Besides the surge margin of the LPC, the characteristics of the EATF are virtually the same. In figure 5.17 the surge margin of the LPC is shown at SLS conditions whereas figure 5.18 shows the surge margins of the LPC at TOC conditions of the GTF. In both cases, the surge margin has increased significantly compared to the DDTF. This increased surge margin now allows the turbofan to operate at its point of maximum efficiency in SLS conditions, while at TOC it is very close to its maximum efficiency point, when the previously mentioned suggested LPC surge margin of 15% is taken into account. Something that is not possible with the subsonic LPC in the DDTF. The results of this analysis therefore largely depend on the selected LPC performance map. If one would design a new LPC, that is meant to be used in an EATF, it might be possible to position the highest efficiency contour further away from the surge line, enlarging the options for electrical power supply.

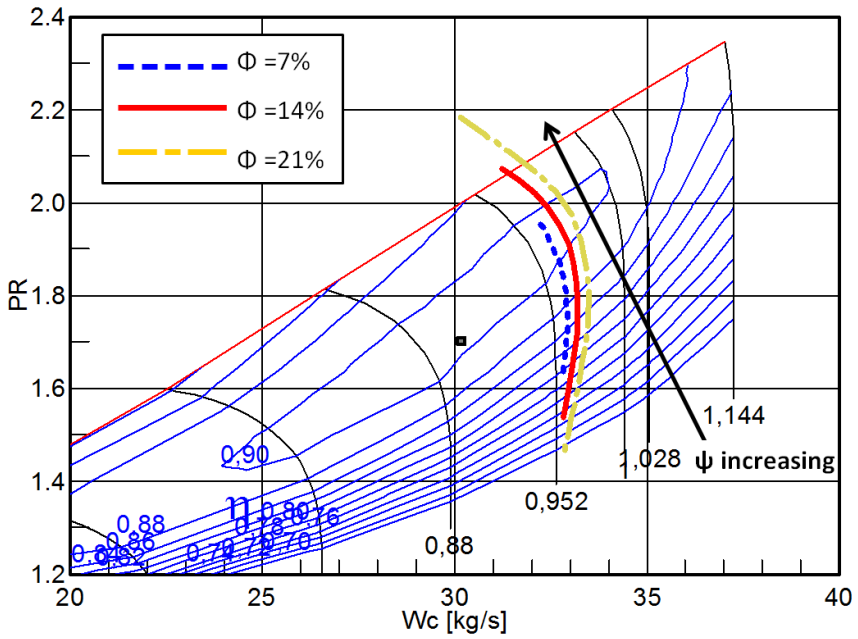

Figure 5.16: Characteristics of the transonic LPC at TOC under electrical power supply

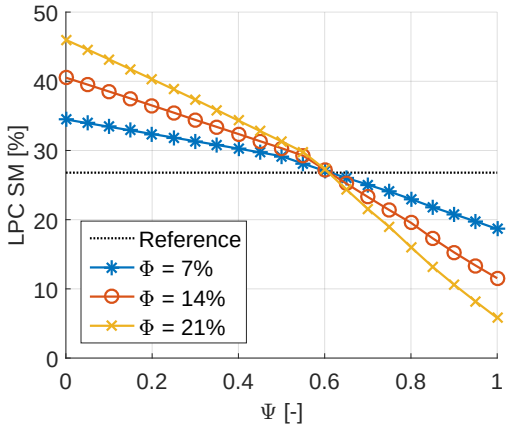

Figure 5.17: GTF LPC surge margin under different power splits and power fractions at SLS conditions

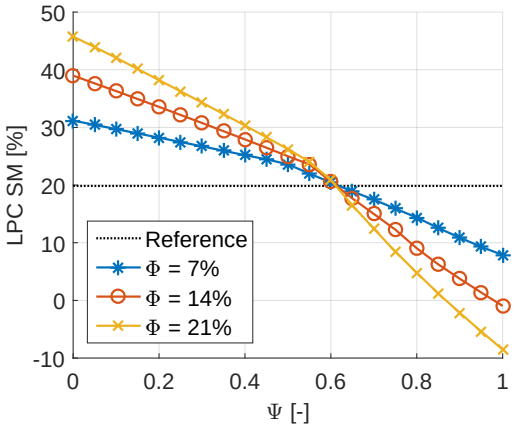

Figure 5.18: GTF LPC surge margin under different power splits and power fractions at TOC conditions

5.2. Redesign of the turbofan for cruise

The efficiency of a gas turbine can be split propulsive efficiency and thermal efficiency, as shown in figure 5.19. It also shows that the thermal efficiency is a function of the components efficiencies, OPR and TIT. Propulsive efficiency is function of the BPR and Fan PR. If there is a way to redesign the gas turbine for maximum efficiency in cruise, it needs to come from one (or several) of these points.

Starting with analysis a possible improvement of the LEAP-1A26's propulsive efficiency by comparing different BPR's and FPR's. By performing a similar analysis as was done in reference [67], figure 5.20 is obtained. It is done by keeping the OPR, TIT and thrust constant, and vary the fan duct pressure ratio, BPR and air mass flow at the reference design point. Every fan duct PR has a specific BPR at which it achieves its maximum efficiency, because of the ideal (exhaust) jet ve-

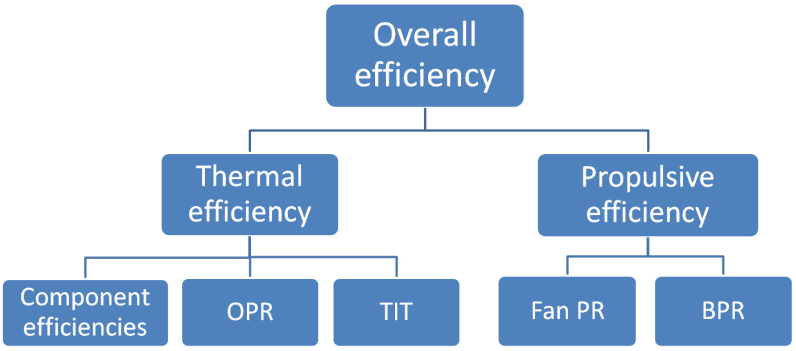

Figure 5.19: Efficiency build-up of a turbofan

locity ratio [77]. The general trend is that lower fan duct PR's can achieve a lower TSFC at higher BPR's. The figure shows it is possible to decrease the TSFC with a higher BPR and lower FPR. Minimum TSFC is obtained at a fan duct PR of 1.48 with a BPR of 12.75. This designs shows an improvement of 1.3% in terms of cruise TSFC, but at the cost of an increased massflow requirement of 12%, compared to the LEAP-1A26 baseline model. When considering this would require a larger fan, nacelle etcetera, it is not a viable option.

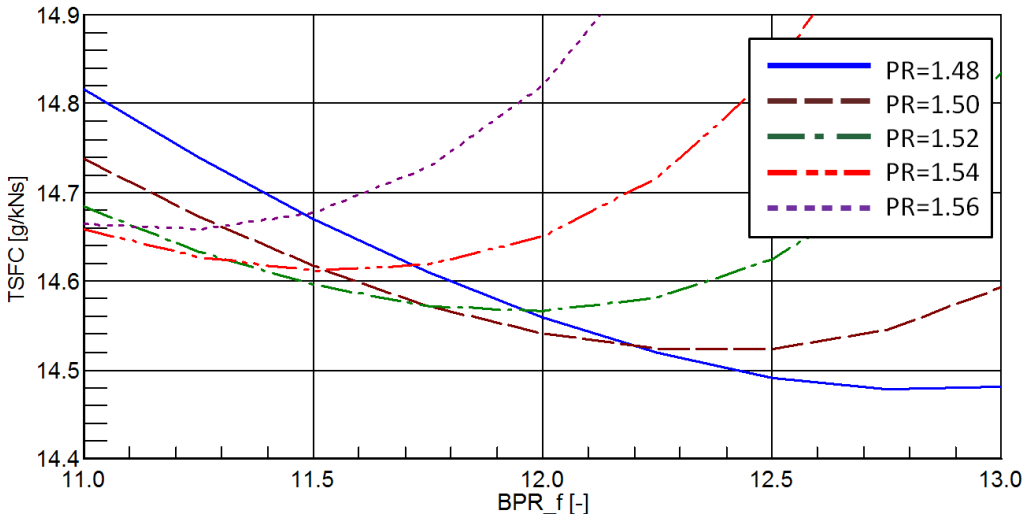

Figure 5.20: Redesign of the LEAP-1A26 turbofan for various fan duct pressure ratios and BPRs at cruise thrust

To see if improvements can be made to the efficiencies any of the following components: fan, LPC, HPC, HPT or LPT, the operating lines in take-off and cruise are compared. In chapter 3 this is already done. Figures 3.8, 3.9 & 3.10 showed these operating lines for the Fan, LPC and HPC respectively. It can be concluded that all these components already work at their maximum efficiencies at cruise. A similar story is true for both turbines, which have because of their very short operating line even more constant performance over all operating conditions. For this analysis, generic performance maps have been used for each component. These where from components designed in the 1980's and 1990's, so today's components maps might differ a bit.

That leaves only two options, the TIT and OPR for possible improvement in cruise performance of the EATF. From the characteristics of an EATF described in section 5.1, it was clear both TIT

and OPR are reduced in take-off as well as TOC. Since in cruise, both the OPR and TIT are not at their maximum, the idea is to increase the OPR and TIT, so it operates closer to its maxima in take-off, TOC as well as cruise for maximum efficiency. The OPR for the redesign can be increased by the same ratio as the OPR is reduced in TOC of the EATF compared to the OPR of the conventional turbofan at TOC. In case of the DDTF LEAP-1A26, the OPR can increased by 2.3% with a power split 14%, whereas with a GTF it can be increases by 3.4% because the surge margin requirement is less stringent for the LPC of the GTF. The LP-power fractions at which the DDTF and GTF can therefore operate are 0.6 and 0.7 respectively in TOC, where 0.7 is more efficient. In terms of TIT reduction in take-off, the DDTF and GTF show almost the same reduction. For the 14% power split case, the TIT is reduced by around 100 K, in take-off as well as in TOC.

Since a GTF with its different LPC performance map shows a larger potential for improvements with an EATF, it will used for the rest of the results. Because the OPR and TIT change for the redesigned EATF, a new propulsive efficiency analysis need to be carried out to find the new optimum fan duct PR and BPR. This is done in a similar manner as before, and is presented in figure 5.21. For these results the TIT was increased from 1550 K to 1650 K, while the OPR increase is obtained by increasing the HPC PR from 14.5 to 15.0. The figure shows the same fan duct PRs as the previous figure, but higher BPRs are incorporated since the optima are located at higher BPRs. Although the cruise TSFC can be reduced by 1.7% in case of the fan duct PR of 1.50 at a BPR of 13.75, it still requires a relatively large increase of the air massflow by 6.5%. If however the fan duct PR of 1.54 is selected with a BPR of 12.75, the TSFC is reduced by 1.0%, while the massflow does not change (-0.01%). This second option is therefore selected and will be used in the rest of this chapter.

It should be noted that the increased TIT will have a negative effect on the lifetime of the combustion chamber and HPT, since the materials will degrade faster. For this study the focus is however on the performance side, so lifetime is not taken into account.

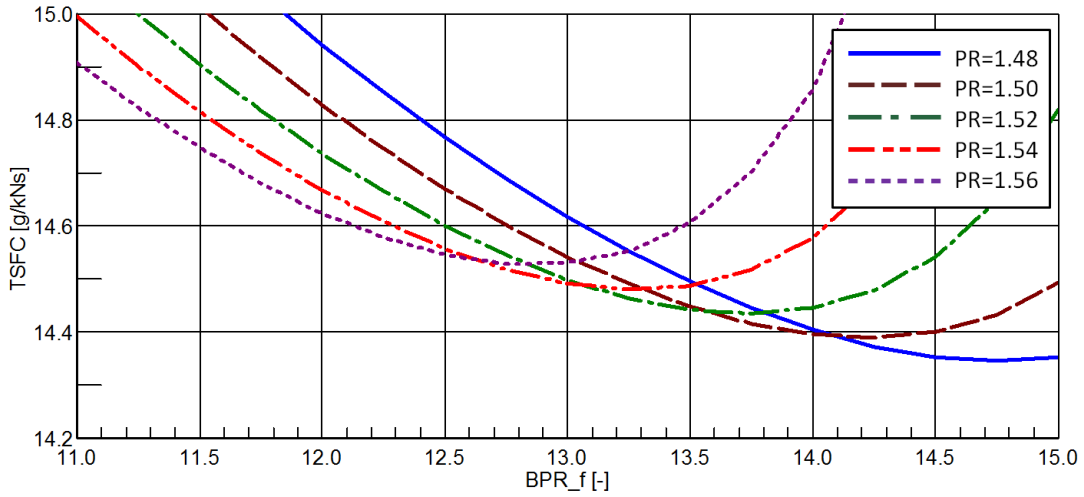

Figure 5.21: Redesign of the EATF for cruise under constant TIT and OPR for various fan duct pressure ratios and BPRs

5.3. Electric motor operation

Operating points of the electric motors in taxi, take-off and climb are plotted in a similar manner to the gas turbine components. The operating points are plotted on top of the performance map, as is done for the electric motor on the LP-spool in figure 5.22. It marks the different flight phases with different markers, while the operating lines are shown with a black line. Take-off takes place at maximum power, at the upper right region with maximum torque at maximum rotational speed. During take-off the speed varies quite a lot, which largely a factor of the exact thrust at a specific speed of the aircraft during the acceleration. Since the thrust and speed during the flight mission are taken from another study, the exact operating line at take-off could be slightly different in reality. The fact that take-off takes place at maximum peak power of the electrical motor, while climb power is the maximum continues. This is possible since with the selected 14% power split in both take-off and climb, the total electric motor power is 2.6 MW in take-off while it is 1.4 MW in climb (for one gas turbine). There is roughly a factor two difference, which is often the difference between the continoues and peak power [41, 85]. Weight and size of the electric motor are therefore minimized in this case. In terms of efficiency this sizing is not the best, because the climb phase (where most electrical energy is supplied) does not take place at maximum efficiency point of the electric motor. Although the required battery size could be reduced by about 1% when the electric motor is sized for maximum efficiency in climb, its weight would increase by about 50%, meaning there is no overall weight benefit in this case. Therefore the decreased energy required from the battery is negated by the increased fuel required for the heavier aircraft. In reality the cooling system weight can be reduced if the electric motor efficiency is increased from 95 to 96%, because the required heat that needs to be removed in reduced by 25% in that case. For this study the cooling system is however out of scope and is not covered in more detail.

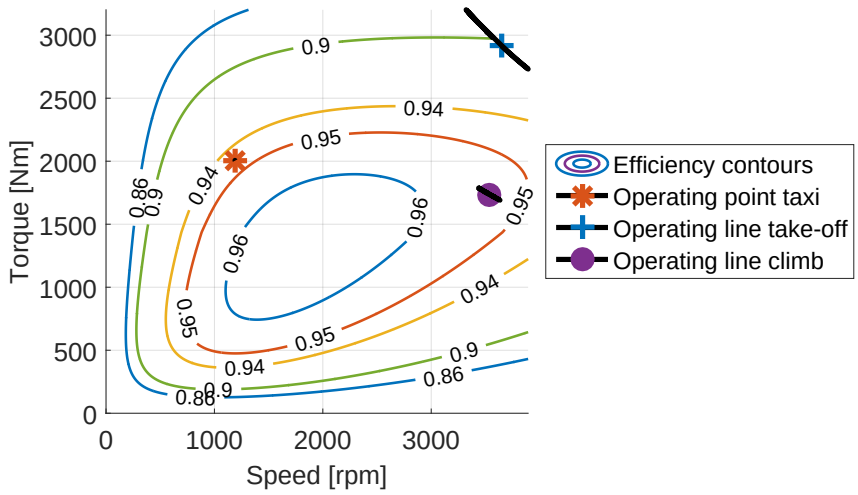

Figure 5.22: LP-spool electric motor operating points

Electric taxiing is carried out by only supplying power to the LP-shaft. To achieve the required thrust of 6 kN total, which is the assumed rolling friction of the aircraft of the research of reference [89], at taxi speed. This would translate into an effective power of 62 kW, for the maximum taxi speed of 20 kts [90]. [91] uses two electric motors with a total power of 100 kW for the electric taxiing. All of these studies where on aircraft of the A320 family. With the gas turbine model, it was found the LPT power is 250 kW to produce 3 kN of thrust per engine. For the electric taxiing, 250 kW of power is therefore required from the LP-shaft electric motor, which is

significantly more than the electric motor power of 50 kW (for one motor) from reference [91]. On one hand this is caused by the relatively lower efficiency of the fan, while on the hand the gas turbine model is not very accurate at lower thrust settings, discussed in section 3.5.1. 250 kW is significantly lower than the maximum continues power of the LP-shaft electric motor, but since the power needs to be supplied at low rotational speeds, the torque needs to be high. Since the electric motor's continues torque limit is around half the maximum torque, see figure 4.9 [85]. Taxiing electrically would require that the electric motor needs to be increased in size (wire thickness). For this study it is however not taken into account as a limiting factor, but the electric motor is sized for the climb and take-off thrust.

For the electric power division between the spool in the figures 5.22 and 5.23 an LP-power fraction of 0.6 was used. The HP-shaft electric motor therefore still has a significant amount of power. Its operating point during a mission a given in figure 5.23. Since the electric taxiing is done by only the LP-shaft electric motor, so this operating point is not present in this figure. The take-off and climb operating point look fairly similar for both electric motors. A large difference is however the HP-shaft electric motor rotational speeds, which are lot higher because of the higher speed of the HP-shaft. Therefore, the torque is a lot lower for the HP-shaft electric motor.

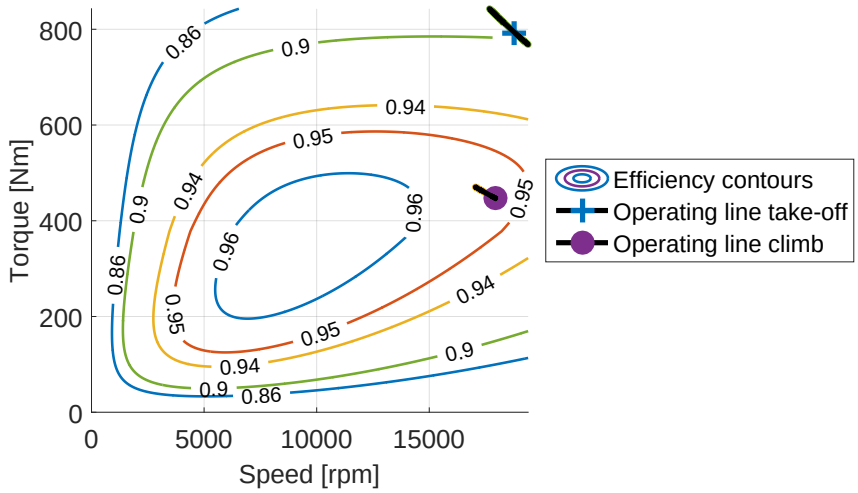

Figure 5.23: HP-spool electric motor operating points

From the operating lines in figures 5.22 and 5.23, the actual efficiencies of the electric motor throughout the mission are calculated. Figures 5.24 and 5.25 show the actual efficiency for the LP-shaft and HP-shaft electric motor in respectively. Both figures are divided between take-off and climb mission segments. The actual efficiency is displayed in a solid line, while the average of the mission phase for the electric motor is plotted with a dashed line. During take-off the efficiency of both electric motors clearly varies, but the average value is never far off. At climb, the efficiency in both the HP- and LP-shaft electric motor are virtually constant, making the simplification of two electric motor efficiency values, one for take-off and one for climb a valid assumption.

5.4. Mission analysis

Two technology levels have been set-up to assess the possible fuel savings and the feasibility of a HEPS. Table 5.1 shows all important technology levels assumed for both 2030 and 2040. Both

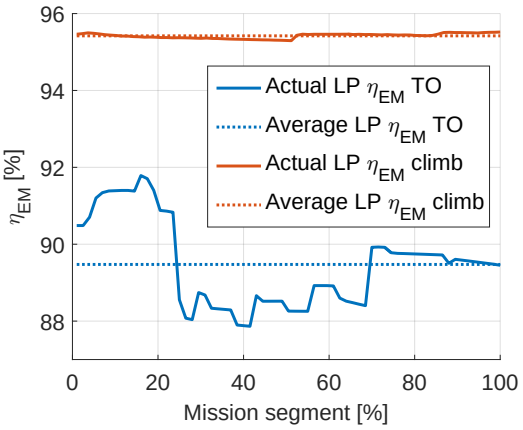

Figure 5.24: LP-spool electric motor operating efficiencies

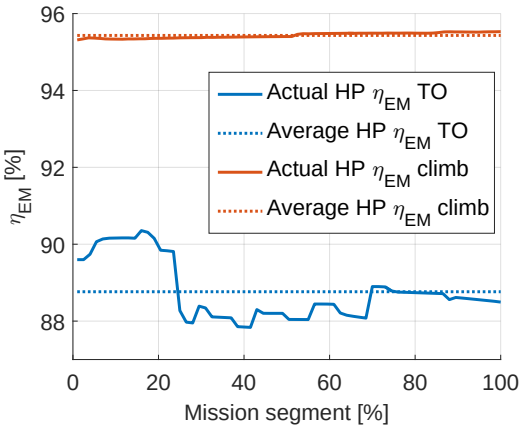

Figure 5.25: HP-spool electric motor operating efficiencies

the battery energy density level and electric motor power density are doubled, while the other parameters see a smaller improvement.

Table 5.1: Different technology levels

Parameter:	Technology level 2030:	Technology level 2040:
Battery energy density:	600 Wh/kg	1200 Wh/kg
Battery discharge efficiency:	97.5%	99%
Electric motor continues power density:	12.5 kW/kg	25 kW/kg
Electric motor maximum efficiency:	97.5%	99%
Inverter power density:	20 kW/kg	25 kW/kg
Inverter efficiency:	99%	99.5%

To provide the reading with insight into the relative importance of the different flight phases, table 5.2 provides the effective power that is supplied by the EM's to the turbofan, together with energy requirement of each phase, which also includes power requirements of the on-board electrical systems. The required battery for this mission is bigger because of the mission of the battery, inverter, electric motor and limit in depth of discharge of the battery itself.

Table 5.2: Useful power and energy supply of the total electrical propulsion system in different flight phases

Segment:	Energy supplied [kWh]:	EM Power [kW]:
Taxi:	83	500
Take-off:	61	5200
Climb:	1213	2800
Cruise:	0	0
Descent:	0	0
Total:	1357	-

Figure 5.26 compares the fuel consumption of the baseline A320neo, together with a HEP A320neo for the technology of 2030 (called $A320HEP_{2030}$) and the $A320HEP_{2040}$ which has the technol-

ogy of 2040. The A320HEP$_{2030}$ shows a total fuel consumption reduction of 4.7%, whereas the A320HEP$_{2040}$ obtains a reduction of 7.3% with respect to the A320neo. Because of the improved technology in the year 2040, the weight penalty of the HEP aircraft is smaller. In cruise, the A320HEP$_{2040}$ therefore shows a reduction in fuel burn compared to the A320HEP$_{2030}$. In table 5.3 the weights of all the aircraft and its HEP components, as well as the relative change with respect to the A320neo are shown. The battery is clearly the heaviest component with both technology levels, and the battery technology will therefore be one of the main factor for the possible fuels savings in parallel HEP aircraft. From the table it can also be seen the maximum landing weight, mentioned before in table 3.1, is exceeded for the A320HEP$_{2030}$. Although the maximum landing weight is exceeded only slightly, the fact that the A320HEP$_{2030}$ as well as the A320HEP$_{2040}$ have a higher landing weight than the A320neo, means that with a new aircraft design, the A320neo's landing gear will be lighter.

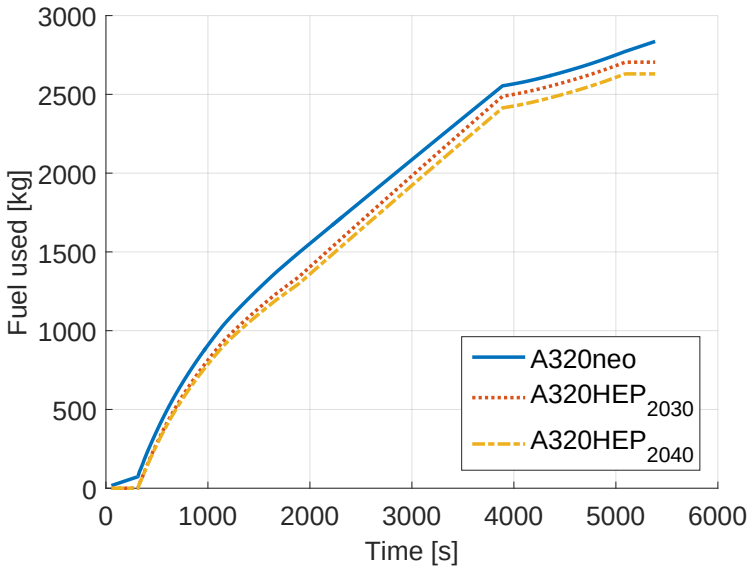

Figure 5.26: Comparison of total fuel consumption between the A320neo and the A320HEP$_{2030}$ and A320HEP$_{2040}$ with redesigned EATFs

Table 5.3: System and Aircraft weights of the A320neo, A320HEP 2030 and 2040

Parameter:	A320neo:	A320HEP$_{2030}$:	Difference w.r.t. neo:	A320HEP$_{2040}$:	Difference w.r.t. neo:
Battery weight:	n/a	3248 kg	n/a	1559 kg	n/a
Inverter weight:	n/a	140 kg	n/a	112 kg	n/a
Electric Motor weight:	n/a	224 kg	n/a	112 kg	n/a
OEW:	44400 kg	48012 kg	8.1%	46183 kg	4.0%
Fuel weight:	2836 kg	2704 kg	-4.7%	2630 kg	-7.3%
Payload:	18400 kg	18400 kg	0%	18400 kg	8.1%
Ramp weight:	65636 kg	69116 kg	5.3%	67213 kg	2.4%
TO weight:	65561 kg	69116 kg	5.4%	67213 kg	2.5%
Landing weight:	62860 kg	66412 kg	5.6%	64583 kg	2.7%

By doing a more in depth analysis of the fuel savings, it is found that taxi phase is where signif-

icant fuel is saved, see table 5.4. It only shows the results of the A320HEP$_{2030}$ compared to the A320neo. Fuel is saved in taxi, take-off & climb, but additional fuel is required in cruise & descent. This also follows from the limited improvement in cruise TSFC of the redesigned EATF, which was 1.0%. Together with the increased weight of around 5.5%, it is impossible to save fuel in cruise with this technology level. When only looking at the actual flight of the mission, so the take-off, climb, cruise and descent, the A320HEP$_{2030}$ consumes more fuel than the A320neo. In case of the A320HEP$_{2040}$, fuel will also be saved during the flight, but the majority of the savings are still thanks to electric taxiing. To show the savings in the mission phases relative to the total savings of the A320HEP$_{2030}$, figure 5.27 is added. It shows that the savings made during taxi are more than the total savings, and has therefore a relative saving of 102%. The relative savings made during take-off and climb (64%) are negated by the relative loss in savings of 66% in cruise and descent. Since the taxi phase is the major contributor to fuel saving, it is examined more extensively in the next section.

Table 5.4: Savings of the A320HEP$_{2030}$ per mission phase

	Taxi	TO & climb	Cruise & descent	Total
A320neo	135 kg	1431 kg	1270 kg	2836 kg
A320HEP$_{2030}$	0 kg	1347 kg	1357 kg	2704 kg
Difference (absolute)	-135 kg	-84 kg	87 kg	-132 kg
Difference (relative)	-100%	-5.9%	6.9%	-4.7%

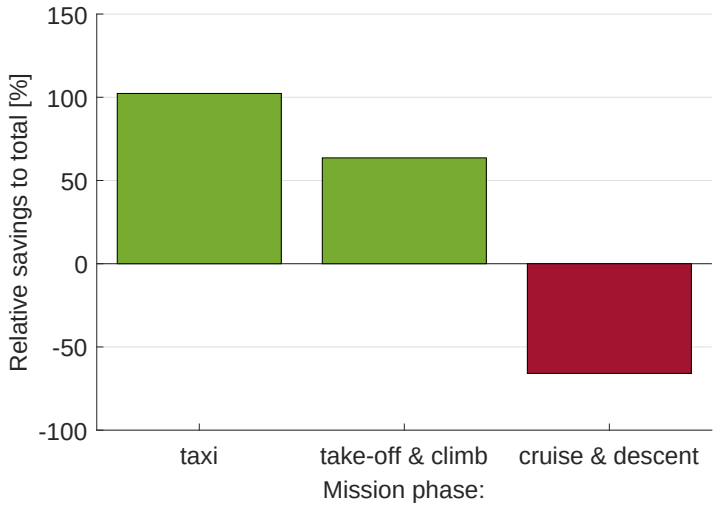

Figure 5.27: Relative mission phase savings of the A320HEP$_{2030}$ to the total savings

5.5. Analysis of taxi phase

In the mission profile considered before, the taxi-out and taxi-in where both 5 minutes. During this time no warm-up or cooling down of the gas turbines was taken into account. This is however required in reality for safety and longevity of the engine. Warm-up takes around 4 minutes, while 3 minutes is required for cooling down after touch down [90]. Because the turbofan needs to work at idle, enough thrust is available, and no additional electric power is required from the electric motors. A mission analysis when warm-up and cooling down are taken into account, and the same total taxi duration, the savings of the A320HEP$_{2030}$ are reduced from 4.7% to 1.8%.

Clearly, the taxi phase is determining the possible fuel savings. In 2007 the average US taxi-out and in time where however a lot longer compared to the taxi phases considered before. Taxi-out was on average 17 minutes and taxi-in took 7 minutes. Combining this longer taxi phase with the warm-up and cooling down, 17 minutes of electric taxi remain. This would allow for reduction of 7.1% with the $A320HEP_{2030}$ compared to the A320neo. Although these savings are significant, the lack of fuel saving capabilities during the flight mean parallel HEP is not very promising. With a much smaller battery and electric motor, electric taxiing can be carried out. By only having an electric taxiing system, the range of the aircraft would not be as limited as in the heavier HEP case, which will beneficial from an operational point of view of the aircraft.

6

Conclusions & Recommendations

This chapter describes the main conclusions of the research project and closes off with recommendations for future research. The conclusions section is divided into two subsections. One deals with conclusions regarding the characteristics of the electrically assisted turbofan; whereas the other contains some conclusions on future outlook of parallel hybrid electric propulsion aircraft.

6.1. Electrically assisted turbofan characteristics

The analyses that were done in this study indicate that none of the assessed power split ratios could operate at maximum efficiency with one electric motor. At top of climb the low pressure compressor surge margin requirement limits the ability to operate the electrically assisted turbofan in its maximum efficiency point, even with two electric motors, one on the LP-spool and another on the HP-spool. In a geared turbofan, the surge margin of the low pressure compressor is larger, compared to a direct drive two-spool turbofan. This allows for a more efficient operation of turbofan in climb.

Due to the added electrical power, the turbine inlet temperature of the gas turbine decreases for a given thrust. When most power is supplied into the LP-spool, the overall pressure ratio decreases as well. Because in a geared turbofan, the low pressure compressor surge margin is less limiting, the overall pressure ratio reduces more. For a redesign of the turbofan in cruise, a geared turbofan can therefore be designed with a slightly higher overall pressure ratio compared to a direct driven two spool turbofan, allowing for a slightly larger efficiency improvement. By applying a power split ratio of 14% in both take-off and climb, the redesigned turbofan show a cruise TSFC reduction of 1.0%.

By investigating the performance of a gas turbine in take-off and cruise with open literature data and operating line characteristics, it was found that the efficiency of the fan, compressor and turbines of a state-of-the-art turbofan during cruise is not limited by take-off thrust or top climb performance requirements. The limitations that do come from the take-off thrust requirement is on the cooling system design and the maximum allowable material temperature of the HP-turbine. For the TOC requirement, the limiting factors are the maximum overall pressure ratio and the maximum corrected airflow.

Designing the electric motor specifically for the turbofan, gives the option to use the electric motor in maximum continues power during climb, while it can operate at peak power during

take-off. This allows it to operate close to the maximum efficiency point in climb, in which most energy is supplied, while the weight of the electric motor is minimised. The considered power split ratio is therefore not limited by the electric motor's operating limits during take-off and climb.

6.2. Outlook on parallel hybrid electric propulsion aircraft

The results of this study indicate that the potential savings for a parallel HEP version of the existing A320 aircraft are limited, mainly due to the mass of the required electrical system. This system increases the total weight of the aircraft by around 5.5% with expected technology for the year, where this is reduced to 2.5% for the year 2040. The study shows that this additional weight cannot sufficiently be offset by the 1.0% reduction of the thrust specific fuel consumption in cruise. Over a complete mission of 1000 km, the 2030 technology shows a fuel saving of 4.7%, whereas 7.3% can be saved in 2040.

The mission analysis shows that the biggest saving is achieved due to electric taxiing. With 2030 technology, the savings during the flight part of the mission are negative. This shows savings can more easily be realised by using only electric taxiing, instead of a complete hybrid electric propulsion system. In the year 2040, the technology would allow for savings during the flight itself, but the majority of the savings are still achieved during electric taxiing.

Commercial parallel HEP aircraft are not expected to be introduced in the coming 2 decades. HEPS will require significant redesigns of the aircraft propulsion system, while a majority of the savings can be achieved by incorporating an electric taxiing system. Such a system will require a lot less effort to be developed than a HEPS.

6.3. Recommendations and limitations

The study uses a constant cooling air flow percentage. With the increased TIT in cruise this would in reality mean a large decrease in lifetime of the hot components. Therefore it is advised to investigate the actual cooling requirements and expected lifetime of the components with the increases TIT.

The possible benefits of removing additional components that could be replaced by the electrical HEP-system (like the axillary power unit, pressure lines and pneumatic starter motors of the turbofans), are not taken into account in this study. Additional research is needed here to assess the additional benefits this weight reduction might have on the performance of a parallel HEP aircraft.

Currently generic performance maps are used in the study. When the components are designed specifically for the use in electrically assisted turbofan, it might provide slightly better performance. Also, a larger surge margin could be made in LPC, so the gas turbine is not limited to operate at its maximum efficiency point.

Although the MTOW is not exceeded with the HEP aircraft, the maximum landing weight is. This would mean that a stronger (and heavier) landing gear is required. In its turn, the fuel consumption would go up for the HEP aircraft, and the savings will go down. A similar story is for the wings and other structures in the aircraft. These where not changed for the heavier HEP aircraft. A study in which two dedicated aircraft designs are compared, a conventional one as well as a HEP aircraft, will result in a more honest comparison.

Bibliography

[1] D.S. Lee, D.W. Fahey, P.M. Forster, P.J. Newton, R.C.N. Wit, L.L. Lim, B. Owen, and R. Sausen. *Aviation and global climate change in the 21st century*. *Atmospheric Environment*, 43(22-23):3520–3537, 2009. doi: 10.1016/j.atmosenv.2009.04.024.

[2] Airbus S.A.S. *Global Market Forecast 2018–2037*, Blagnac, France, 2018.

[3] Boeing. *Commercial Market Outlook 2018–2037*, Chicago, Illinois, USA, 2018.

[4] European Environment Agency, European Union Aviation Safety Agency, and Eurocontrol. *European Aviation Environmental Report 2019*. Technical report, 2019.

[5] A. Klauber and I. Toussie. *A Radical New Plan for Aviation*. In *World Economic Forum*, Davis, Switzerland, 2019.

[6] IATA. *Fact Sheet: Climate Change CORSIA, A CO2 standard for aircraft*, 2018.

[7] Intergovernmental Panel on Climate Change (IPCC). *Climate Change 2014: Mitigation of Climate Change- Technical Summary*. Technical report, Cambridge, United Kingdom, 2014.

[8] R. Babikian, S.P. Lukachko, and I.A. Waitz. *The historical fuel efficiency characteristics of regional aircraft from technological, operational, and cost perspectives. Journal of Air Transport Management*, 8(6):389–400, 2002. doi: 10.1016/S0969-6997(02)00020-0.

[9] National Academies of Sciences Engineering and Medicine. *Commercial Aircraft Propulsion and Energy Systems Research: Reducing Global Carbon Emissions*. The National Academies Press, Washington DC, United States of America, 2016. ISBN 978-0-309-44096-7. doi: 10.17226/23490.

[10] C.E. Hughes, D.E. van Zante, and J.D. Heidmann. *Aircraft Engine Technology for Green Aviation to Reduce Fuel Burn*. In *3rd AIAA Atmospheric Space Environments Conference*, number June, pages 1–18, Honolulu, Hawaii, USA, 2011. doi: 10.2514/6.2011-3531.

[11] Pratt & Whitney. *Pratt & Whitney geared turbofan engine fast facts*, 2019.

[12] A.H. Lefebvre and D.R. Ballal. *Gas Turbine Combustion: Alternative Fuels and Emissions*. CRC Press, 3rd edition, 2010.

[13] European-Commission. *Flightpath 2050: Europe's Vision for Aviation*, 2011.

[14] NASA. *Green Aviation: Safeguarding Our Future on Earth*, 2015.

[15] J.C. Gladin, C. Perullo, J.C. Tai, and D.N. Mavris. *A Parametric Study of Hybrid Electric Gas Turbine Propulsion as a Function of Aircraft Size Class and Technology Level*. In *55th AIAA Aerospace Sciences Meeting*, pages 1–38, 2017. ISBN 978-1-62410-447-3. doi: 10.2514/6.2017-0338.

[16] A.W.X. Ang, A. Gangoli Rao, T. Kanakis, and W. Lammen. *Performance analysis of an electrically assisted propulsion system for a short-range civil aircraft. Proceedings of the Institution of Mechanical Engineers, Part G: Journal of Aerospace Engineering*, 233(4):1490–1502, 2019. doi: 10.1177/0954410017754146.

[17] M. Hoogreef, R. Vos, R. de Vries, and L.L. Veldhuis. *Conceptual Assessment of Hybrid Electric Aircraft with Distributed Propulsion and Boosted Turbofans.* In *AIAA Scitech 2019 Forum*, number January, pages 1–16, 2019. doi: 10.2514/6.2019-1807.

[18] A. Seitz, M. Nickl, A. Stroh, and P.C. Vratny. *Conceptual study of a mechanically integrated parallel hybrid electric turbofan. Proceedings of the Institution of Mechanical Engineers, Part G: Journal of Aerospace Engineering*, 232(14):2688–2712, 2018. doi: 10.1177/0954410018790141.

[19] V. Kloos, T.H. Speak, R.J. Sellick, and P. Jeschke. *Dual Drive Booster for a Two-Spool Turbofan: High Shaft Power Offtake Capability for More Electric Aircraft and Hybrid Aircraft Concepts. Journal of Engineering for Gas Turbines and Power*, 140(12):121201, 2018. doi: 10.1115/1.4040822.

[20] GSP Development Team. *GSP manual*, Amsterdan, The Netherlands, 2015.

[21] The MathWorks Inc. *Matlab R2015b (8.6.0)*, Natick, United States, 2015.

[22] W. Visser. *Generic Analysis Methods for Gas Turbine Engine Performance.* PhD thesis, TU Delft, 2015.

[23] A. Gangoli Rao. *Aero Engine Technology lecture 1: Introduction*, TU Delft, 2015.

[24] B. Fehrm. *Bjorn's Corner: Turbofan engine challenges, Part 4*, 2016. URL `https://leehamnews.com/2016/11/18/bjorns-corner-turbofan-engine-challenges-part-4/`. Accessed on 3-7-2019.

[25] K. Ghorbanian and M. Gholamrezaei. *An artificial neural network approach to compressor performance prediction. Applied Energy*, 86(7-8):1210–1221, 2009. doi: 10.1016/j.apenergy.2008.06.006.

[26] W. Visser. *Aero Engine Technology lecture: Gas Turbine Performance Characteristics*, TU Delft, 2015.

[27] P.P. Walsh and P. Fletcher. *Gas Turbine Performance.* Blackwell, Oxford, United Kingdom, 2nd edition, 2004.

[28] F. Yin and A. Gangoli Rao. *Off-Design Performance of an Interstage Turbine Burner Turbofan Engine. Journal of Engineering for Gas Turbines and Power*, 139(8), 2017. doi: 10.1115/1.4035821.

[29] E.S. Hendricks and M.T. Tong. *Performance and Weight Estimates for an Advanced Open Rotor Engine.* In *48th AIAA/ASME/SAE/ASEE Joint Propulsion Conference & Exhibit*, pages 1–12, Atlanta, Georgia, USA, 2012. doi: 10.2514/6.2012-3911.

[30] N. Peake and A.B. Parry. *Modern Challenges Facing Turbomachinery Aeroacoustics. Annual Review of Fluid Mechanics*, 44:227–250, 2012. doi: 10.1146/annurev-fluid-120710-101231.

[31] C. Lambert. *Open Rotor Engines.* Technical report, Society of British Aerospace Companies Limited, London, United Kingdom, 2015.

[32] J. Brouckaert. *Engine Demonstration Programmes in Clean Sky & Clean Sky 2*, London, United Kingdom, 2015.

[33] A. Gangoli Rao, F. Yin, and J.P. van Buijtenen. *A hybrid engine concept for multi-fuel blended wing body. Aircraft Engineering and Aerospace Technology*, 86(6):483–493, 2014. doi: 10.1108/AEAT-04-2014-0054.

[34] C. Liu, G. Doulgeris, P. Laskaridis, and R. Singh. *Turboelectric Distributed Propulsion System Modelling for Hybrid-Wing-Body Aircraft.* In *48th AIAA/ASME/SAE/ASEE Joint Propulsion Conference & Exhibit*, number August, pages 1–13, Atlanta, Georgia, USA, 2012. doi: 10.2514/6.2012-3700.

[35] D.K. Hall, A.C. Huang, A. Uranga, E.M. Greitzer, M. Drela, and S. Sato. *Boundary Layer Ingestion Propulsion Benefit for Transport Aircraft. Journal of Propulsion and Power*, 33(5): 1–12, 2017. doi: 10.2514/1.B36321.

[36] M.K. Bradley and C.K. Droney. *Subsonic Ultra Green Aircraft Research: Phase I Final Report.* Technical report, NASA, 2011.

[37] J.L. Felder, G.V. Brown, H.D. Kim, and J. Chu. *Turboelectric Distributed Propulsion in a Hybrid Wing Body Aircraft. Isabe-2011-1340*, pages 1–20, 2011.

[38] The Boeing Company. *2014 Environment Report: Build a Better Planet*, 2014.

[39] K. San-Hoon. *Electric Motor Control.* Elsevier, Chuncheon, South Korea, 1st edition, 2017.

[40] Ming Cheng, Le Sun, Giuseppe Buja, and Lihua Song. *Advanced Electrical Machines and Machine-Based Systems for Electric and Hybrid Vehicles. Energies*, 8(9):9541–9564, 2015. doi: 10.3390/en8099541.

[41] D. Moreels and P. Leijnen. *High Efficiency Axial Flux Machines.* Technical report, MAGNAX, 2018.

[42] WEG-Group. *Motors Specification of Electric Motors.* WEG Group, Jaraguá do Sul - SC-Brazil, 2016.

[43] O. Schmitz and M. Hornung. *Methods for simulation and analysis of hybrid electric propulsion systems. CEAS Aeronautical Journal*, 6(2):245–256, 2015. doi: 10.1007/s13272-014-0137-9.

[44] Siemens AG. *Aerobatic Airplane "Extra 330LE" with world-record electric motor from Siemens*, 2016.

[45] C.A. Luongo, P.J. Masson, T. Nam, D. Mavris, H.D. Kim, G.V. Brown, M. Waters, and D. Hall. *Next Generation More-Electric Aircraft: A Potential Application for HTS Superconductors. IEEE Transactions on Applied Superconductivity*, 19(6):1055–1068, 2009. doi: 10.1109/TASC.2009.2019021.

[46] Y. Miyairi, C. Perullo, and D.N. Mavris. *A Parametric Environment for Weight and Sizing Prediction of Motor/Generator for Hybrid Electric Propulsion. 51st AIAA/SAE/ASEE Joint Propulsion Conference*, pages 1–19, 2015. doi: 10.2514/6.2015-3887.

[47] M.K. Bradley and C.K. Droney. *Subsonic Ultra Green Aircraft Research: Phase II – Volume II – Hybrid Electric Design Exploration.* Technical report, NASA, 2015.

[48] E. Ganev. *Selecting the best electric machines for electrical power-generation systems: High-performance solutions for aerospace More electric architectures. IEEE Electrification Magazine*, 2(4):13–22, 2014. doi: 10.1109/MELE.2014.2364731.

[49] A.T. Isikveren, Y. Fefermann, C. Maury, C. Level, K. Zarati, J.P. Salanne, C. Pornet, and B. Thoraval. *Pre-design of a commuter transport utilising Voltaic-Joule/Brayton motive power systems. The Aeronautical Journal*, 122(1248):205–237, 2017. doi: 10.1017/aer.2017.126.

[50] G. Cinar, D.N. Mavris, M. Emeneth, A. Schneegans, C. Riediger, Y. Fefermann, and A. Isikveren. *Sizing, Integration and Performance Evaluation of Hybrid Electric Propulsion Subsystem Architectures.* In *55th AIAA Aerospace Sciences Meeting*, number January, Grapevine, Texas, USA, 2017. doi: 10.2514/6.2017-1183.

[51] C. Friedrich and P.A. Robertson. *Design of Hybrid-Electric Propulsion Systems for Light Aircraft.* In *14th AIAA Aviation Technology, Integration, and Operations Conference*, number June, pages 1–17, Atlanta, Georgia, USA, 2014. doi: 10.2514/6.2014-3008.

[52] N. Madavan. *Hybrid-Electric and Distributed Propulsion Technologies for Large Commercial Air Transports : A NASA Perspective "Advanced Air Transport Technology Project"*. In *Presentation at Special Session on Future Electric Aircraft-Systems*, 2015.

[53] M. Voskuijl, J. van Bogaert, and A. Gangoli Rao. *Analysis and design of hybrid electric regional turboprop aircraft. CEAS Aeronautical Journal*, 2017. doi: 10.1007/s13272-017-0272-1.

[54] Panasonic. *Datasheet Panasonic NCR18650B*, 2012.

[55] K. Field. *Tesla Model 3 Battery Pack & Battery Cell Teardown Highlights Performance Improvements*, 2019. URL `https://cleantechnica.com/2019/01/28/tesla-model-3-battery-pack-cell-teardown-highlights-performance-improvements/`. Accessed on 3-7-2019.

[56] J. Ryu, H. Jang, J. Park, Y. Yoo, M. Park, and J. Cho. *Seed-mediated atomic-scale reconstruction of silver manganate nanoplates for oxygen reduction towards high-energy aluminum-air flow batteries. Nature Communications*, 9(1):1–10, 2018. doi: 10.1038/s41467-018-06211-3.

[57] B. Roberts. *Capturing Grid Power. IEEE Power & Energy Magazine*, 7(4):32–41, 2009.

[58] MagniX. *MagniDrive*, 2019. URL `https://www.magnix.aero/products/`. Accessed on 10-7-2019.

[59] P.C. Vratny, P. Forsbach, A. Seitz, and M. Hornung. *Investigation of Universally Electric Propulsion Systems for Transport Aircraft. 29th Congress of the International Council of the Aeronautical Sciences*, pages 1–13, 2014.

[60] G. Brown. *Weights and Efficiencies of Electric Components of a Turboelectric Aircraft Propulsion System. 49th AIAA Aerospace Sciences Meeting including the New Horizons Forum and Aerospace Exposition*, (January), 2011. doi: 10.2514/6.2011-225.

[61] Japan Aircraft Development Corporation. *Worldwide Market Forecast 2018 – 2037.* Technical Report March, Tokio, 2018.

[62] Airbus S.A.S. *Airbus A320 Aircraft Characteristics and Maintenance Planning*. Technical report, Blagnac, France, 2018.

[63] IHS Markit. *Airbus A320*. In *Jane's All the World's Aircraft*, 2017.

[64] Lissys Limited. *PianoX*, Woodhouse Eaves, United Kingdom, 2010.

[65] D. Scholz, R. Seresinhe, I. Staack, and C. Lawson. *Fuel Consumption Due To Shaft Power Off-Takes From the Engine*. In *4th International Workshop on Aircraft System Technologies (AST 2013)*, pages 169–179, Hamburg, Germany, 2013.

[66] ICAO. *LEAP-1A26*. In *ICAO ENGINE EXHAUST EMISSIONS DATA BANK*, 2019.

[67] N.A. Cumpsty. *Preparing for the Future: Reducing Gas Turbine Environmental Impact—IGTI Scholar Lecture*. *Journal of Turbomachinery*, 132(4):041017, 2010. doi: 10.1115/1.4001221.

[68] IHS Markit. *CFM International CFM56*. In *Jane's Areo-Engines*, 2018.

[69] CFM International. *CFM LEAP Brochure*, 2010.

[70] EASA. *LEAP-1A and LEAP-1C*. In *Type-certificate data sheet*, number No. E110, Issue: 07, 2018.

[71] E. Hall, R. Delaney, S. Lynn, and J. Veres. *Energy Efficient Engine low pressure subsystem aerodynamic analysis*. In *34th Propulsion*, pages 1–15, 1998. doi: 10.2514/6.1998-3119.

[72] J. Kurzke. *Smooth C 8.2: Preparing Compressor Maps for Gas Turbine Performance Modeling*, 2009.

[73] GasTurb GmbH. *GasTurb 13: Design and Off-Design Performance of Gas Turbines*, 2018.

[74] R.M. Plencer. *Plotting Component Maps in Navy/NASA Engine Program (NNEP) - A Method and Its Usage*. Technical report, NASA Lewis Research Center, Ohio, Cleveland, USA, 1989.

[75] A.W.X. Ang. *Hybrid Electric Propulsion Systems: Integrated performance analysis applied on short-range aircraft*. Master's thesis, TU Delft, 2016.

[76] E. Roux. *Turbofan and turbojet engines: database handbook*. lulu.com, Blagnac, France, 2007. ISBN 978-2-9529380-1-3.

[77] J. Kurzke and I. Halliwell. *Propulsion and Power: An Exploration of Gas Turbine Performance Modeling*. Springer International Publishing, Cham, Switzerland, 2018. ISBN 978-3-319-75977-7. doi: 10.1007/978-3-319-75979-1.

[78] V. Bhaskara. *ANALYSIS: A320neo vs. 737 MAX: Airbus is Leading*, 2016. URL `https://web.archive.org/web/20160206082857/http://airwaysnews.com/blog/2016/02/05/a320neo-vs-737-max-pt-ii/`. Accessed on 24-5-2019.

[79] Airbus S.A.S. *Family Figures*, Blagnac Cedex, France, 2019.

[80] M. Gubisch. *What operators have to say about the A320neo*, 2019. URL `https://www.flightglobal.com/news/articles/analysis-what-operators-have-to-say-about-the-a320n-454247/`. Accessed on 22-7-2019.

[81] G. Evans. *Frankfurt to Rome flight 1401*, 2019. URL http://fuelplanner.com/index.php. Accessed on 24-7-2019.

[82] J. Larminie and J. Lowry. *Electric Vehicle Technology Explained*. John Wiley & Sons, Incorporated, second edition, 2012. doi: 10.1002/9781118361146.ch7.

[83] R.A. McDonald. *Electric Propulsion Modeling for Conceptual Aircraft Design*. In *52nd Aerospace Sciences Meeting*, number January, National Harbor, Maryland, 2014. doi: 10.2514/6.2014-0536.

[84] J. Pyrhönen, T. Jokinen, and V. Hrabovcová. *Design of Rotating Electrical Machines*. John Wiley & Sons, Ltd, 2008. ISBN 9780470695166. doi: 10.1002/9780470740095.

[85] Emrax. *Technical Data and Manual for EMRAX Motors / Generators*, 2018. URL http://emrax.com/wp-content/uploads/2017/10/user{_}manual{_}for{_}emrax{_}motors.pdf. Accessed on 2-6-2019.

[86] M.U. Lampérth, A.C. Malloy, A. Mlot, and M. Cordner. *Assessment of Axial Flux Motor Technology for Hybrid Powertrain Integration*. *World Electric Vehicle Journal*, 7:187–194, 2015.

[87] MAGNAX. *Efficiency Map axial flux motor Magnax AXF275*. URL https://www.magnax.com/. Accessed on 24-5-2019.

[88] G.L. Converse. *Extended Parametric Representation of Compressors, Fans and Turbines Vol III*, NASA-CR-174647, 1984.

[89] Michael Schier, Frank Rinderknecht, and Heribert Hellstern. *Electric wheel hub motor for aircraft application*. *International Journal of Renewable Energy Research*, 1(4):298–305, 2011.

[90] Y. Nicolas. *eTaxi, taxiing aircraft with engines stopped*. *Airbus Technical Magazine - FAST 51*, January, 2013.

[91] Guy Norris. *Electric Taxi Puts On A Show At Paris*, 2013. URL https://awin.aviationweek.com/ArticlesStory/ArticlesPrint.aspx?id=0c52d3dd-7565-45d6-bdae-6503a5b994ab{&}p=1{&}printView=true. Accessed on 29-7-2019.

[92] J.D. Anderson Jr. *Introduction to Flight*. McGraw-Hill, seventh edition, 2008. ISBN 9780071086059.

[93] OpenSky Network. *Open Air Traffic Data for Research*, 2019. URL https://opensky-network.org/. Accessed on 11-6-2019.

[94] R.M. Rosenkrantz. *Finding the climate optimal cruise altitude for a selection of aircraft and mission combinations*. Master's thesis, TU Delft, 2019.

[95] V. Singh. *Fuel consumption minimization of transport aircraft using real-coded genetic algorithm*. *Proceedings of the Institution of Mechanical Engineers, Part G: Journal of Aerospace Engineering*, 232(10):1925–1943, 2018. doi: 10.1177/0954410017705899.

[96] H. Khadilkar and H. Balakrishnan. *Estimation of aircraft taxi fuel burn using flight data recorder archives*. *Transportation Research Part D: Transport and Environment*, 17(7):532–537, 2012. doi: 10.1016/j.trd.2012.06.005.

[97] B. Goldberg and D. Chesser. *Bureau of Transportation Statistics Special Report Sitting on the Runway: Current Aircraft Taxi Times Now Exceed Pre-9/11 Experience Figure 1: Average Taxi-Out Times by Year*. Technical report, U.S. Department of Transportation, 2008.

A

International Standard Atmosphere

The International Standard Atmosphere (ISA) model is set-up as described in reference [92]. From standard sea level conditions of 1.225 kg/m^3, 101325 Pa and 15 ^oC (288.16 K) the other conditions can be calculated. In the lower region of the atmosphere, called troposphere the temperature decreases linearly with altitude. This trend remains the same until a height of 11 km where the tropopause begins. In this layer, which reaches above cruise altitude of commercial aircraft, the temperature remains the same as at 11 km altitude. From this the pressure can be calculated at every altitude, as well as the density and speed of sound. Table A.1 shows the properties of the ISA up to an altitude of 12 km.

Table A.1: International Standard Atmosphere

Altitude [km]	Density [kg/m^3]	Pressure [Pa]	Temperature [K]	Speed of Sounds [m/s]
0	1.2250	101325	288.16	340.30
1000	1.1116	89877	281.66	336.44
2000	1.0065	79502	275.16	332.54
3000	0.9092	70122	268.67	328.59
4000	0.8193	61662	262.18	324.60
5000	0.7364	54050	255.69	320.55
6000	0.6601	47219	249.20	316.46
7000	0.5900	41107	242.71	312.31
8000	0.5258	35653	236.23	308.11
9000	0.4671	30802	229.74	303.85
10000	0.4135	26501	223.26	299.54
11000	0.3648	22701	216.78	295.16
12000	0.3119	19401	216.66	295.08

B

Mission Profile Validation

With a real flight profile of a Lufthansa Airbus A320neo from Frankfurt, Germany to Rome, Italy on 20th of November 2018 the mission profile is validated. The Lufthansa flight data was obtained with data from The Opensky Network [93]. With the help of the author of reference [94], this data was analysed to be able to present it in a simple manner and clear manner.

The upper left plot of figure B.1 shows the thrust of both engines during the entire mission. No additional validation data was available, but the thrust shows good agreement to the thrust requirements from table 3.3. On the lower left plot, showing the altitude, the climb, cruise and descent are very similar. During climb the reference data shows a sharp peak which is physically impossible for the aircraft and must be a measurement error. At TOC the reference mission shows a much sharper edge compared to the simulation model, explaining why the thrust value of the simulation mission at TOC is so close to the cruise thrust. Cruise of the reference mission is taking place slightly higher, around 12 km compared to 11.28 km. The majority of the descent shows very good overlap as well, but where the simulation model shows a constant descent, the reference mission showed a decreased descent speed. On the two right plots in the figure, airspeed and Mach number are shown. Overall the trends of the simulation and reference mission are very similar, but halfway during climb it can be seen the reference mission increases its Mach number faster and reaching cruise speed before it reaches TOC. From these two plots it can also clearly be seen that the reference mission does not have data of the take-off and touch-down. Data from Opensky Network is limited, and on-ground data is present. It is however easy to see, especially at the end of descent, the simulation decreases speed extremely fast after reaching Mach 0.4, indicating touch-down. The same is true for lift-off, which seems to take place Mach 0.4 as well. These values are way too high for the A320, but since both take-off and touch-down are relatively short mission phases, the total fuel consumption is not very high and is therefore not having a large impact on the overall mission. Taxi duration is relatively short with 5 minutes taxi-out and 5 minutes taxi-in, when looking at other sources [95, 96]. In 2007 the average US taxi-out and taxi-in times where 17 and 7 minutes respectively [97]. Despite some errors and shortcomings, the mission flight profile is appropriate for this study.

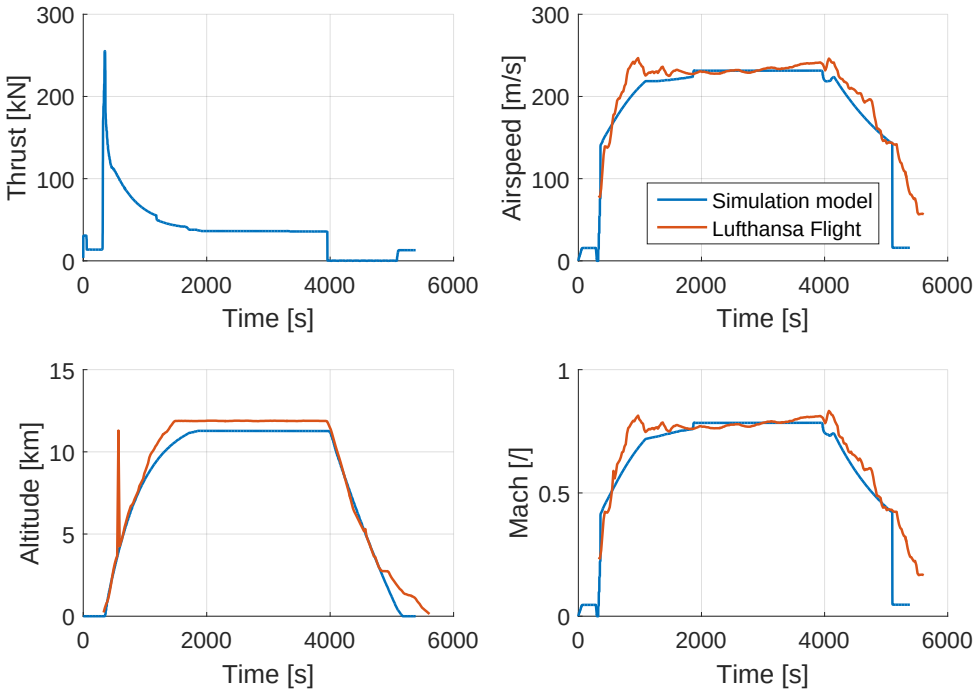

Figure B.1: Mission profile validation, data adapted from [75]

C

Research Paper

Paper on the performed master thesis, planned to be submitted for the 2020 ASME Turbo Expo.